Supporting Information for:

Selective Anion Binding Drives the Formation of $Ag^{I}_{8}L_{6}$ and $Ag^{I}_{12}L_{6}$ Six-Stranded Helicates

Charlie T. McTernan, Tanya K. Ronson, and Jonathan R. Nitschke*

Department of Chemistry, University of Cambridge, Lensfield Road, Cambridge, CB2 1EW

*E-mail: jrn34@cam.ac.uk

S1. Contents

S2. Experimental Procedure

Unless otherwise specified, all starting materials, solvents and reagents were used as supplied and without further purification. Flash column chromatography was performed using Silica Gel high purity grade (pore size 60 Å, 230-400 mesh particle size, Sigma-Aldrich). All anhydrous reactions were carried out in oven-dried glassware and under an inert atmosphere of nitrogen provided by a balloon. All reactions were stirred with magnetic followers Centrifugation of samples was carried out using a Grant-Bio LMC-3000 low speed benchtop centrifuge.

S3. Instrumentation and Characterisation Methods

Mass Spectrometry

Low-resolution electrospray ionisation (ESI) mass spectra were obtained on a Micromass Quattro LC mass spectrometer (cone voltage 20 eV; desolvation temp. 313 K; ionisation temp. 313 K) infused from a Harvard syringe pump at a rate of 4-10 μL min^{-1}. High-resolution ESI mass spectra were obtained using a Thermo Scientific LTQ Orbitrap XL hybrid ion trap-orbitrap mass spectrometer or a Xevo quadrupole time-of-flight mass spectrometer.

NMR Spectroscopy

NMR spectra were recorded on a 400 MHz Avance III HD Smart Probe, Bruker Avance 500 Cryo, Bruker 500 TCI-ATM Cryo and Bruker 700 TCI-ATM Cryo. Chemical shifts (δ) for ^{1}H NMR spectra are reported in parts per million (ppm) and are reported relative to the solvent residual peak. DOSY experiments were carried out on a Bruker DRX-400 spectrometer. Coupling constants (*J*) are reported in hertz (Hz). The following abbreviations are used to describe signal multiplicity in ^{1}H, ^{13}C and ^{19}F NMR spectra: s: singlet, d: doublet, t: triplet, dd: doublet of doublets; dt: doublet of triplets; m: multiplet, br: broad. DOSY NMR experiments were performed on a 400 MHz Avance III HD Smart Probe NMR spectrometer. Maximum gradient strength was 6.57 G/cm A. The standard Bruker pulse program, ledbpgp2s, employing a stimulated echo and longitudinal eddy-current delay (LED) using bipolar gradient pulses for diffusion using 2 spoil gradients was utilised. Rectangular gradients were used with a total duration of 1.5 ms. Gradient recovery delays were 875-1400 μs. Individual rows of the S4 quasi-2D diffusion databases were phased and baseline corrected.

S4. Synthesis and Characterisation

S4.1 Six-Stranded Helicate 9

To 2,2'-dimethyl-[1,1'-biphenyl]-4,4'-diamine (**3**) (10.8 mg, 0.051 mmol, 6 eq.), 2-formyl-1,8-naphthyridine (**1**) (16.0 mg, 0.101 mmol, 12 eq.), and silver triflimide (42.6 mg, 0.110 mmol, 12 eq.) was added a magnetic stirrer and acetonitrile (5 ml). The assembly was sonicated until a homogenous solution was formed. TBA iodide (6.28 mg, 0.017 mmol, 2 eq.) was then added, and the assembly stirred for 5 minutes. The assembly was filtered, concentrated to a fifth of the original volume, and diethyl ether was added until a pale yellow precipitate was formed. The precipitate was collected by centrifugation, washed with diethyl ether (3 x 10 mL), and dried under a stream of nitrogen. The solid product was then collected as a fine yellow powder (33.4 mg, 68%).

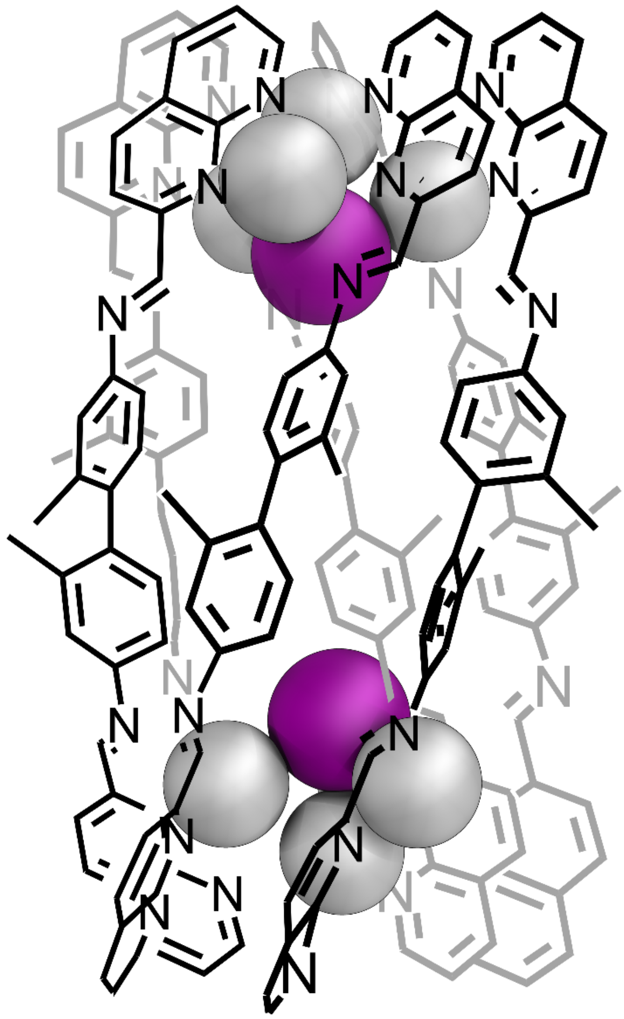

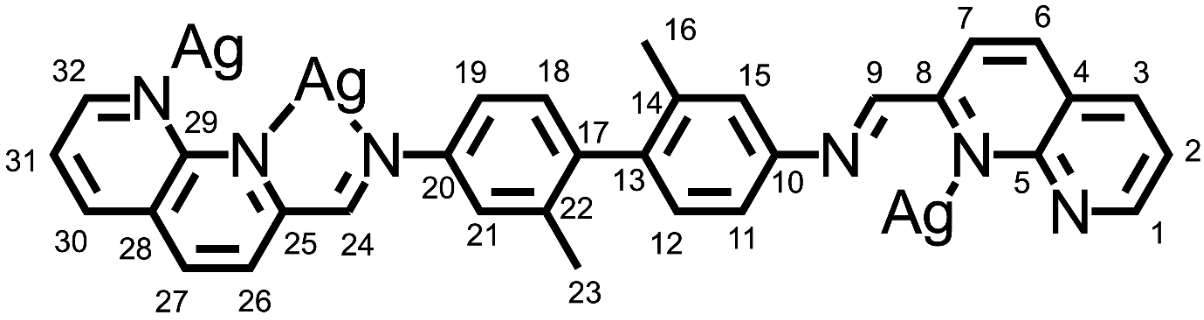

^{1}H NMR (500 MHz, CD_3CN) δ: 9.33 (1H, dd, *J* = 4.6, 1.9 Hz, H_{32}), 9.01 (1H, s, H_{24}), 8.95 (1H, s, H_9), 8.38 – 8.36 (2H, m, H_{11} + H_{27}), 8.35 (1H, d, *J* = 8.4 Hz, H_6), 8.20 (1H, dd, *J* = 8.6, 1.7 Hz, H_3), 7.98 (1H, dd, *J* = 8.6, 1.7 Hz, H_{30}), 7.95 (1H, d, *J* = 8.4 Hz, H_7), 7.89 (1H, d, *J* = 8.1 Hz, H_{26}), 7.41 (1H, s, H_{15}), 7.24 (1H, dd, *J* = 8.1, 4.3 Hz, H_2), 7.17 (1H, s, H_{21}), 7.10 (1H, dd, *J* = 8.0, 4.6 Hz, H_{31}), 7.02 (1H, dd, *J* = 4.4, 1.7 Hz, H_1), 6.89 (1H, dd, *J* = 7.7, 1.7 Hz, H_{19}), 5.94 (1H, d, *J* = 7.8 Hz, H_{12}), 5.87 (1H, d, *J* = 7.8 Hz, H_{18}), 1.91 (3H, s, H_{16}), 1.76 (3H, s, H_{23}).

^{13}C NMR (126 MHz, CD_3CN) δ: 159.5 (C_{32}), 158.8 (C_{24}), 158.1 (C_9), 155.7 (C_8), 154.7 (C_1), 154.1 (C_{25}), 152.7 (C_4), 152.5 (C_{28}), 149.0 (C_{20}), 147.5 (C_{10}), 143.4 (C_{13}), 143.1 (C_{27}), 142.1 (C_{17}), 141.6 (C_6), 140.9 (C_{30}), 139.1 (C_{14}), 138.9 (C_3), 138.7 (C_{22}), 131.3 (C_{12}), 130.2 (C_{18}), 128.9 (C_{21}), 126.9 (C_{26}), 126.6 (C_{11}), 125.8 (C_{29}), 125.4 (C_2), 124.9 (C_5), 124.5 (C_{31}), 121.4 (C_7), 120.4 (C_{15}), 120.8 (q, *J* = 320.8 Hz, NTf_2), 114.6 (C_{19}), 19.9 (C_{16}), 19.7 (C_{23}).

^{19}F NMR (376 MHz, CD_3CN) δ: − 80.17.

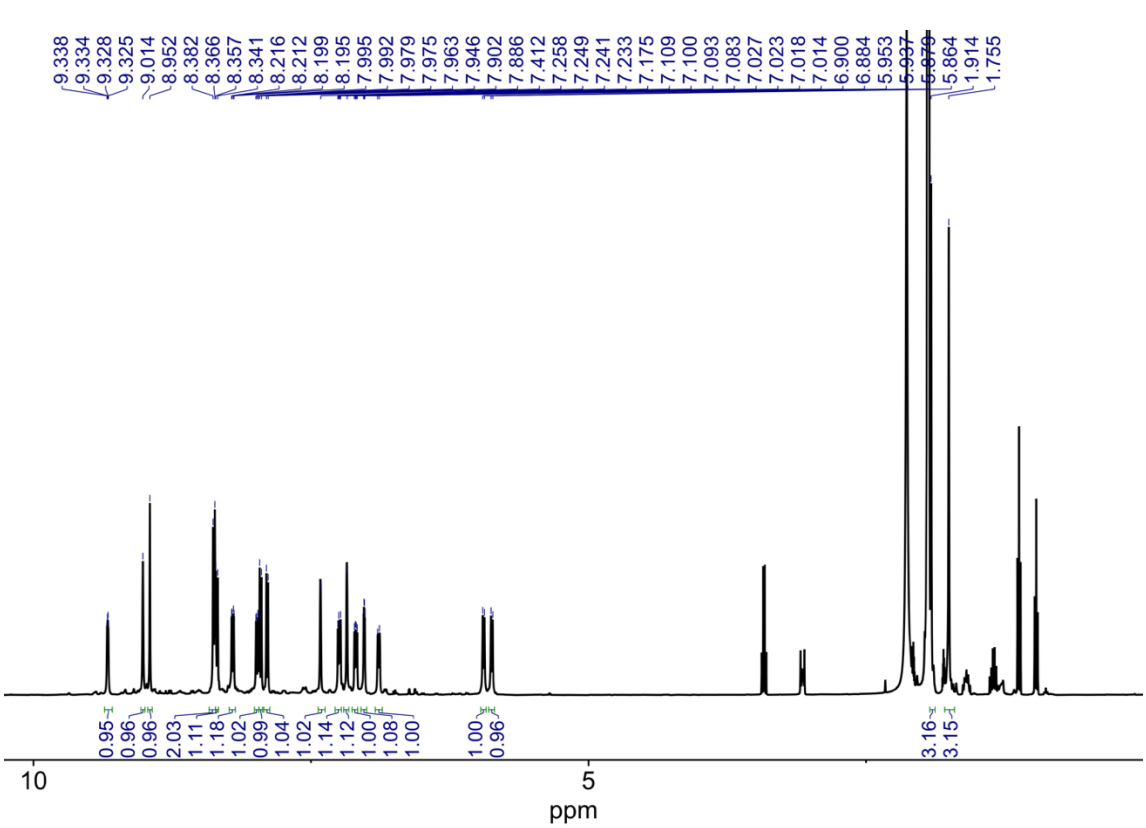

Figure S1: ^{1}H NMR spectrum (500 MHz, 298 K, CD_3CN) of **9**.

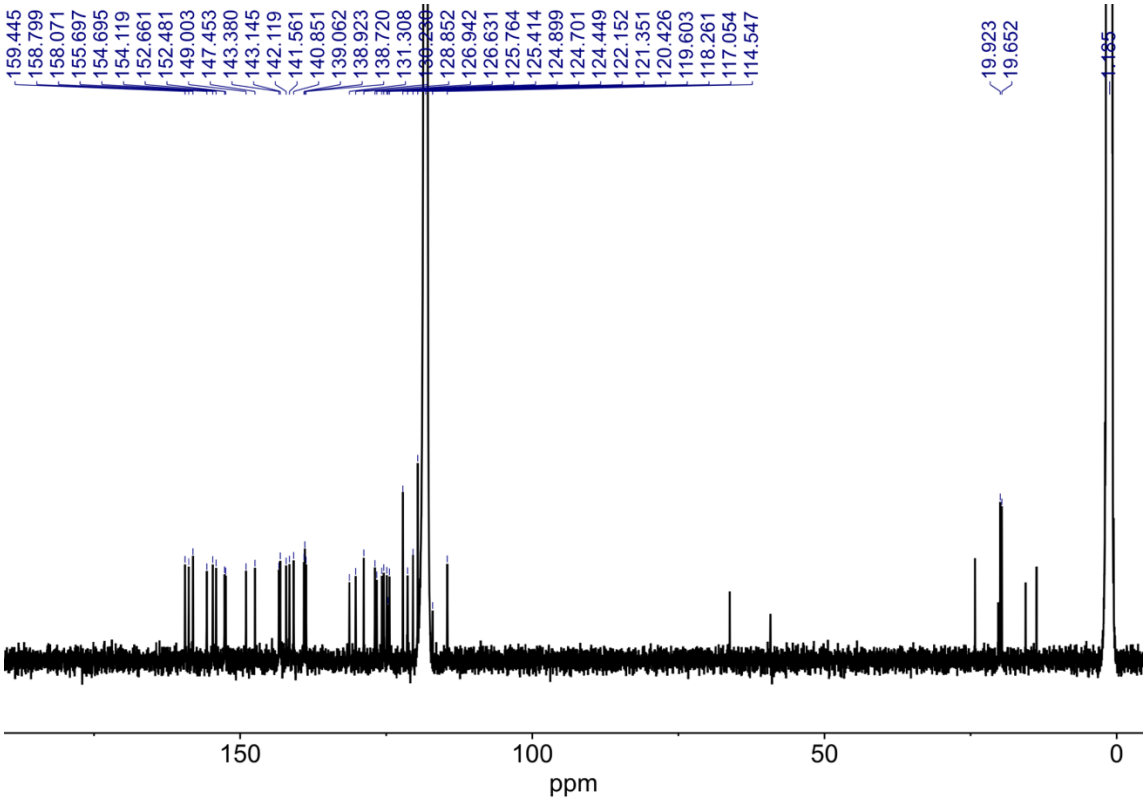

Figure S2: ^{13}C NMR spectrum (125 MHz, 298 K, CD_3CN) of **9**.

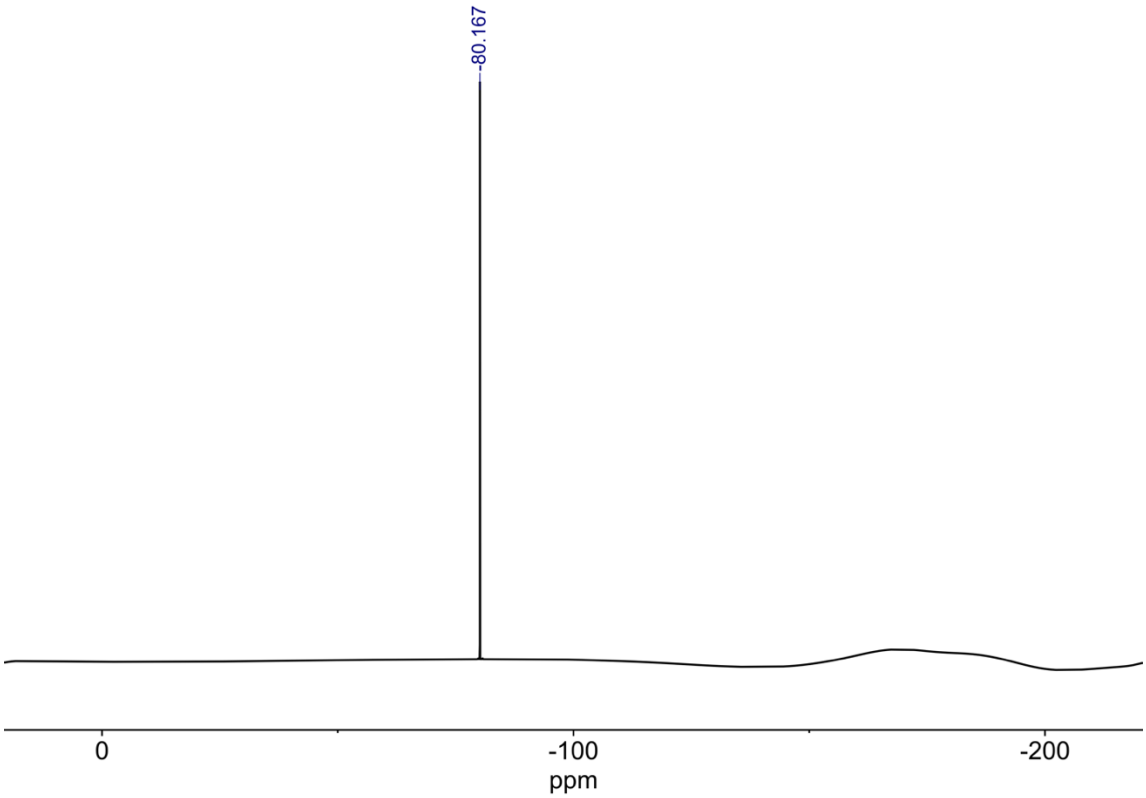

Figure S3: ^{19}F NMR spectrum (376 MHz, 298 K, CD_3CN) of **9**.

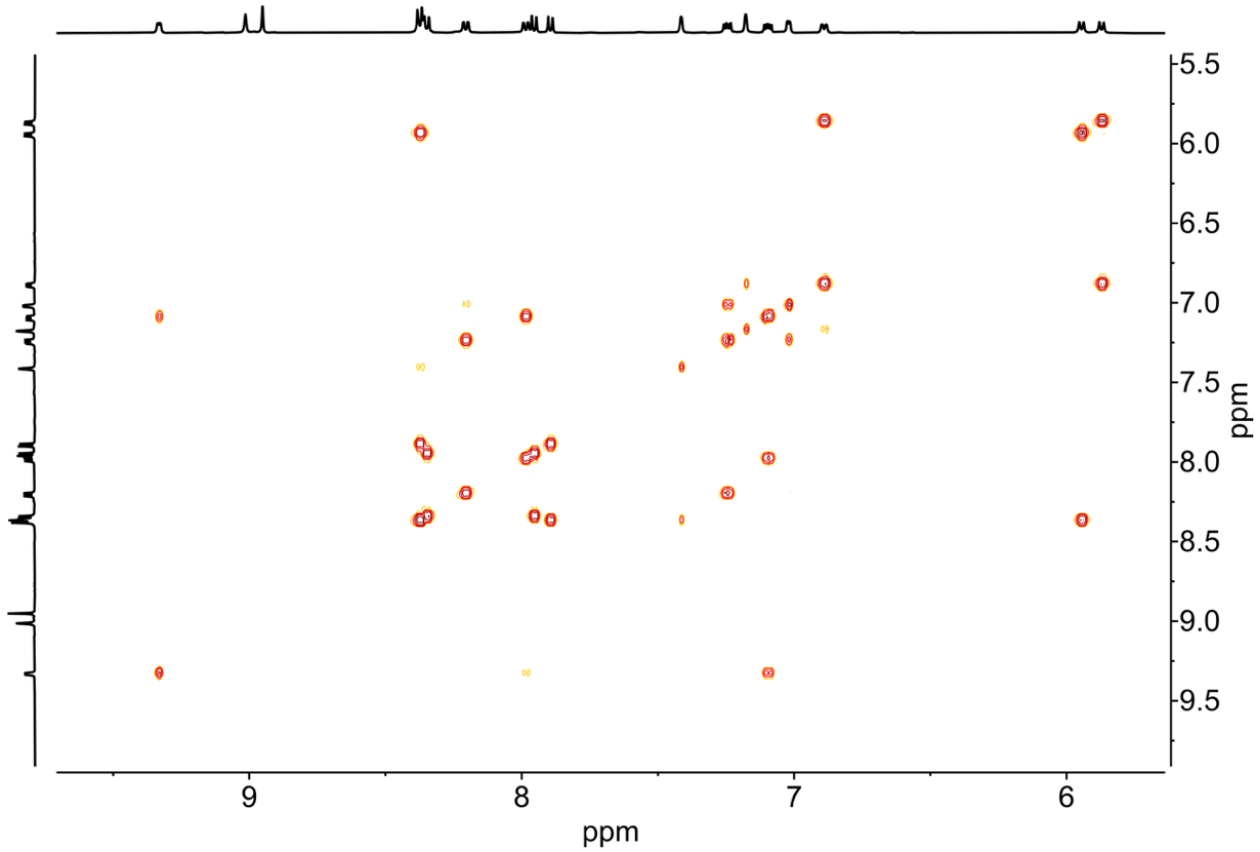

Figure S4: Aromatic region of the ^{1}H-^{1}H COSY NMR spectrum (500 MHz, 298 K, CD_3CN) of **9**.

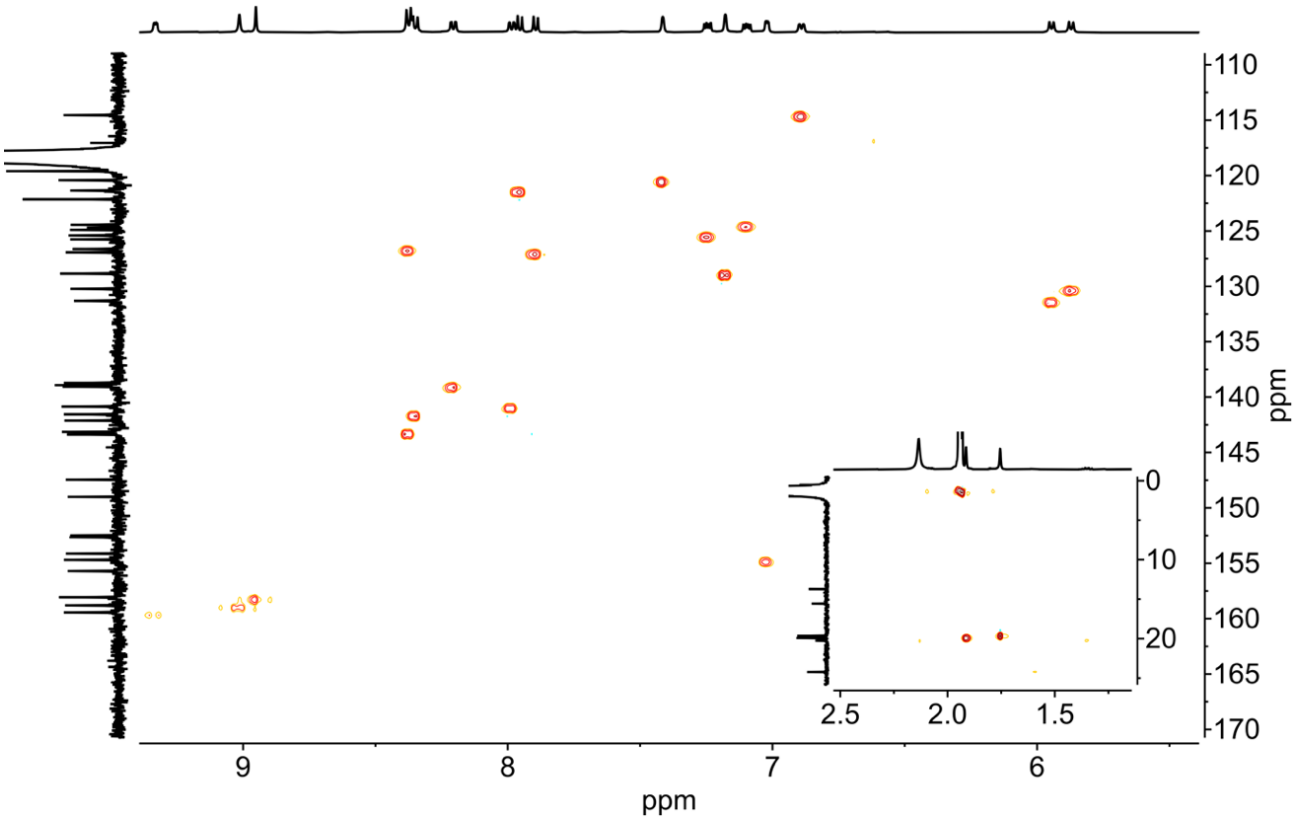

Figure S5: Aromatic region of the ^{1}H-^{13}C HSQC NMR spectrum (500 MHz, 298 K, CD_3CN) of **9**.

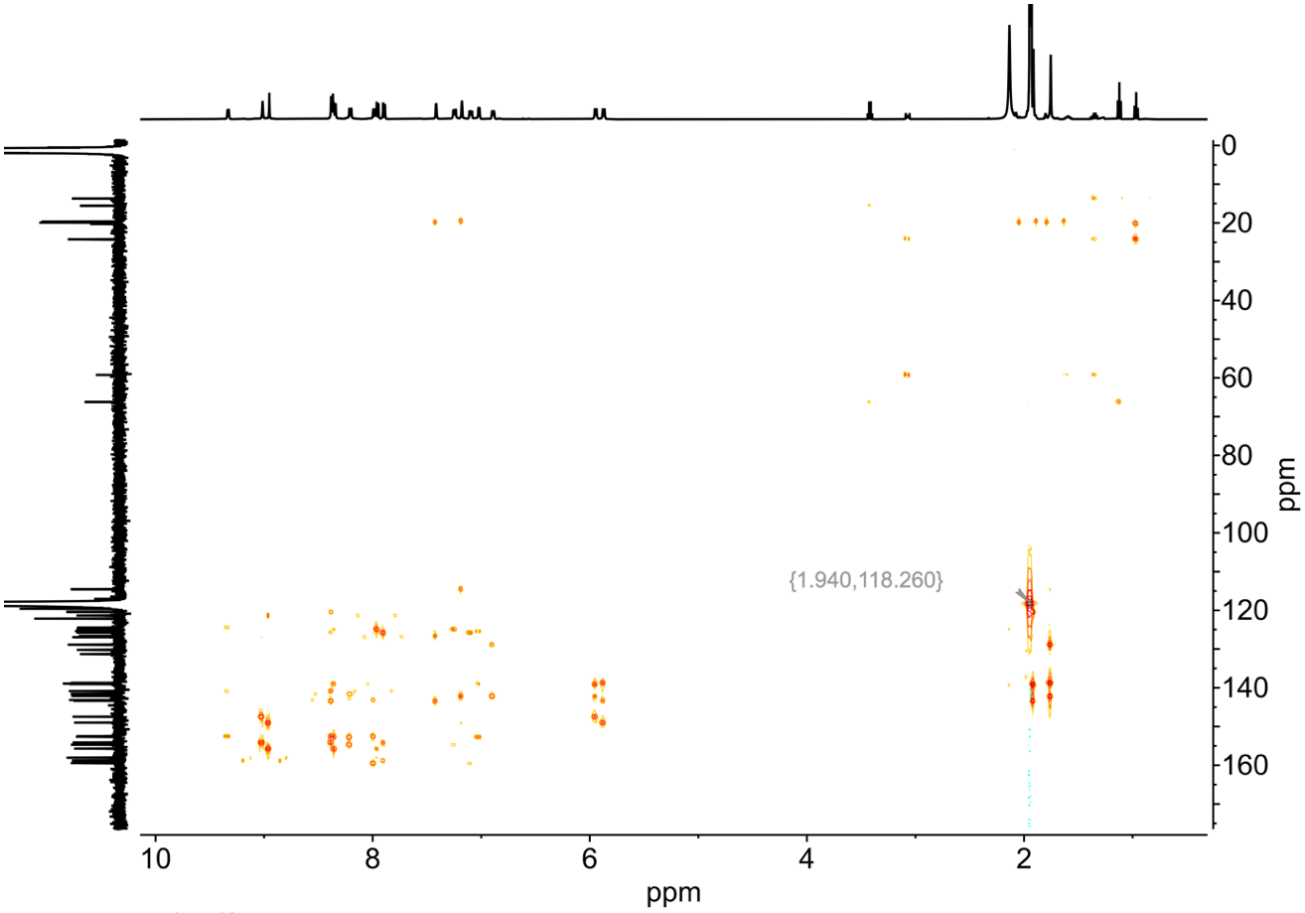

Figure S6: ^{1}H-^{13}C HMBC NMR spectrum (500 MHz, 298 K, CD_3CN) of **9**.

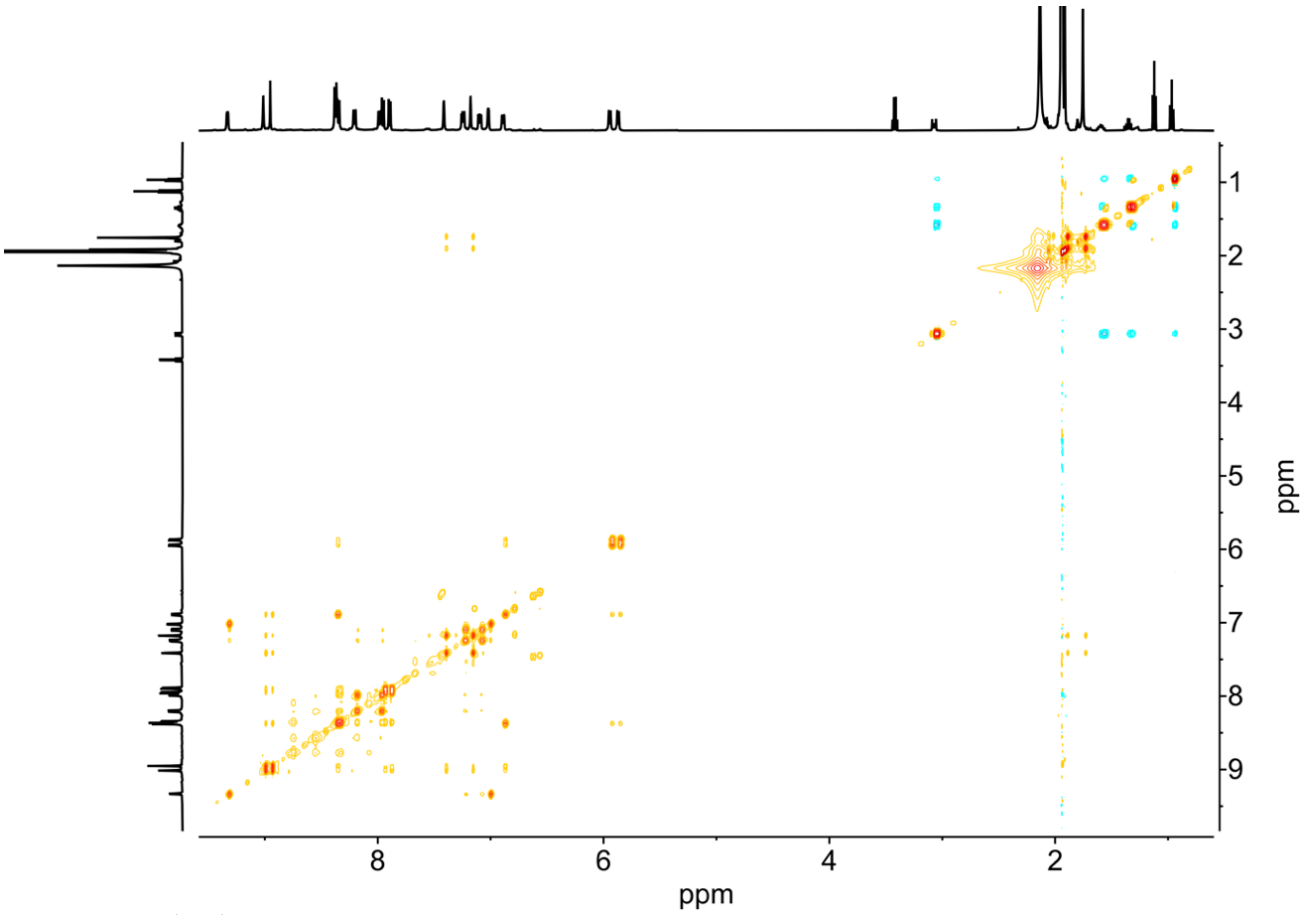

Figure S7: ^{1}H-^{1}H NOESY NMR spectrum (500 MHz, 298 K, CD_3CN) of **9**.

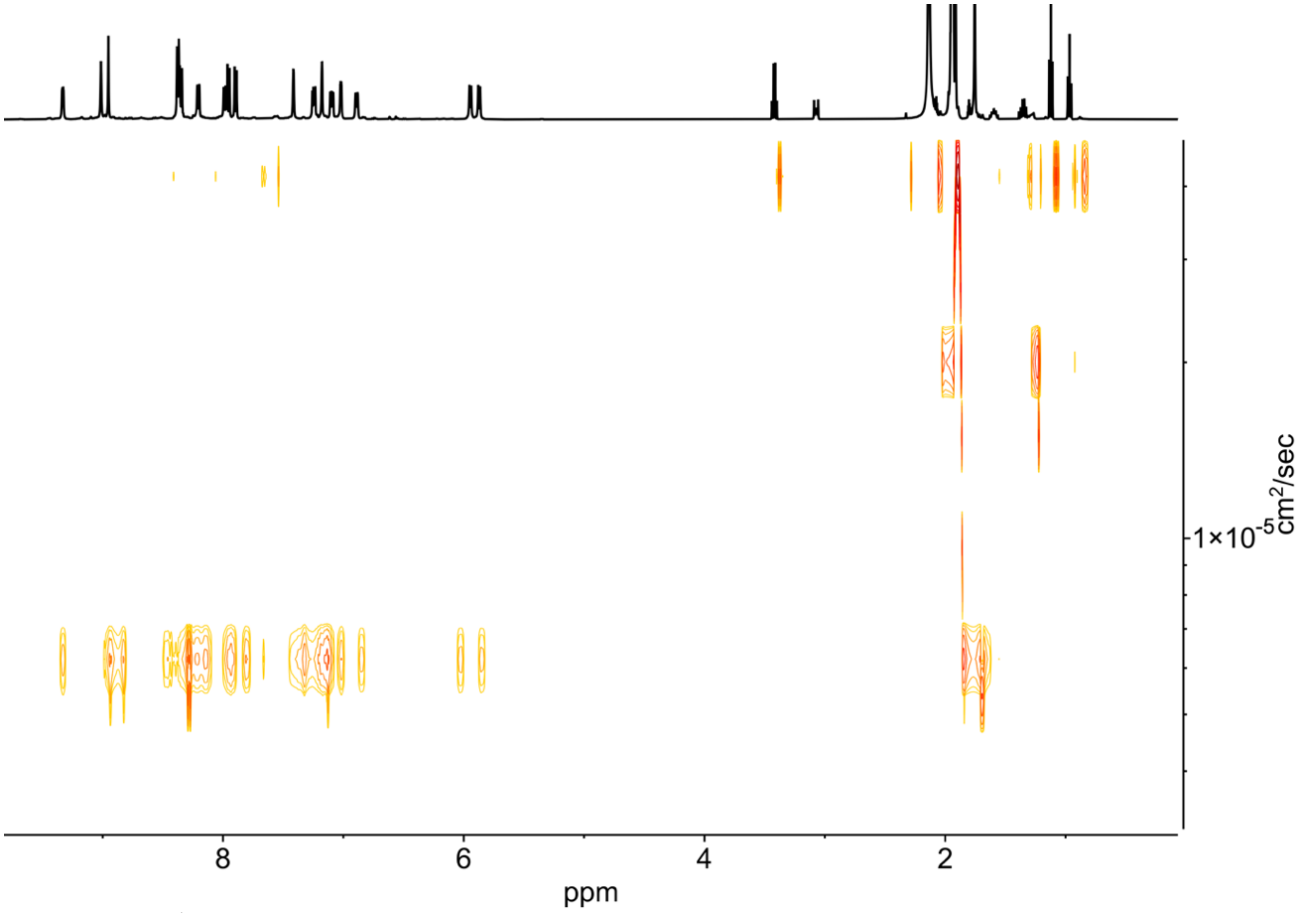

Figure S8: ^{1}H DOSY NMR spectrum (400 MHz, 298 K, CD_3CN) of **9**. The diffusion coefficient of **9** was measured to be 5.56 x 10^{-6} cm^2 s^{-1}, giving a solvodynamic radius of 11.4 Å. This value is comparable to those measured from the crystal structure of **9** (24 to 16 Å along the various axes of the six-stranded helicate).

S4.2 Six-Stranded Helicate 10

To 2,2'-dimethyl-[1,1'-biphenyl]-4,4'-diamine (**3**) (5.4 mg, 0.025 mmol, 6 eq.), 2-formyl-1,8-naphthyridine (**1**) (8.0 mg, 0.051 mmol, 12 eq.), and silver triflimide (21.3 mg, 0.055 mmol, 12 eq.) was added a magnetic stirrer and acetonitrile (2.5 ml). The assembly was sonicated until a homogenous solution was formed. TMA sulfate (6.11 mg, 0.025 mmol, 6 eq.) was then added, and the assembly stirred for 6 hours. The assembly was filtered, concentrated to a fifth of the original volume, and diethyl ether was added until a pale yellow precipitate was formed. The precipitate was collected by centrifugation, washed with diethyl ether (3 x 10 mL), and dried under a stream of nitrogen. The solid product was then collected as a fine yellow powder (17.6 mg, 74%).

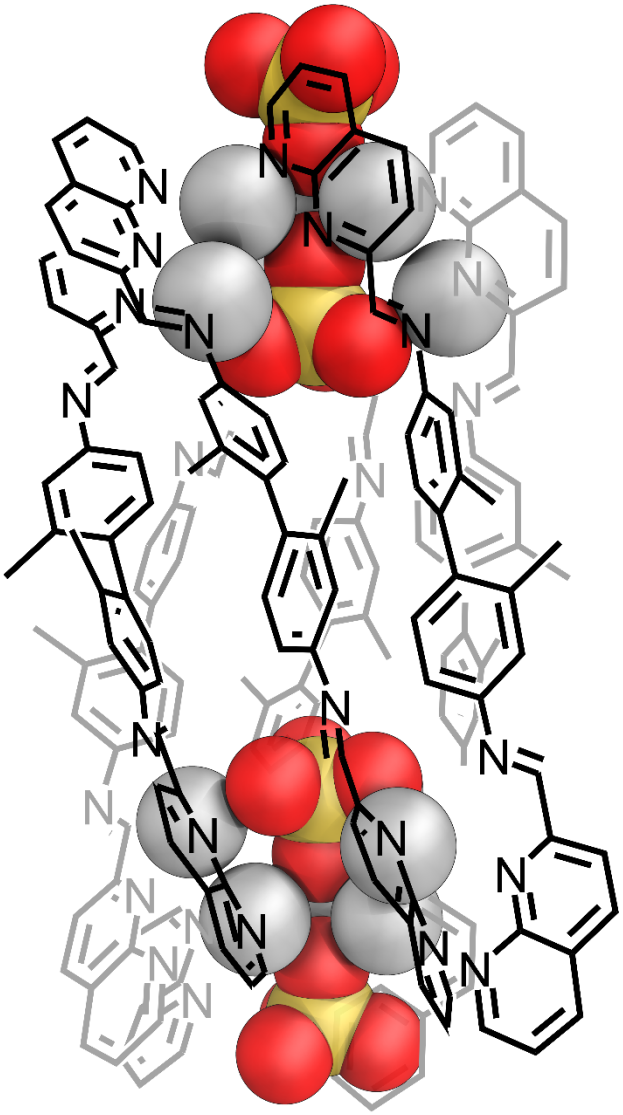

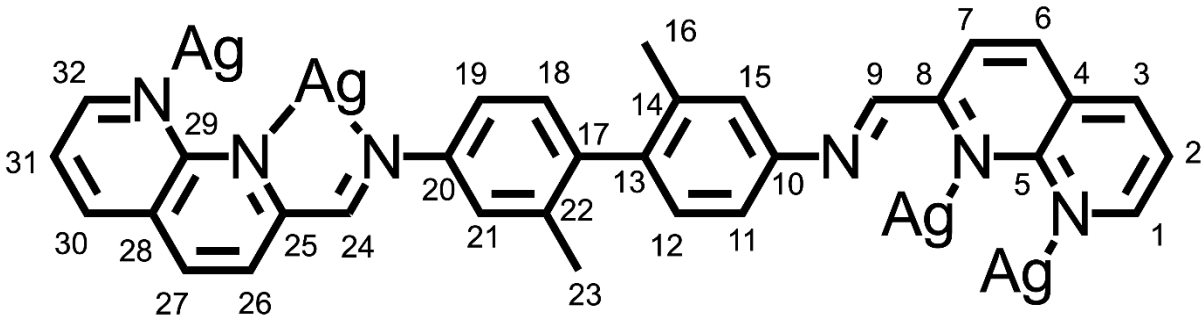

^{1}H NMR (500 MHz, CD_3CN) δ: 9.77 (1H, s, H_1), 8.96 (1H, s, H_9), 8.72 – 8.68 (2H, m, H_{24} + H_{31}), 8.49 – 8.46 (2H, m, H_6 + H_{27}), 8.18 (1H, s, H_{19}), 8.09 (1H, s, H_{32}), 8.02 (1H, s, H_3), 7.79 (1H, s, H_{30}), 7.75 – 7.71 (1H, s, H_7 + H_{11}), 7.44 (1H, s, H_{26}), 7.36 (1H, s, H_2), 7.09 (1H, s, H_{21}), 7.00 (1H, s, H_{15}), 5.98 (1H, s, H_{18}), 5.76 (1H, s, H_{12}), 1.96 (1H, s, H_{23}), 1.80 (1H, s, H_{16}).

^{13}C NMR (125 MHz, CD_3CN) δ: 160.8 (C_{32}), 159.4, 158.8 (C_{24}), 158.8 (C_1), 158.0 (C_9), 154.3, 153.9, 151.9, 149.2, 147.8, 143.2 (C_{31}), 143.0, 142.5 (C_3), 141.3, 140.9 (C_6 or C_{27}), 140.0 (C_6 or C_{27}), 138.5, 137.9, 132.1 (C_{18}), 130.9 (C_{12}), 129.9 (C_{15}), 129.2, 127.4 (C_{30}), 127.1, 126.7, 126.3, 125.7 (C_7), 125.5, 125.2 (C_{26}), 124.7, 120.8 (q, *J* = 320.8 Hz, NTf_2), 120.2 (C_2), 120.0 (C_{21}), 117.4 (C_{11}), 20.1 (C_{23}), 19.8 (C_{16}).

^{19}F NMR (376 MHz, CD_3CN) δ: − 80.21.

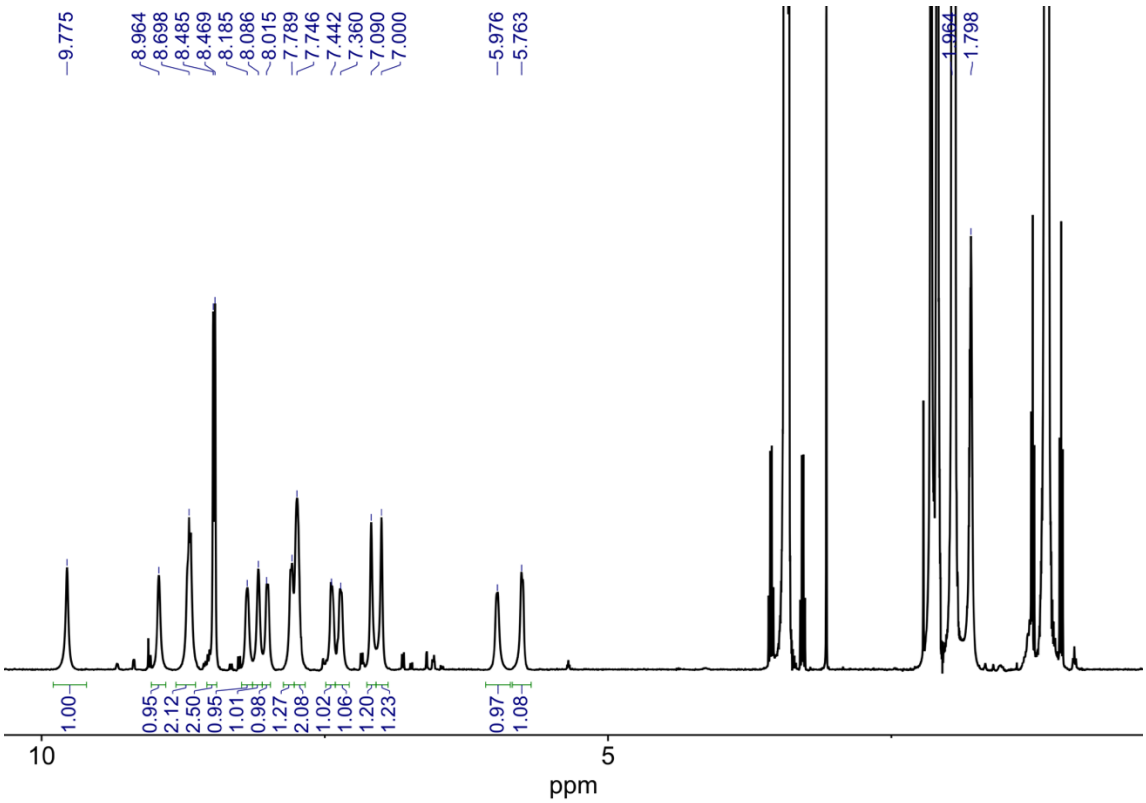

Figure S9: ^{1}H NMR spectrum (500 MHz, 298 K, CD_3CN) of **10**. The peaks at c. 6 ppm are indicative of significant π-stacking in this structure, as compared to **5** and **6**.

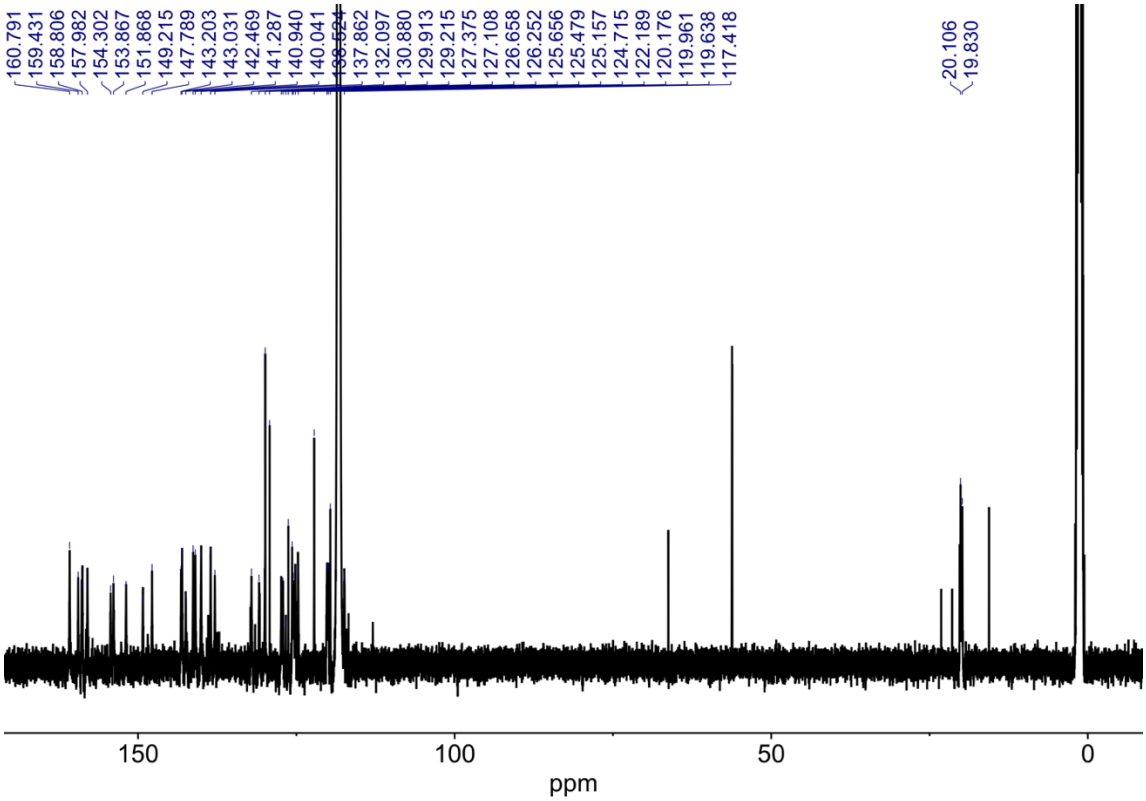

Figure S10: ^{13}C NMR spectrum (125 MHz, 298 K, CD_3CN) of **10**.

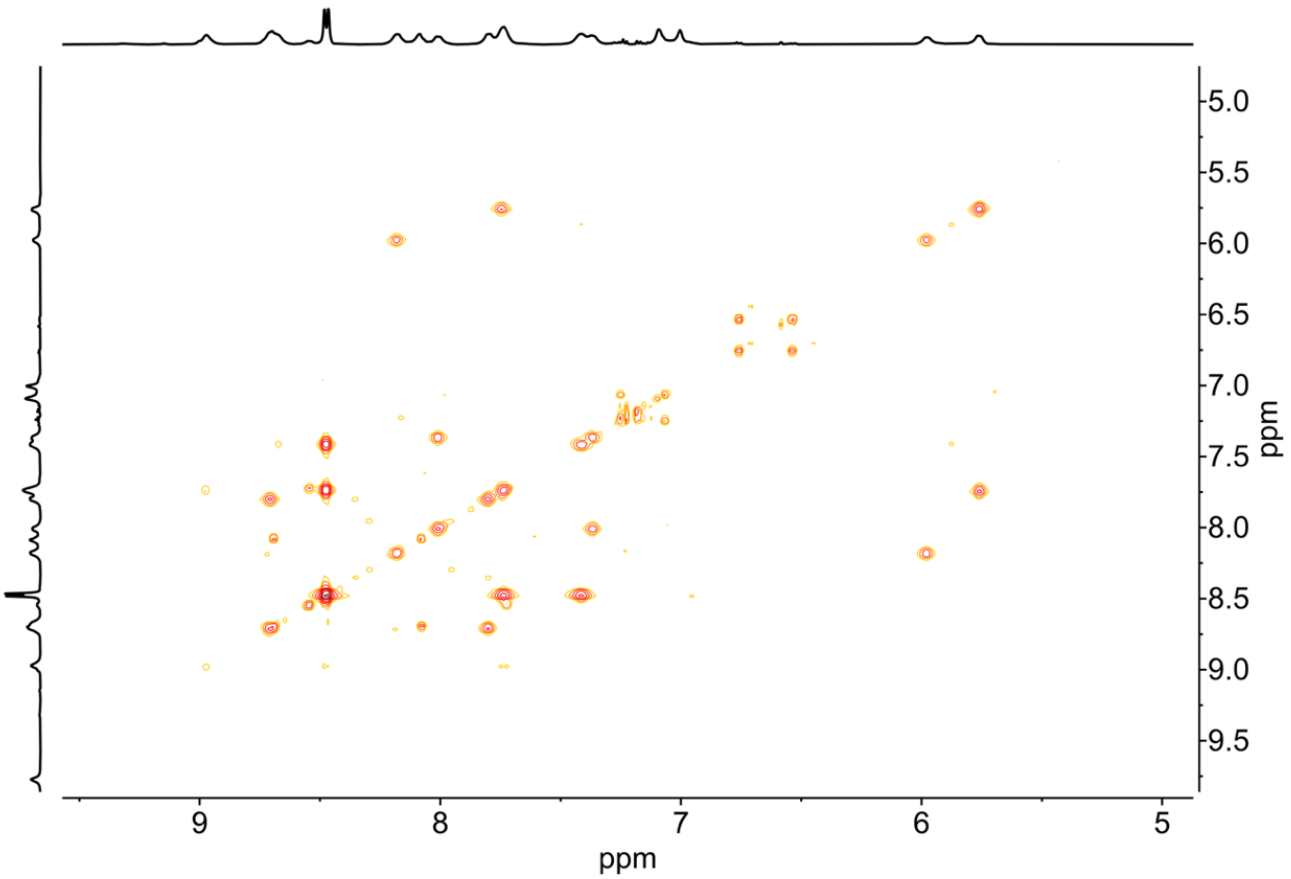

Figure S11: Aromatic region of the ^{1}H-^{1}H COSY NMR spectrum (500 MHz, 298 K, CD_3CN) of **10**.

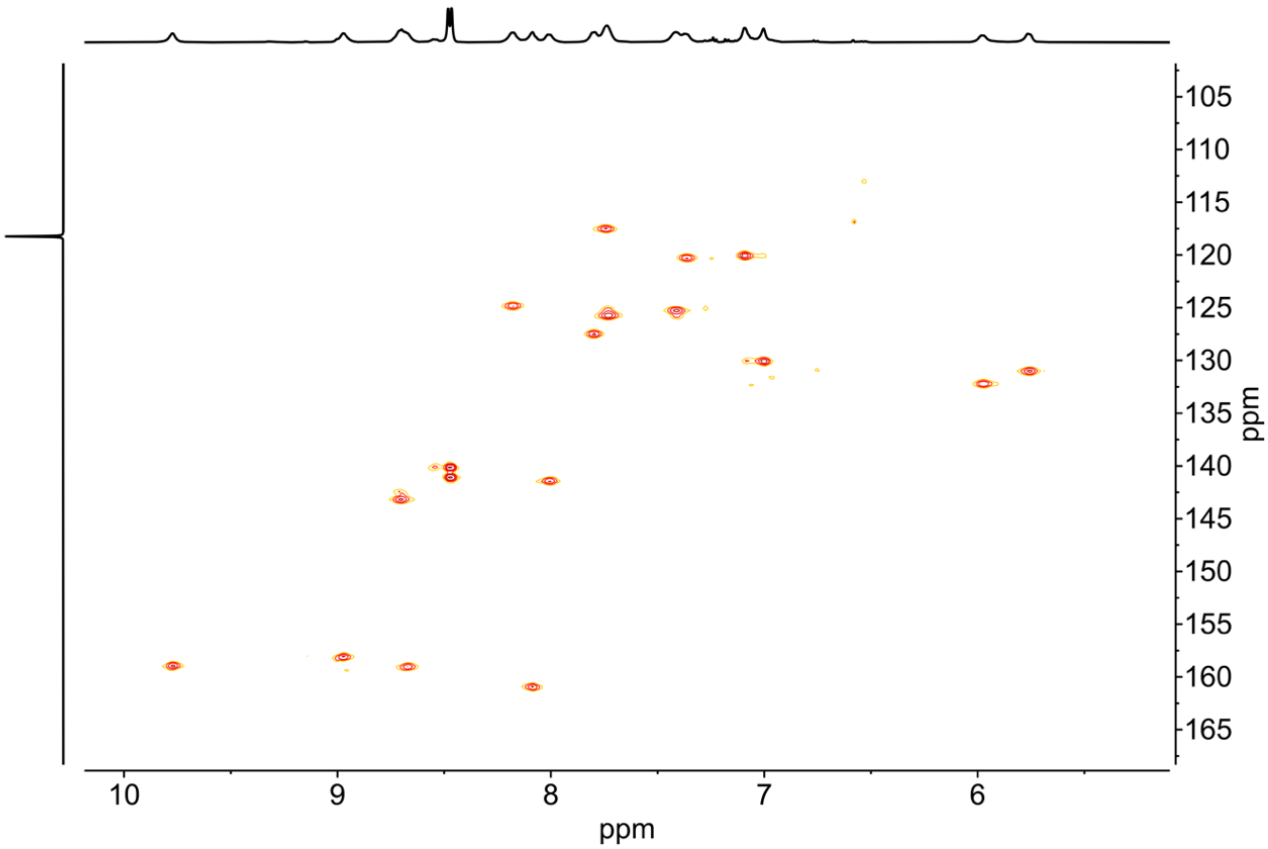

Figure S12: Aromatic region of the ^{1}H-^{13}C HSQC NMR spectrum (500 MHz, 298 K, CD_3CN) of **10**.

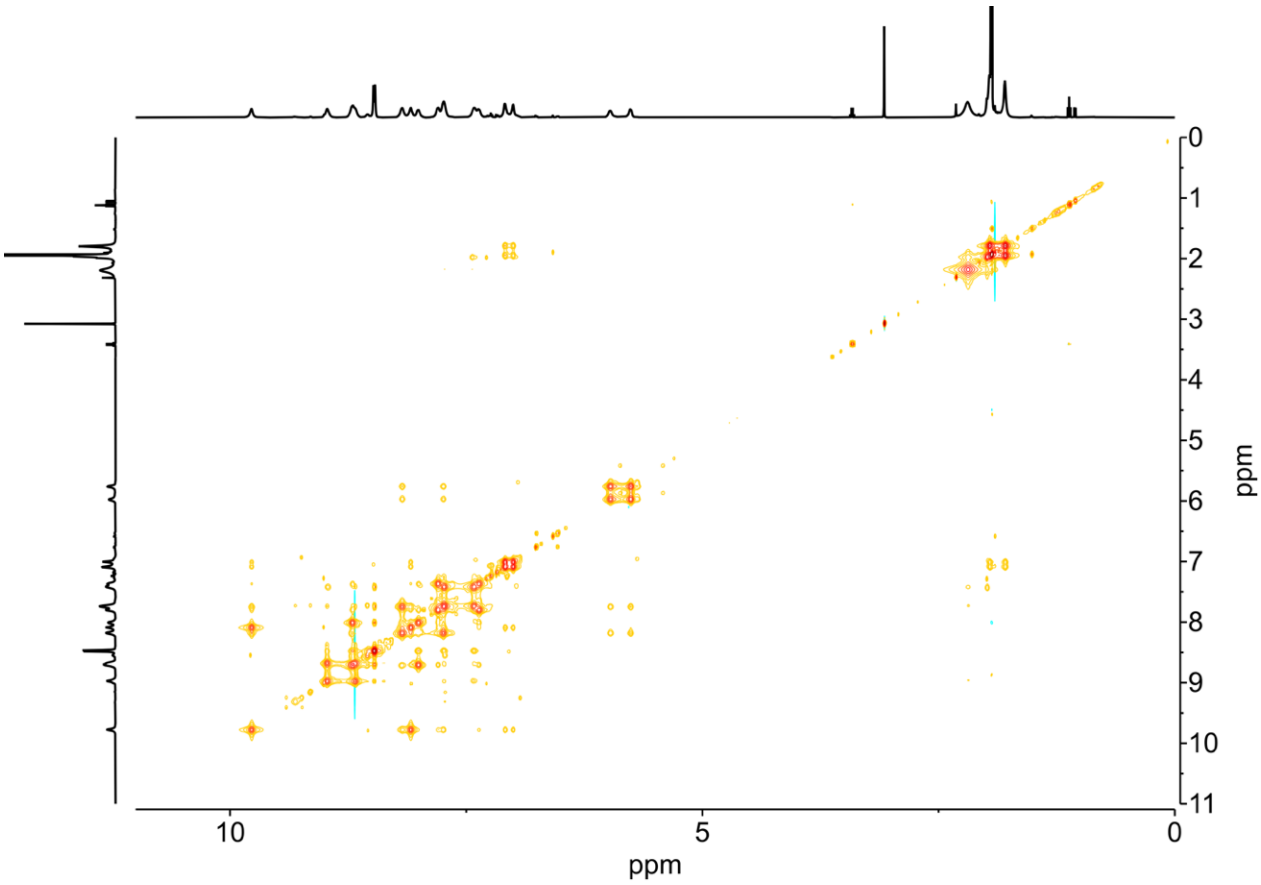

Figure S13: ^{1}H-^{1}H NOESY NMR spectrum (500 MHz, 298 K, CD_3CN) of **10**.

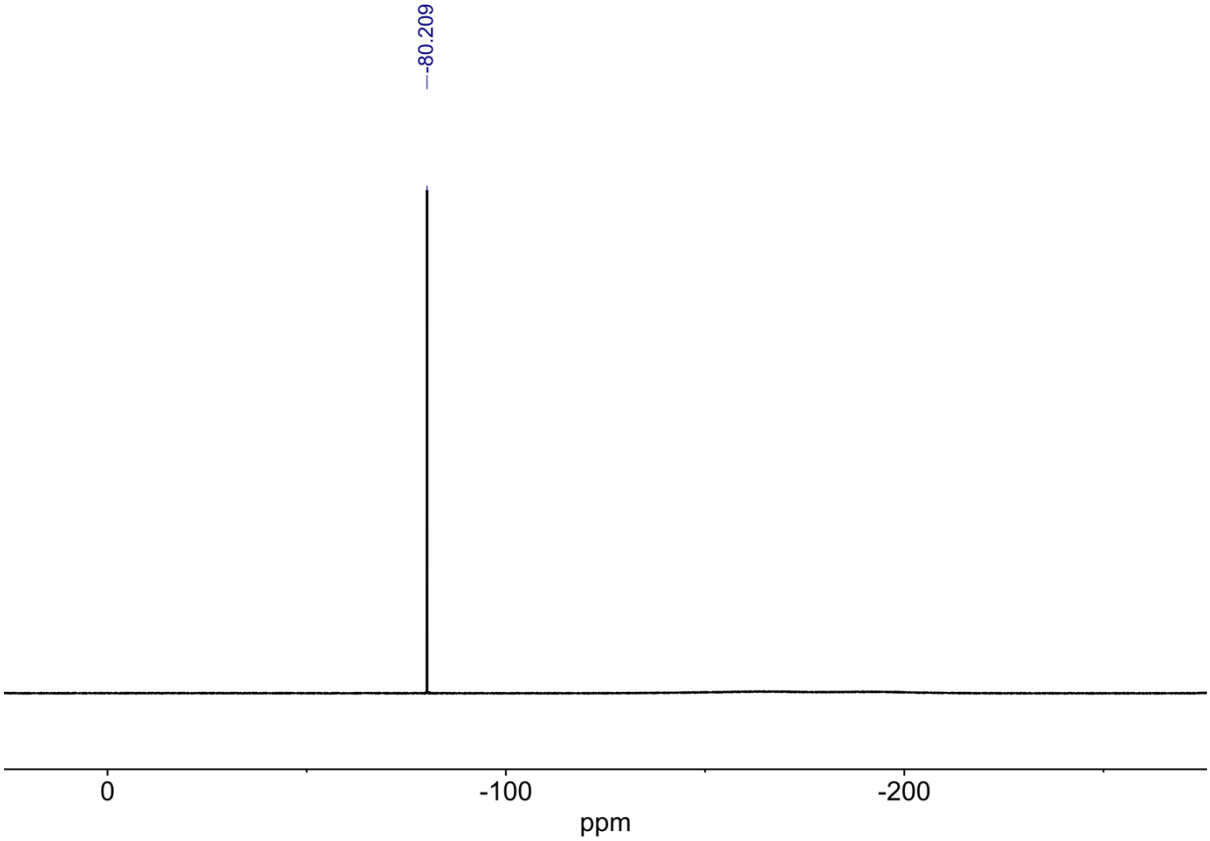

Figure S14: ^{19}F NMR spectrum (471 MHz, 298 K, CD_3CN) of **10**.

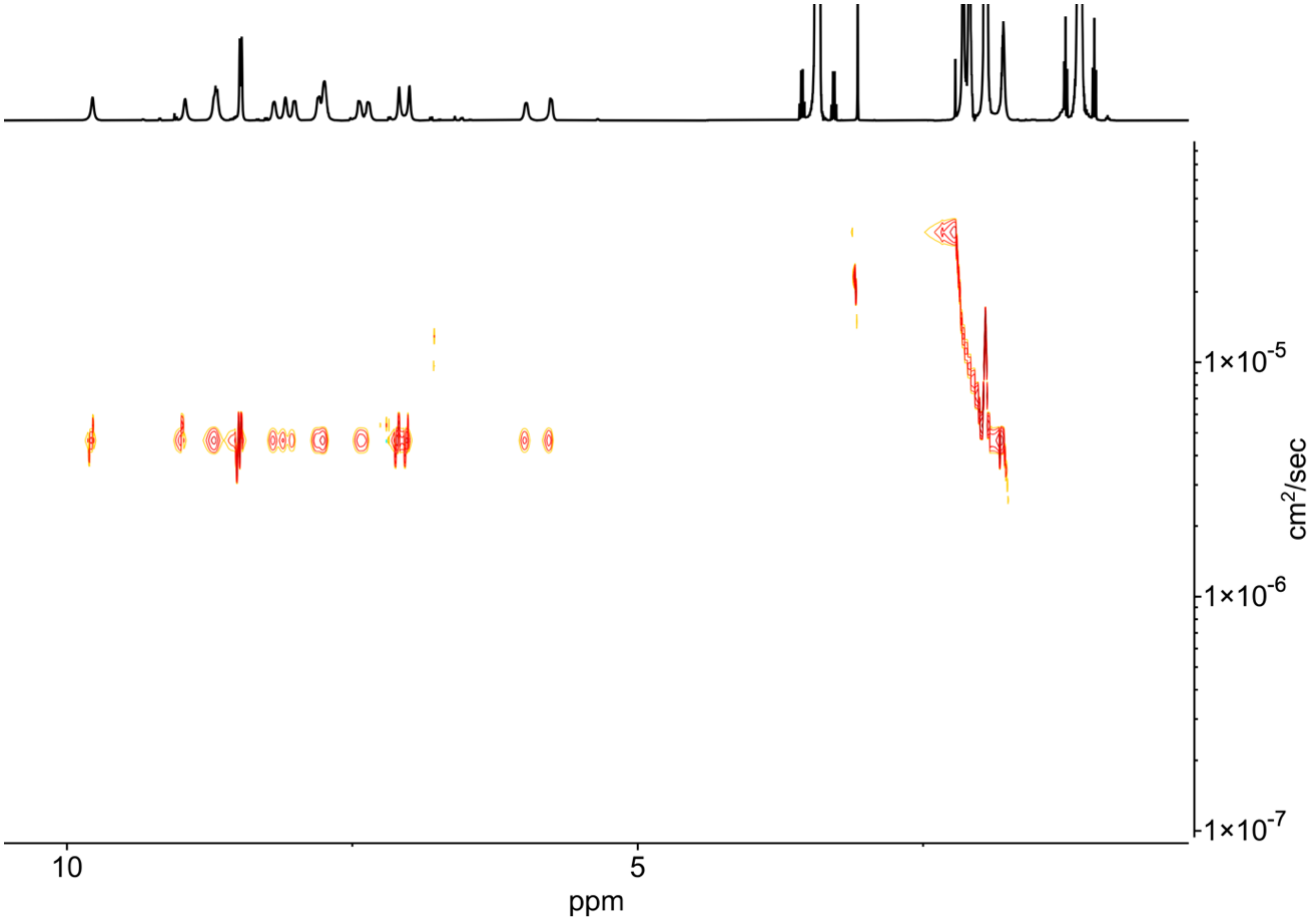

Figure S15: ^{1}H DOSY NMR spectrum (400 MHz, 298 K, CD_3CN) of **10**. The diffusion coefficient of **10** was measured to be 4.62 x 10^{-6} cm^2 s^{-1}, giving a solvodynamic radius of 13.8 Å. This value is comparable to those measured from the crystal structure of **10** (26 to 15 Å along the various axes of the six-stranded helicate).

S4.3 Six-Stranded Helicate 11

To 2,2'-dimethyl-[1,1'-biphenyl]-4,4'-diamine (**3**) (5.4 mg, 0.025 mmol, 6 eq.), 2-formyl-1,8-naphthyridine (**1**) (8.0 mg, 0.051 mmol, 12 eq.), and silver triflimide (21.3 mg, 0.055 mmol, 12 eq.) was added a magnetic stirrer and acetonitrile (2.5 ml). The assembly was sonicated until a homogenous solution was formed. Potassium bromide (2.0 mg, 0.017 mmol, 4 eq.) was then added, and the assembly stirred for 5 minutes. The assembly was filtered, concentrated to a fifth of the original volume, and diethyl ether was added until a pale yellow precipitate was formed. The precipitate was collected by centrifugation, washed with diethyl ether (3 x 10 mL), and dried under a stream of nitrogen. The solid product was then collected as a fine yellow powder (15.4 mg, 65%).

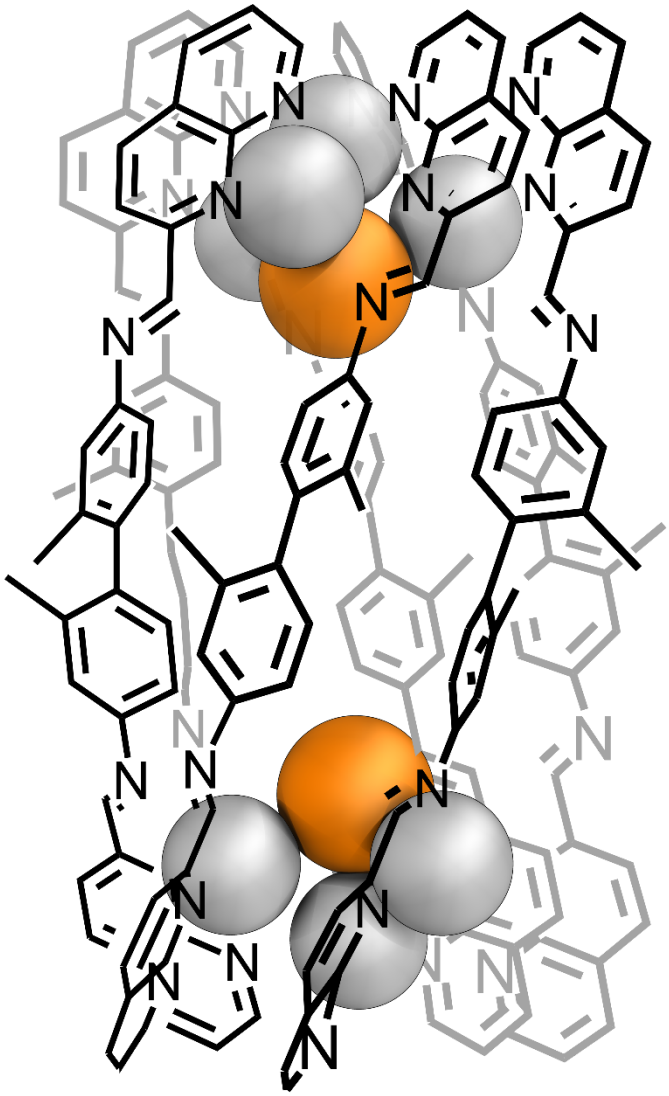

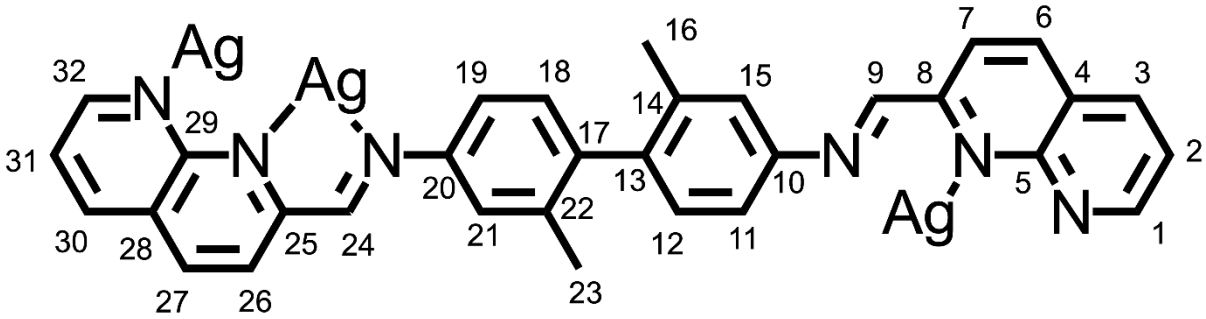

^{1}H NMR (500 MHz, CD_3CN) δ: 9.38 (1H, s, H_{32}), 8.98 (1H, s, H_{24}), 8.87 (1H, s, H_9), 8.35 – 8.30 (2H, m, H_6 + H_{27}), 8.26 (1H, s, H_{11}), 8.18 (1H, d, *J* = 7.6 Hz, H_3), 8.03 – 7.90 (1H, m, H_7 + H_{30}), 7.85 (1H, d, *J* = 7.2 Hz, H_{26}), 7.37 (1H, s, H_{15}), 7.21 (1H, s, H_2), 7.19 – 7.14 (2H, m, H_{21} + H_{31}), 7.06 (1H, s, H_1), 6.89 (1H, d, *J* = 6.3, H_{19}), 6.07 (1H, d, *J* = 6.3 Hz, H_{12}), 5.90 (1H, d, *J* = 7.2 Hz, H_{18}), 1.89 (3H, s, H_{16}), 1.74 (3H, s, H_{23}).

^{13}C NMR (126 MHz, CD_3CN) δ: 159.7 (C_{32}), 159.1 (C_{24}), 158.3 (C_9), 155.8 (C_8), 154.8 (C_1), 154.2 (C_{25}), 152.7 (C_4), 152.5 (C_{Ar}), 148.7 (C_{Ar}), 147.7 (C_{Ar}), 143.3 (C_{10}), 143.1 (C_{27}), 142.2 (C_{20}), 141.5 (C_6), 140.9 (C_{30}), 139.1 (C_{Ar}), 139.0 (C_3), 138.7 (C_{Ar}), 131.8 (C_{12}), 130.3 (C_{18}), 129.1 (C_{21}), 127.0 (C_{26}), 126.2 (C_{11}), 126.0 (C_{Ar}), 125.4 (C_2), 124.9 (C_{31}), 124.8 (C_{Ar}), 121.2 (C_7), 120.8 (q, J = 320.7 Hz, NTf_2), 120.6 (C_{15}), 114.7 (C_{19}), 19.9 (C_{16}), 19.7 (C_{23}).

^{19}F NMR (376 MHz, CD_3CN) δ: − 80.19.

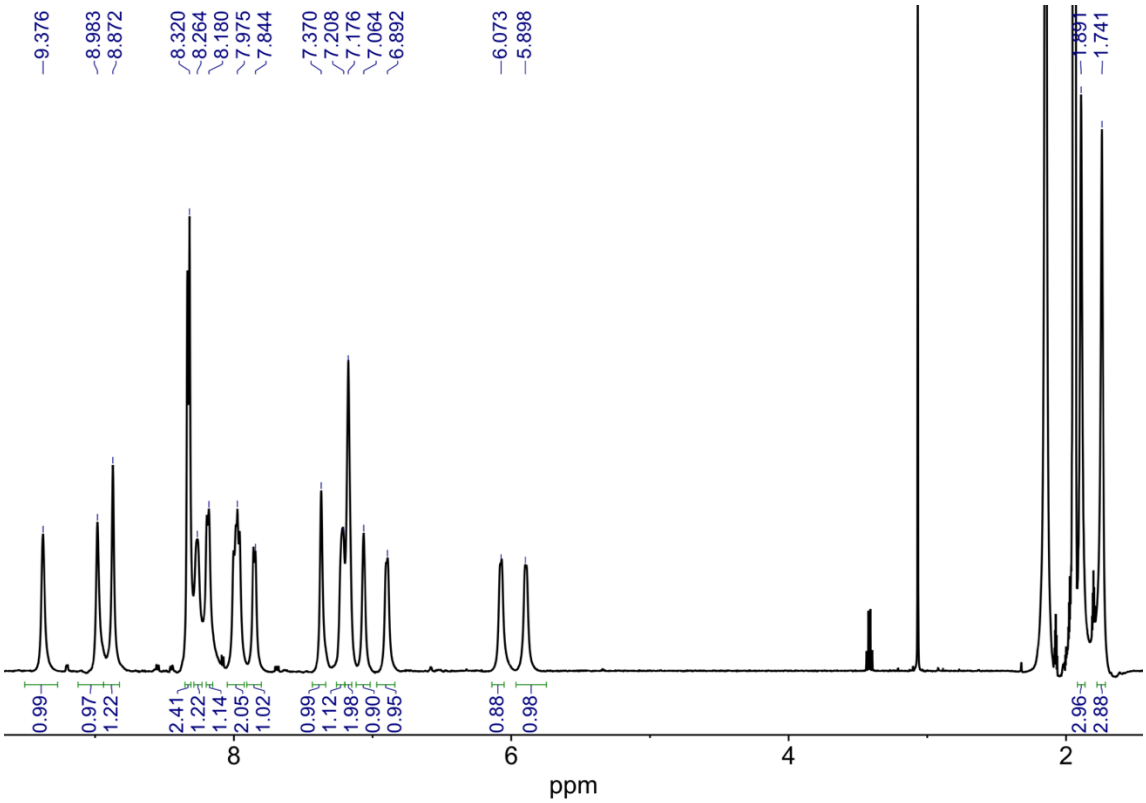

Figure S16: ^{1}H NMR spectrum (500 MHz, 298 K, CD_3CN) of **11**.

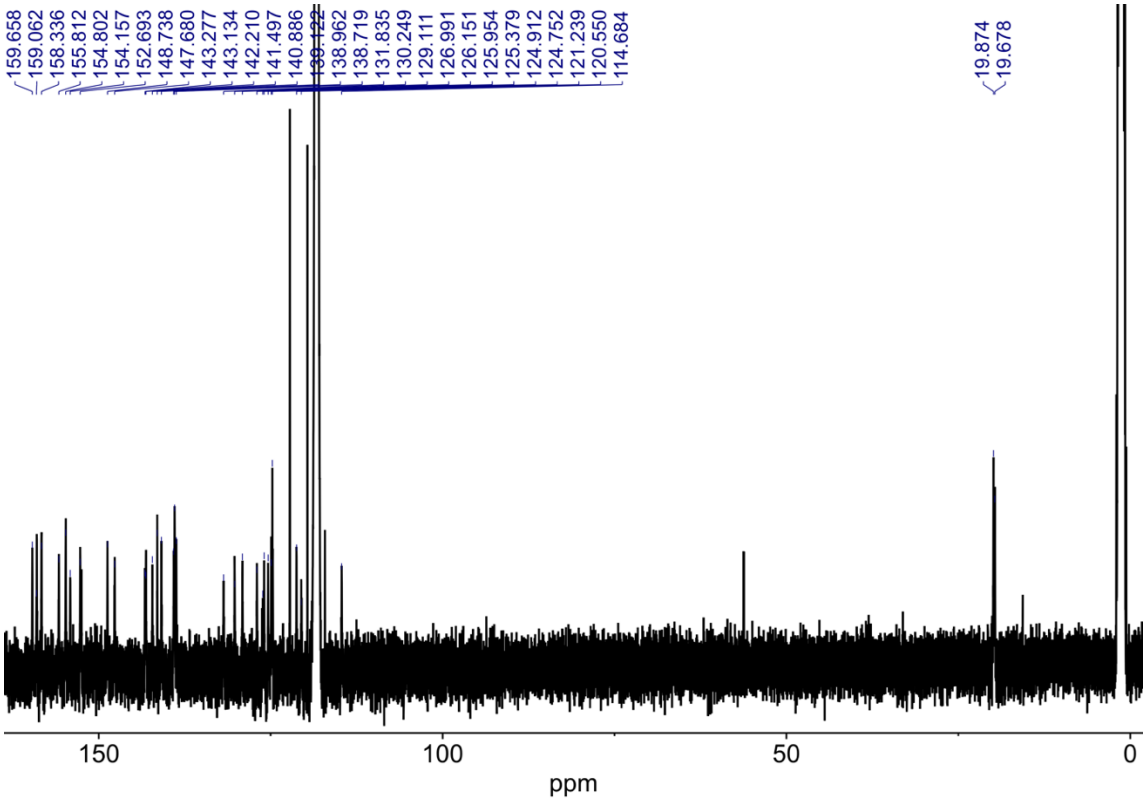

Figure S17: ^{13}C NMR spectrum (125 MHz, 298 K, CD_3CN) of **11**.

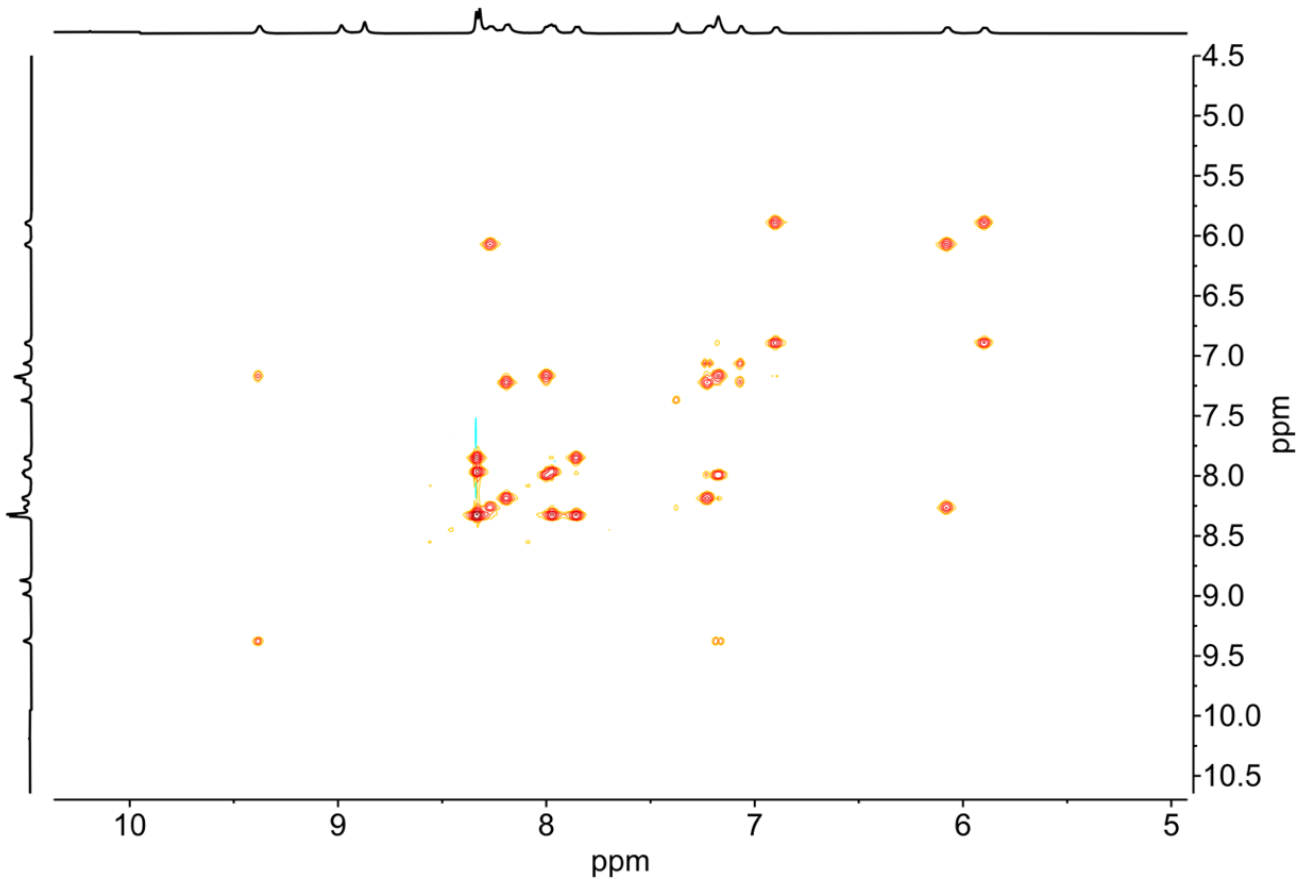

Figure S18: Aromatic region of the ^{1}H-^{1}H COSY NMR spectrum (500 MHz, 298 K, CD_3CN) of **11**.

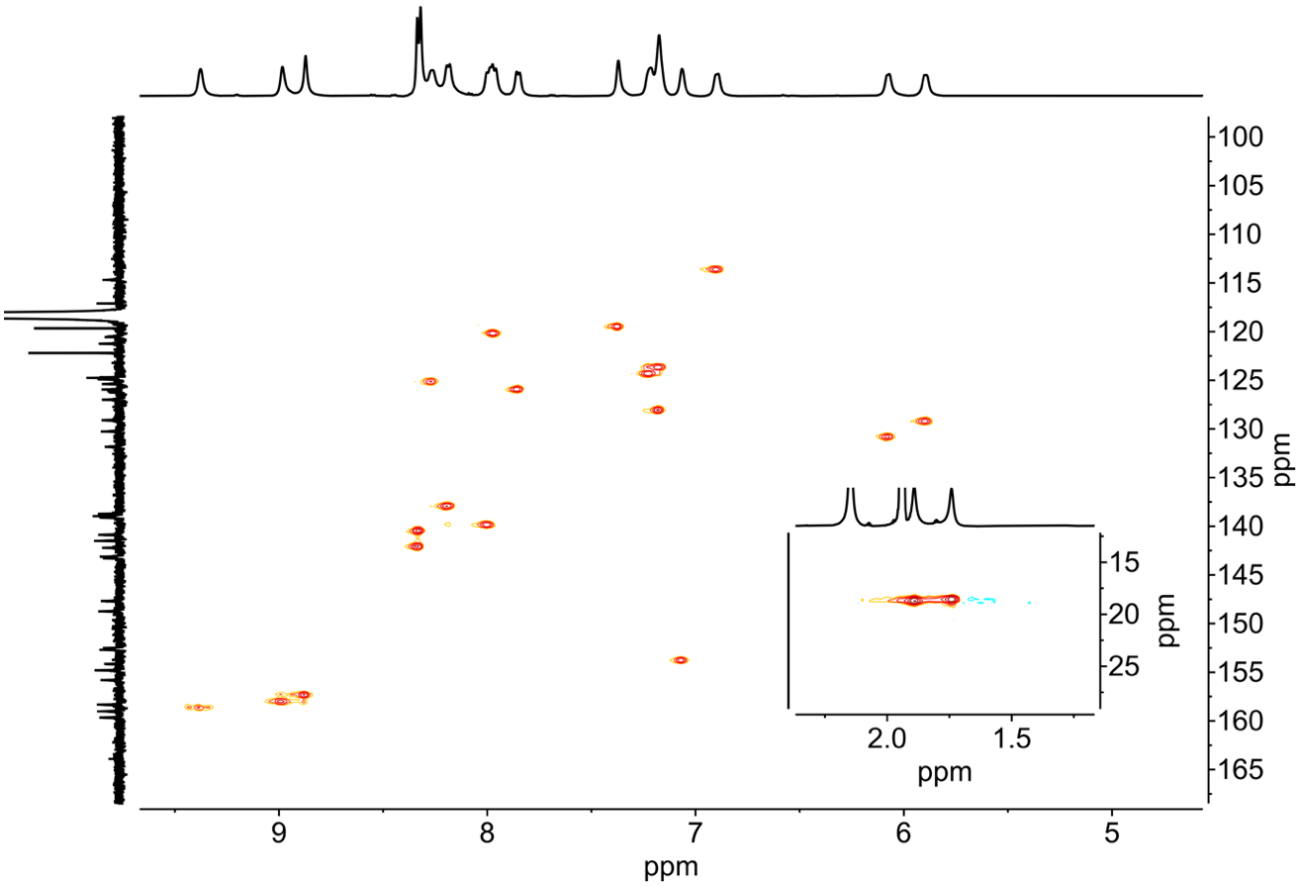

Figure S19: Aromatic region of the ^{1}H-^{13}C HSQC NMR spectrum (500 MHz, 298 K, CD_3CN) of **11**.

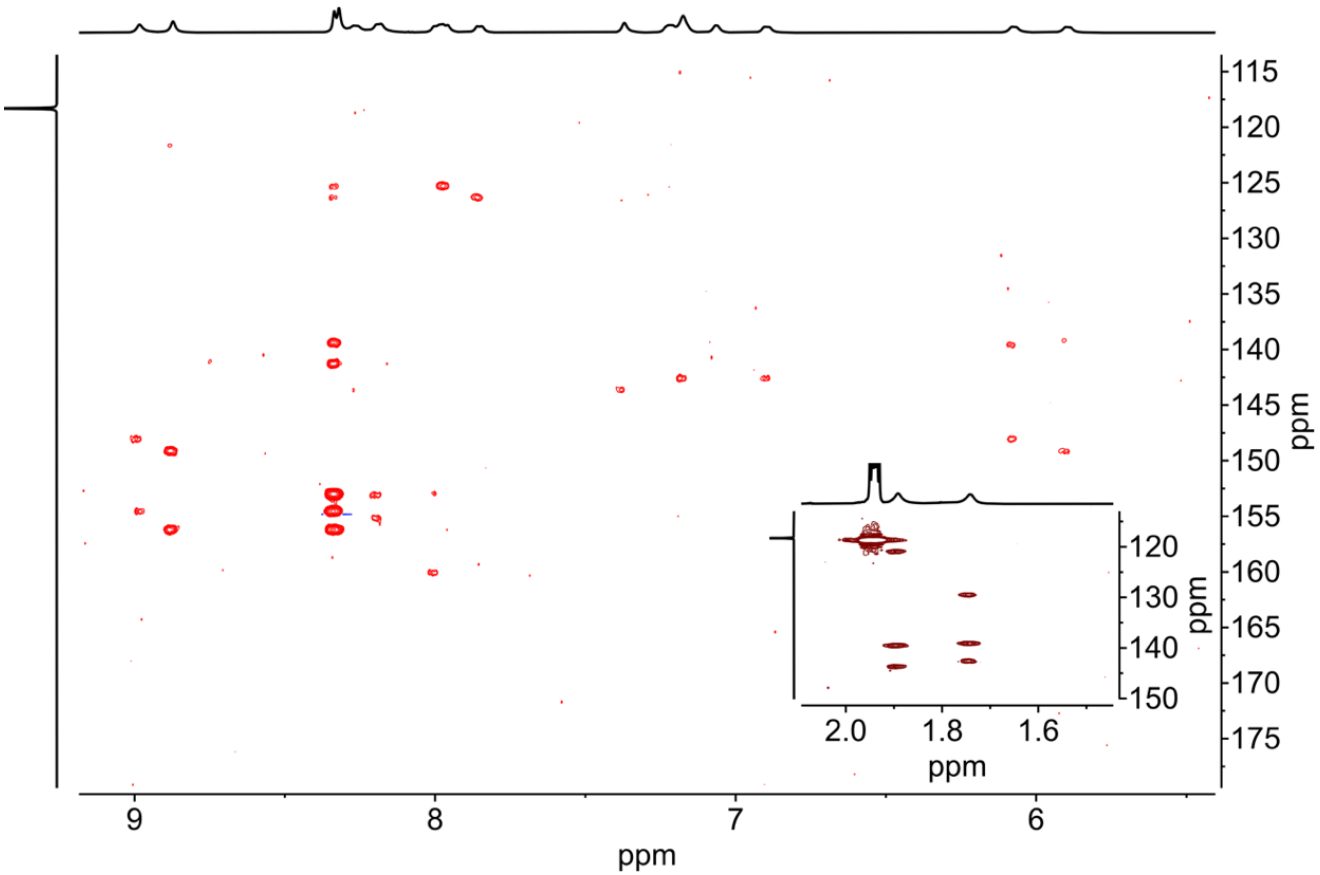

Figure S20: ^{1}H-^{13}C HMBC NMR spectrum (500 MHz, 298 K, CD_3CN) of **11**.

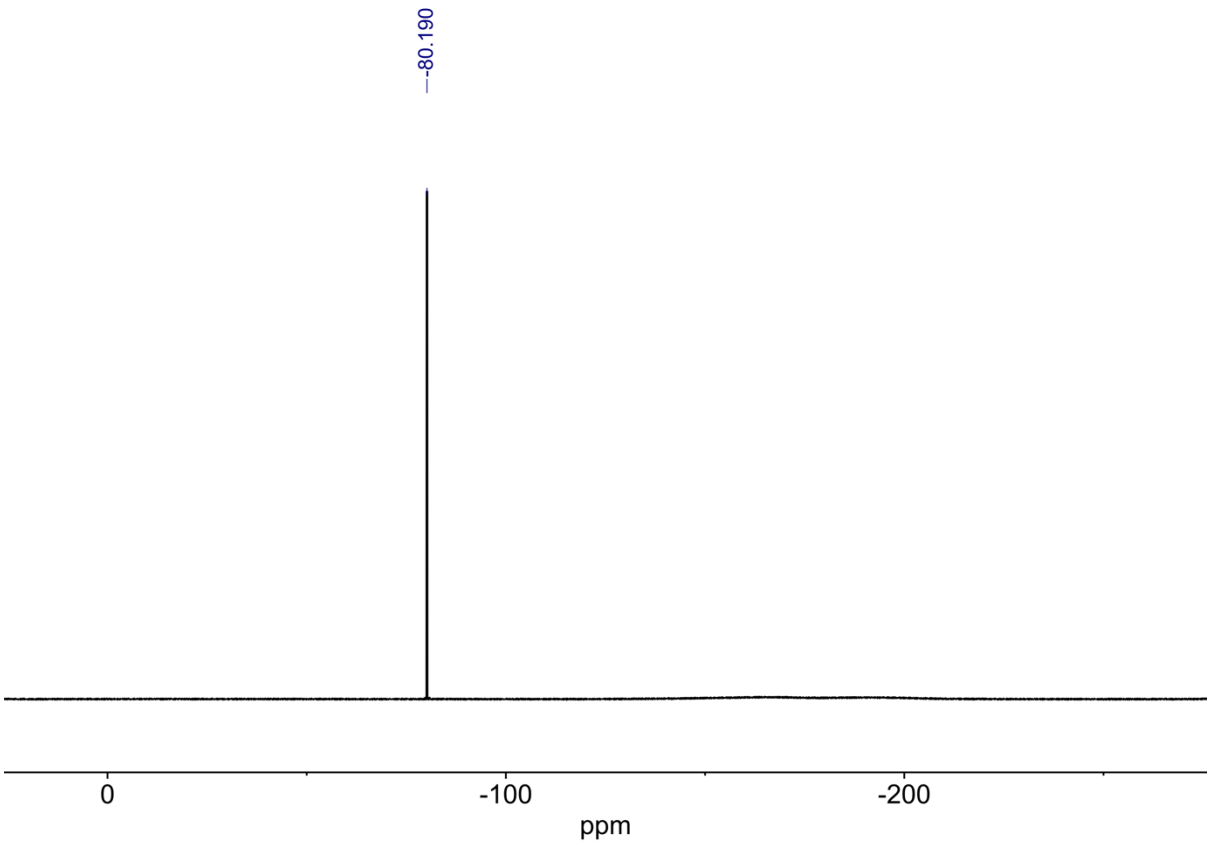

Figure S21: ^{19}F NMR spectrum (471 MHz, 298 K, CD_3CN) of **11**.

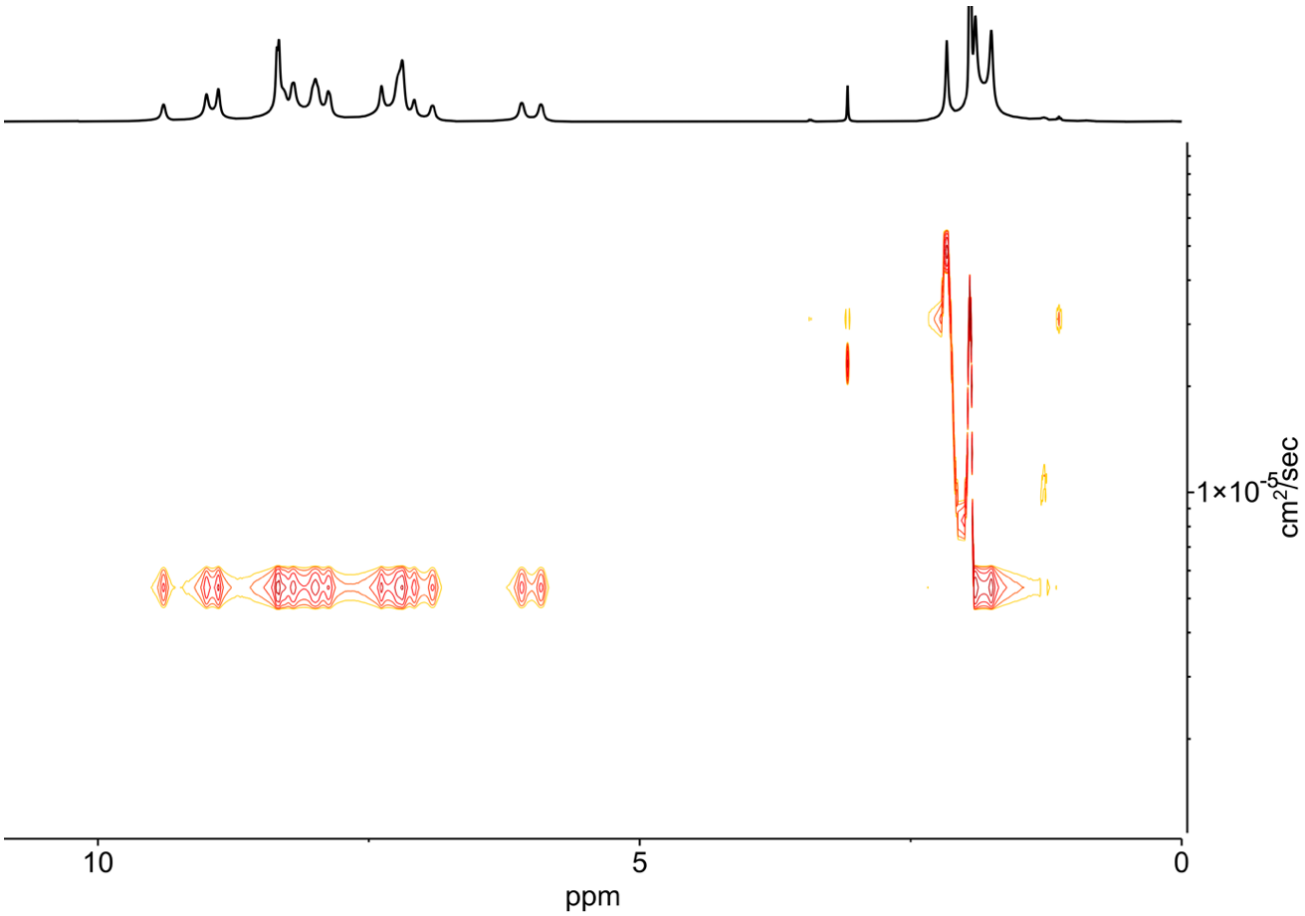

Figure S22: ^{1}H DOSY NMR spectrum (400 MHz, 298 K, CD_3CN) of **11**. The diffusion coefficient of **11** was measured to be 5.35 x 10^{-6} cm^2 s^{-1}, giving a solvodynamic radius of 11.9 Å. This value is comparable to those expected from the crystal structures of six-stranded helicates **9** and **10**.

S4.4 Tetrahedron 6 and helicate 5

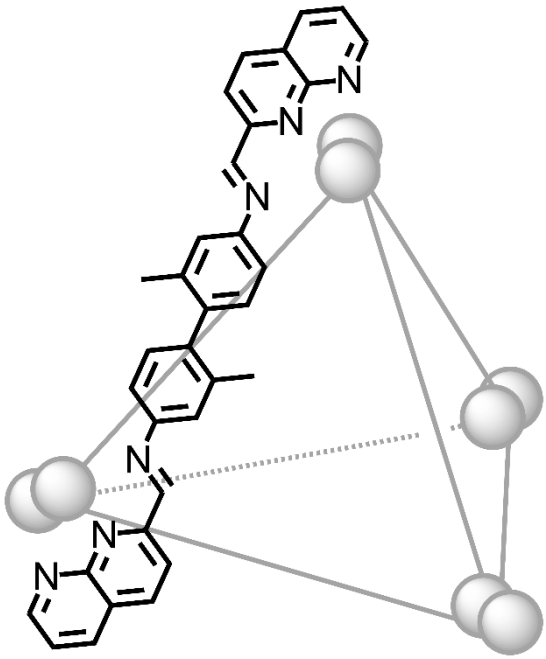

To 2,2'-dimethyl-[1,1'-biphenyl]-4,4'-diamine (**3**) (5.4 mg, 0.025 mmol, 6 eq.), 2-formyl-1,8-naphthyridine (**1**) (8.0 mg, 0.051 mmol, 12 eq.), and silver triflimide (21.3 mg, 0.055 mmol, 12 eq.) was added a magnetic stirrer and acetonitrile (2.5 ml). The assembly was sonicated until a homogenous solution was formed. This system could not be recovered after precipitation (insoluble polymers were formed) and so was analysed without further purification.

^{1}H NMR (500 MHz, CD_3CN) δ: 9.29 (1H, s, $H_{1\text{-tet}}$), 9.16 (1H, s, $H_{1\text{-hel}}$), 9.00 (1H, s, $H_{9\text{-hel}}$), 8.96 (1H, s, $H_{9\text{-tet}}$), 8.77 (1H, d, *J* = 8.2 Hz, $H_{6\text{-tet}}$), 8.69 (1H, d, *J* = 8.5 Hz, $H_{6\text{-hel}}$), 8.60 (1H, d, *J* = 7.9 Hz, $H_{3\text{-tet}}$), 8.56 (1H, d, *J* = 8.3 Hz, $H_{3\text{-hel}}$), 8.17 (1H, d, *J* = 8.1 Hz, $H_{7\text{-tet}}$), 8.05 (1H, d, *J* = 8.3 Hz, $H_{7\text{-hel}}$), 7.76 (1H, dd, *J* = 7.4, 3.3 Hz, H_2), 7.35 (1H, s, $H_{15\text{tet+hel}}$), 7.28 (1H, d, *J* = 7.4 Hz, $H_{11\text{-tet}}$), 7.20 (1H, d, *J* = 9.5 Hz, $H_{11\text{-hel}}$), 7.05 (1H, d, *J* = 8.1 Hz, $H_{12\text{-hel}}$), 6.97 (1H, d, *J* = 7.9 Hz, $H_{12\text{-tet}}$), 2.07 (3H, s, $H_{16\text{-hel}}$, extracted from HSQC), 1.94 (3H, s, $H_{16\text{-tet}}$, extracted from HSQC). Relative integrals are consistent within species, and the two species were observed in a 1:0.3 tetrahedron:helicate ratio.

^{13}C NMR (126 MHz, CD_3CN) δ: 159.0, 158.1, 158.0, 157.9, 157.4, 157.4, 154.1, 153.9, 147.6, 147.2, 144.4, 142.8, 142.3, 141.5, 139.8, 139.7, 139.3, 138.6, 137.3, 132.4, 131.6, 130.9, 126.8, 126.5, 125.6, 125.5, 124.9, 120.9 (q, *J* = 319 Hz), 120.5, 117.2, 113.4, 20.3, 20.2.

^{19}F NMR (376 MHz, CD_3CN) δ: − 80.16.

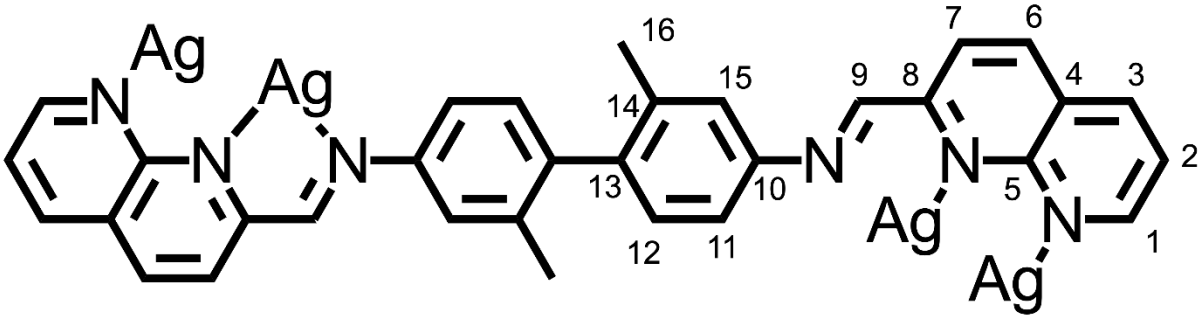

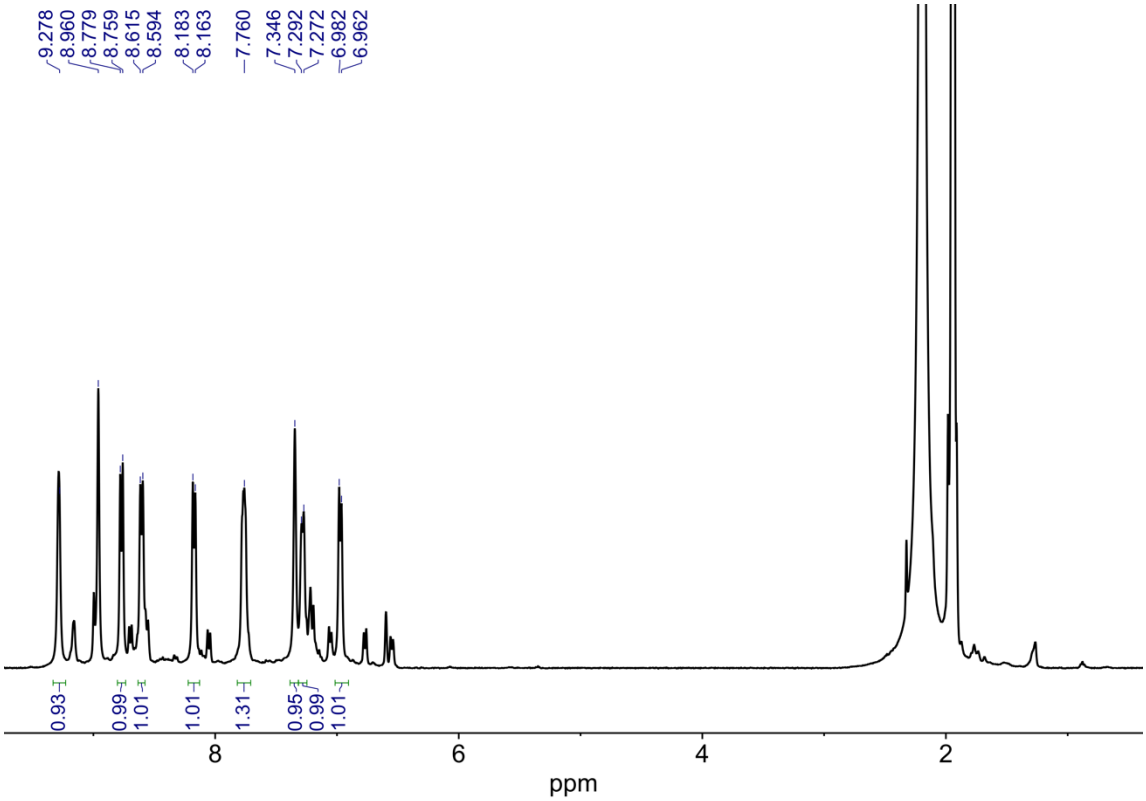

Figure S23: ^{1}H NMR spectrum (500 MHz, 298 K, CD_3CN) of **5** and **6**.

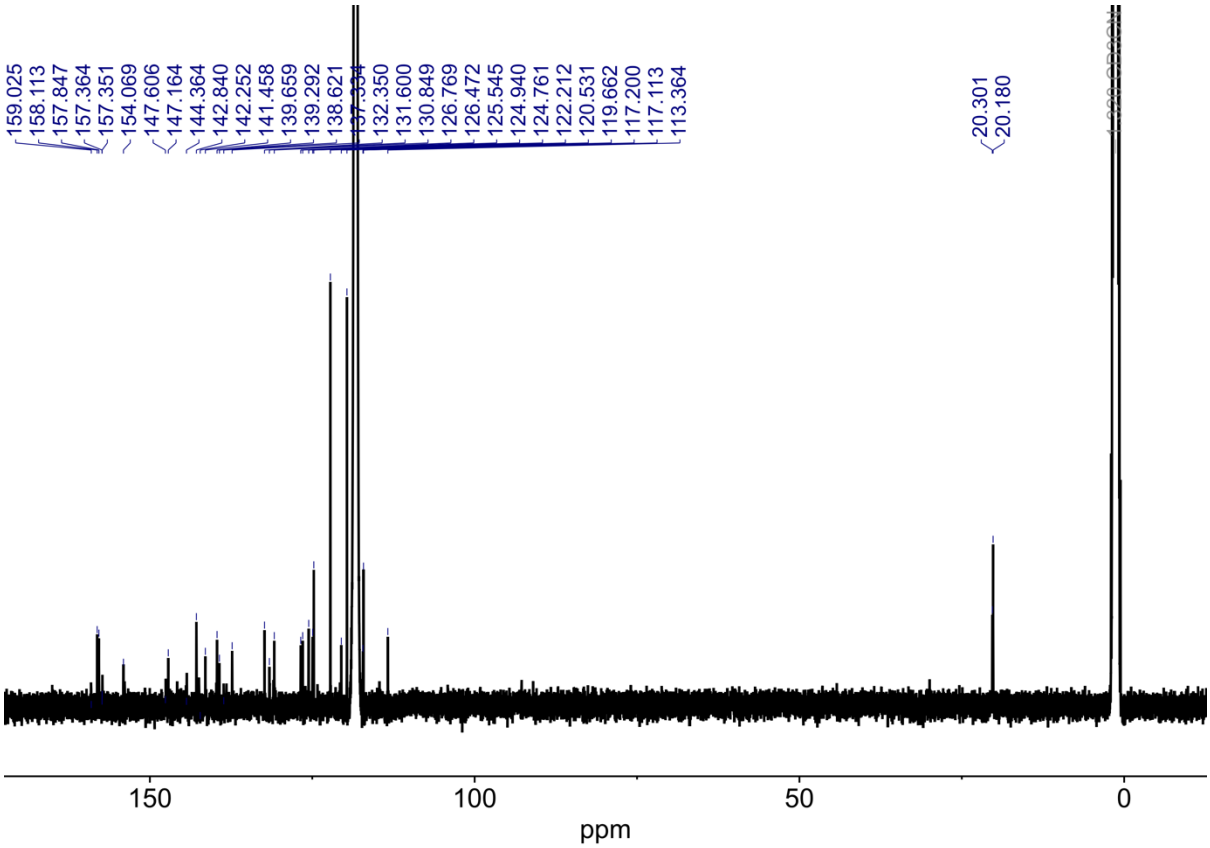

Figure S24: ^{13}C NMR spectrum (125 MHz, 298 K, CD_3CN) of **5** and **6**.

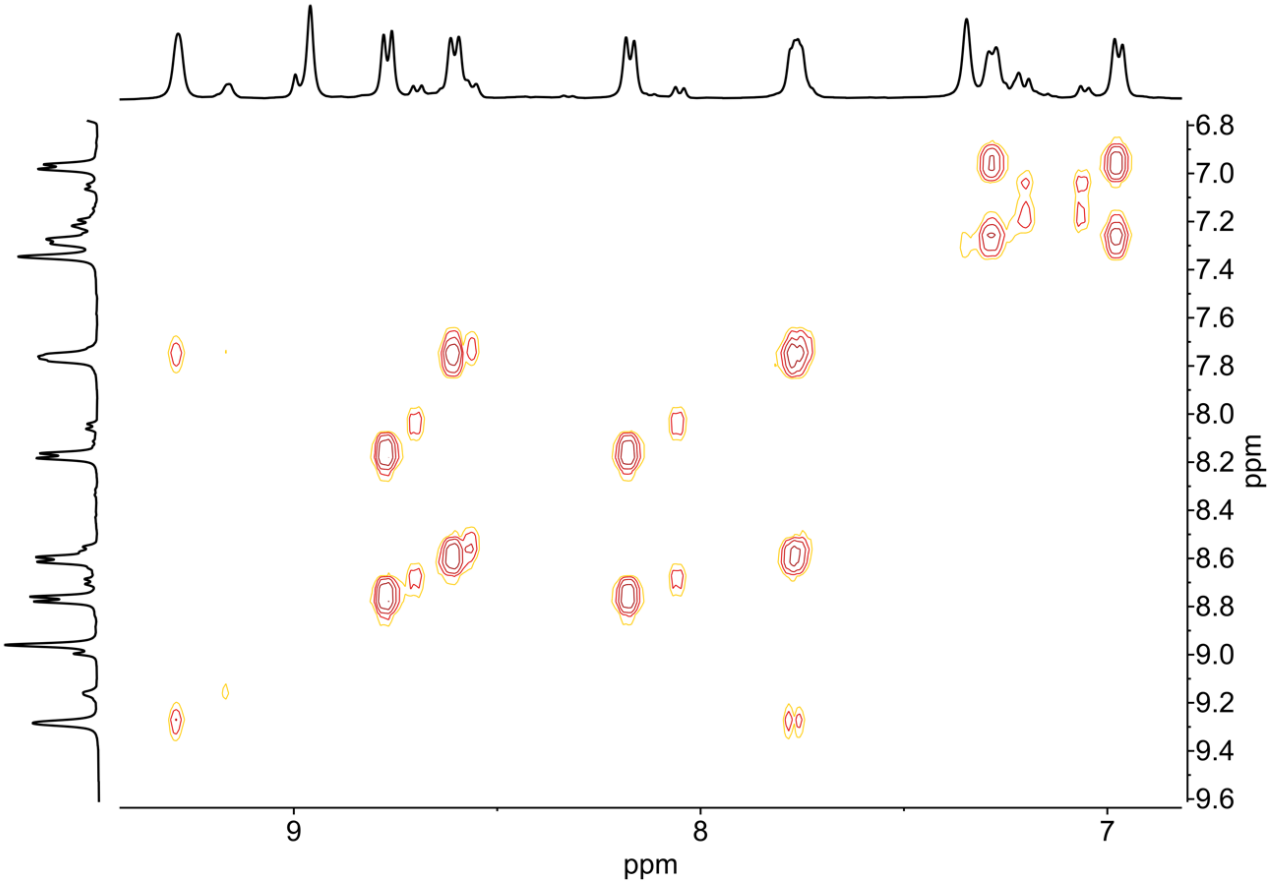

Figure S25: Aromatic region of the ^{1}H-^{1}H COSY NMR spectrum (500 MHz, 298 K, CD_3CN) of **5** and **6**.

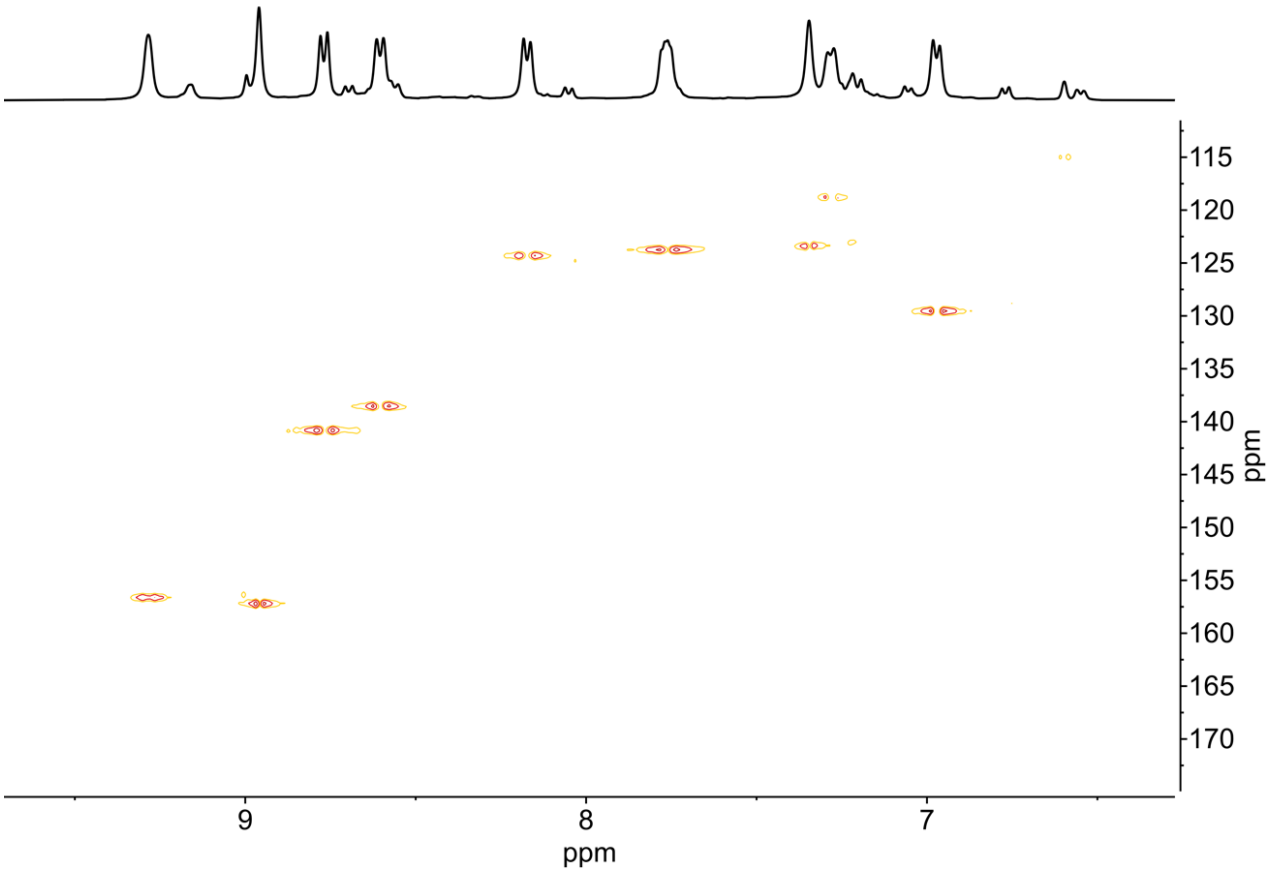

Figure S26: Aromatic region of the ^{1}H-^{13}C HSQC NMR spectrum (500 MHz, 298 K, CD_3CN) of **5** and **6**.

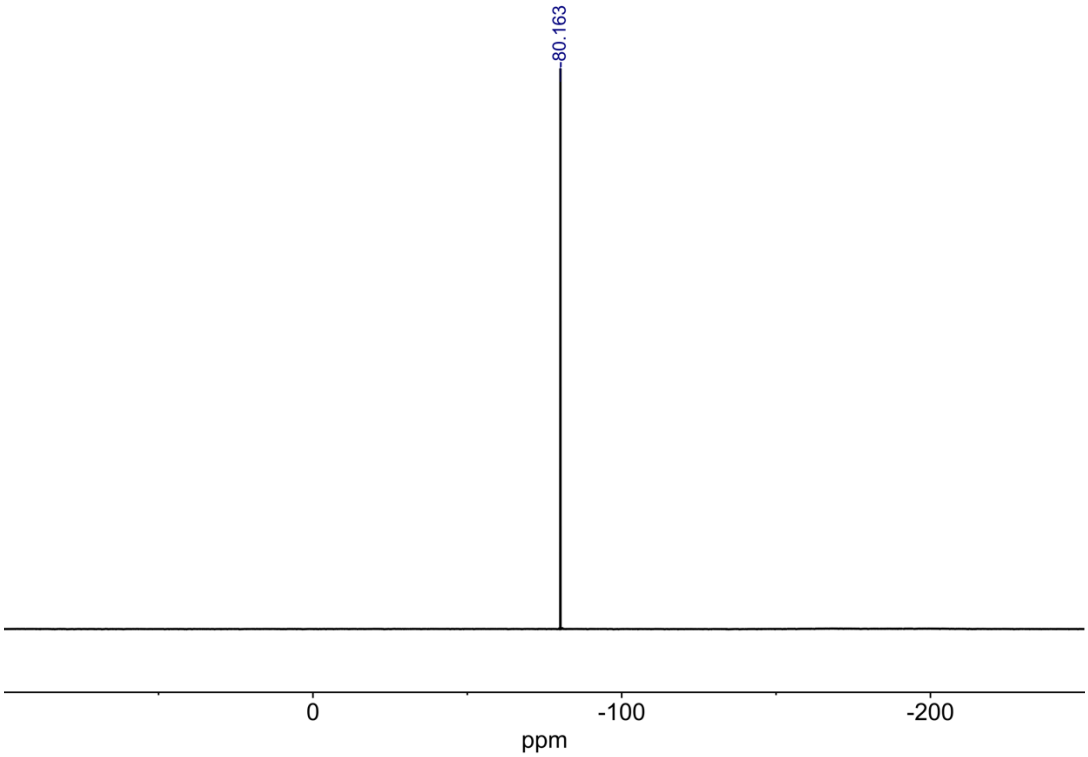

Figure S27: ^{19}F NMR spectrum (471 MHz, 298 K, CD_3CN) of **5** and **6**.

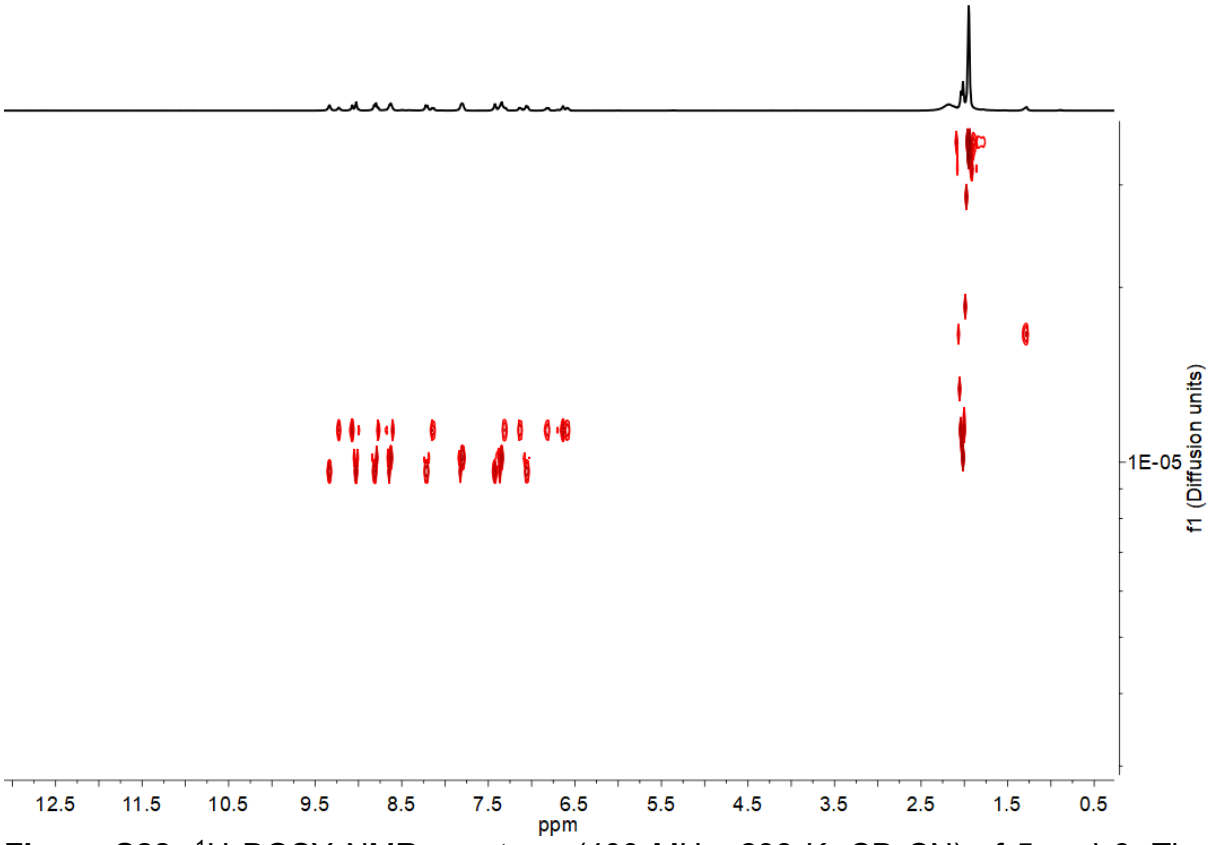

Figure S28: ^{1}H DOSY NMR spectrum (400 MHz, 298 K, CD_3CN) of **5** and **6**. The diffusion coefficient of **5** was measured to be 1.14 x 10^{-5} cm^2 s^{-1}, and of **6** to be 9.62 x 10^{-6} cm^2 s^{-1} giving solvodynamic radii of 5.58 Å and 6.61 Å. These values are comparable with those generated by molecular models of the proposed structures.

S4.5 Assembly in absence of iodide with alternate silver salts

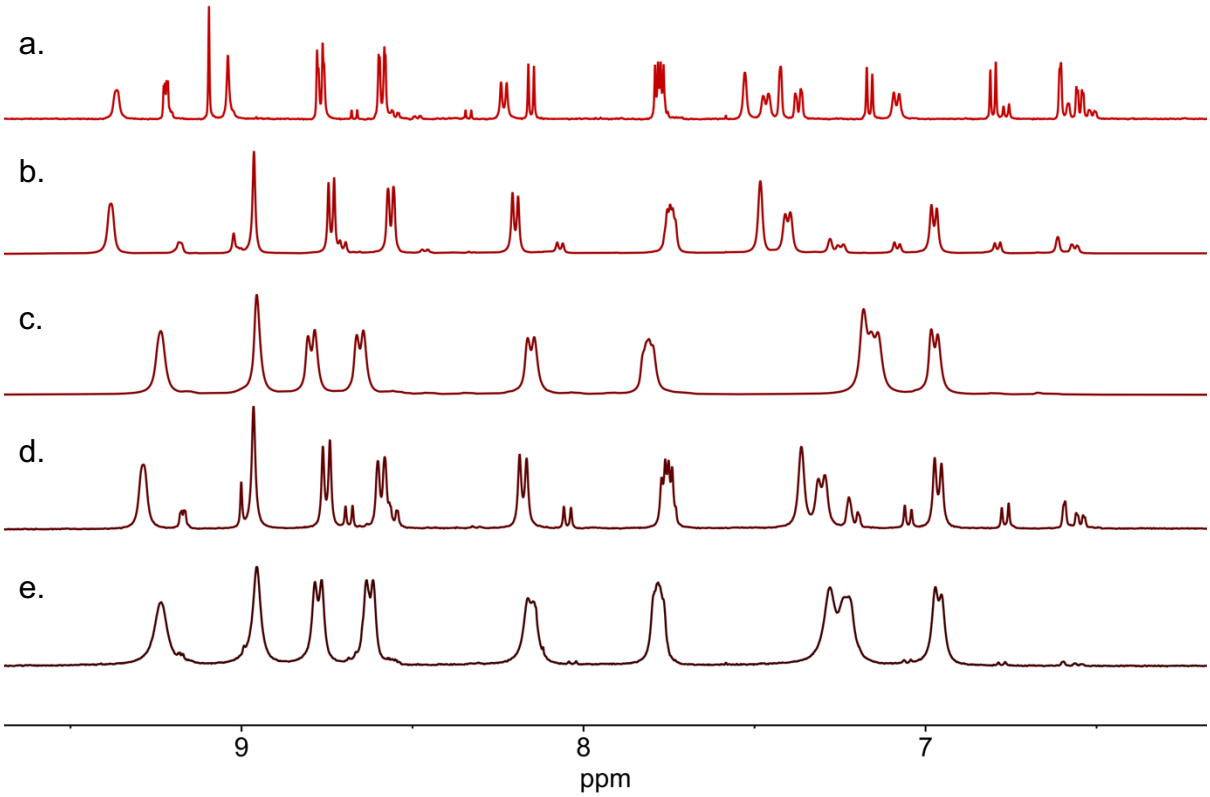

Figure S29: ^{1}H NMR (500 MHz, 298 K, CD_3CN) of assemblies of **1**, **3**, and a. $AgClO_4$, b. $AgNTf_2$, c. $AgPF_6$, d. AgOTf or e. $AgBF_4$. Note maximal small component in $AgClO_4$ and exclusive formation of large component in $AgPF_6$

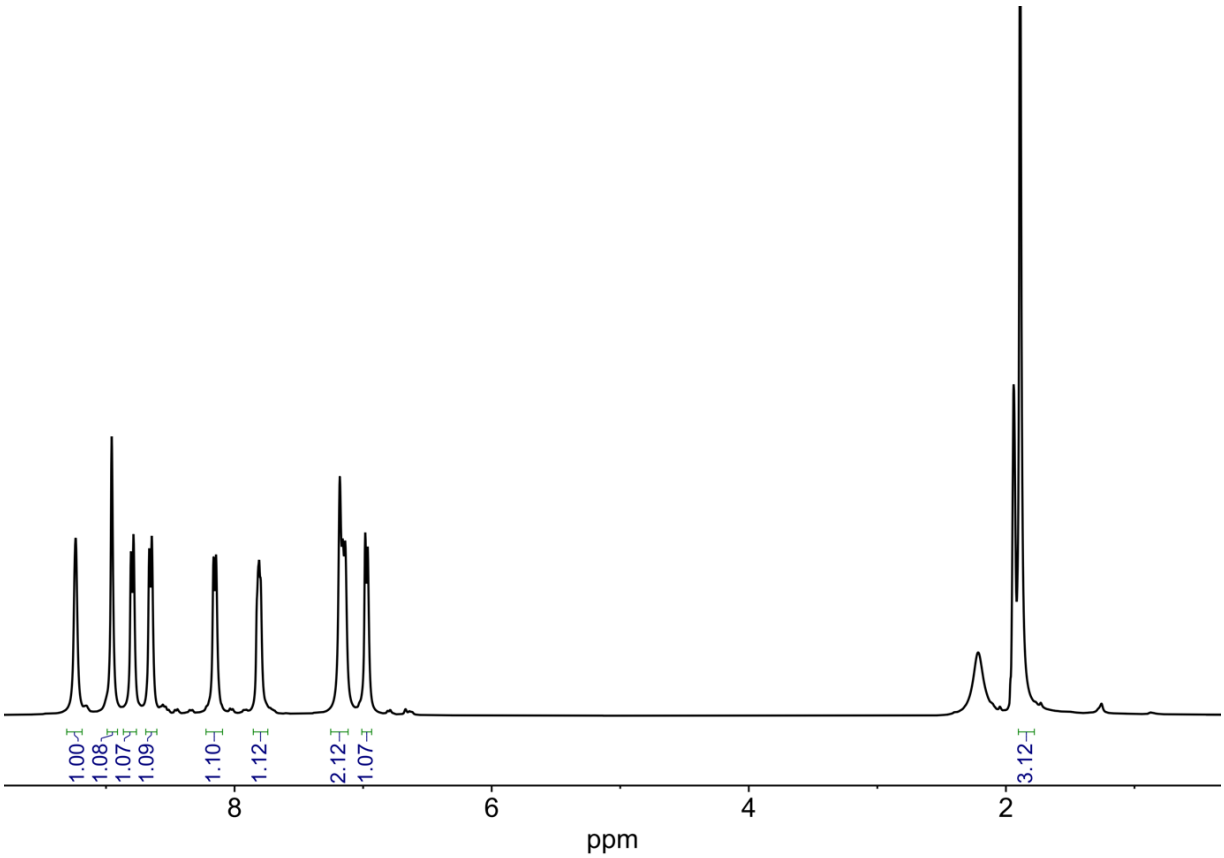

Figure S30: ^{1}H NMR spectrum (500 MHz, 298 K, CD_3CN) of **6** formed from $AgPF_6$.

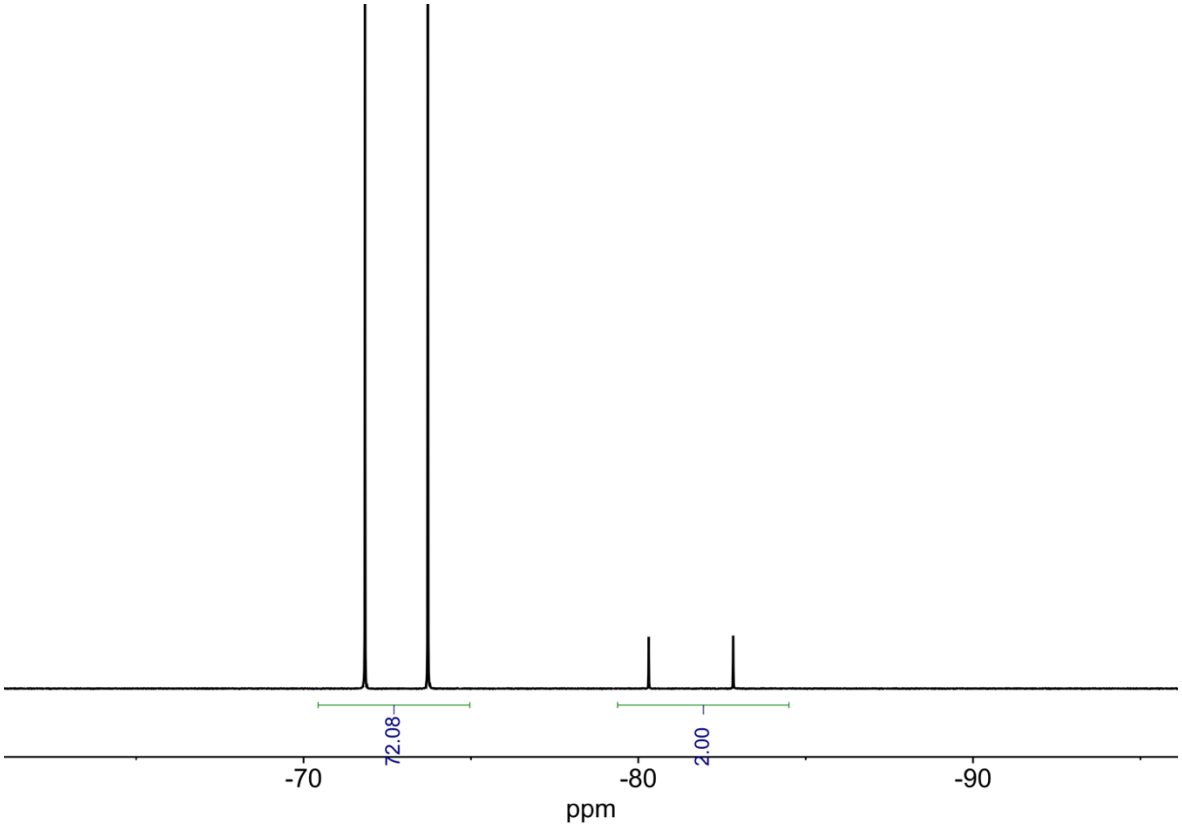

Figure S31: ^{19}F NMR spectrum (376 MHz, 298 K, CD_3CN) of **6** formed from $AgPF_6$. Ratio of two species 12:1 PF_6:PO_2F_2.

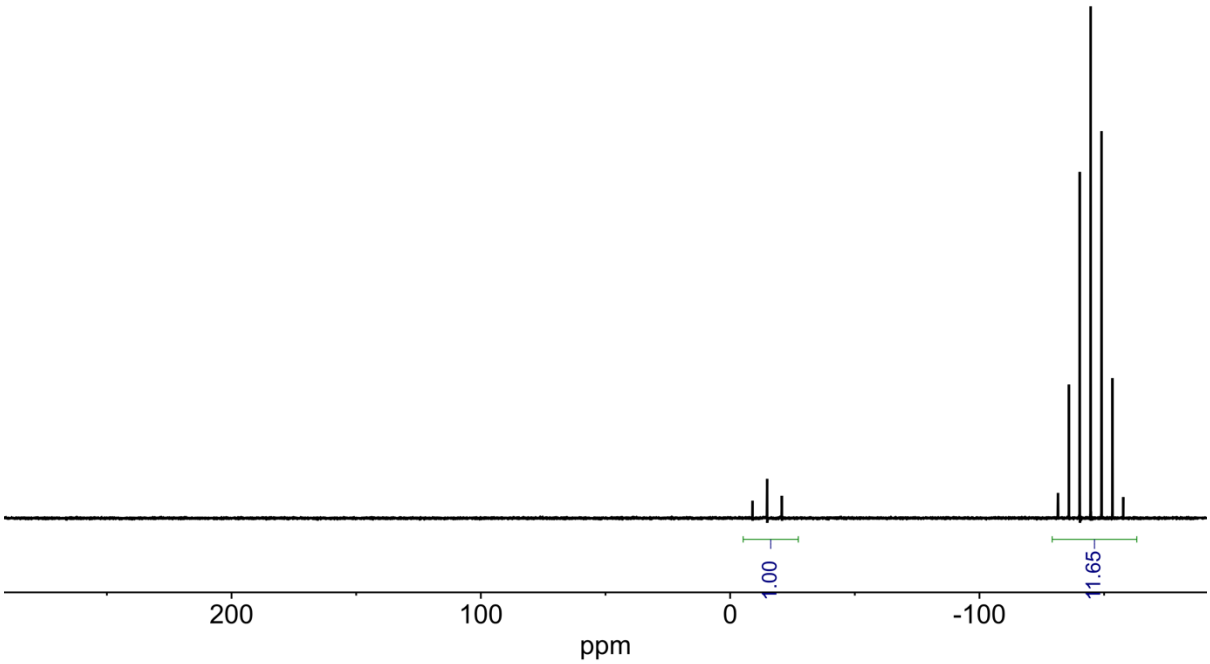

Figure S32: ^{31}P NMR spectrum (162 MHz, 298 K, CD_3CN) of **6** formed from $AgPF_6$. Ratio of two species 12:1 PF_6:PO_2F_2.

S5. Assignment of Six-Stranded Helicate 11 as $Ag_8L_6Br_2$

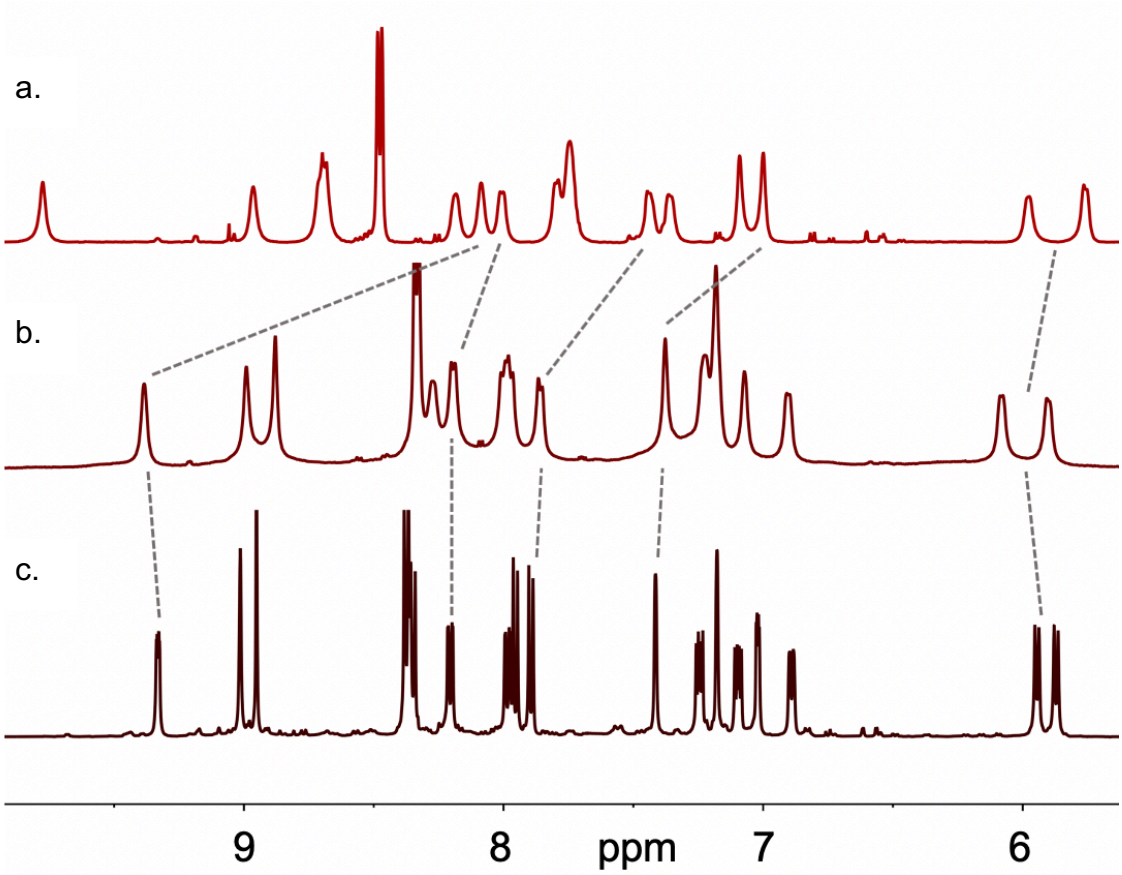

Figure S33: ^{1}H NMR spectrum (500 MHz, 298 K, CD_3CN) of a. **10** (SO_4), b. **11** (Br) and c. **9** (I). Note the family of 6 peaks around 7 ppm in **9** is mirrored (with overlap) in **11**, but not in **10**. This is repeated in the families of peaks at 8 ppm and 9 ppm.

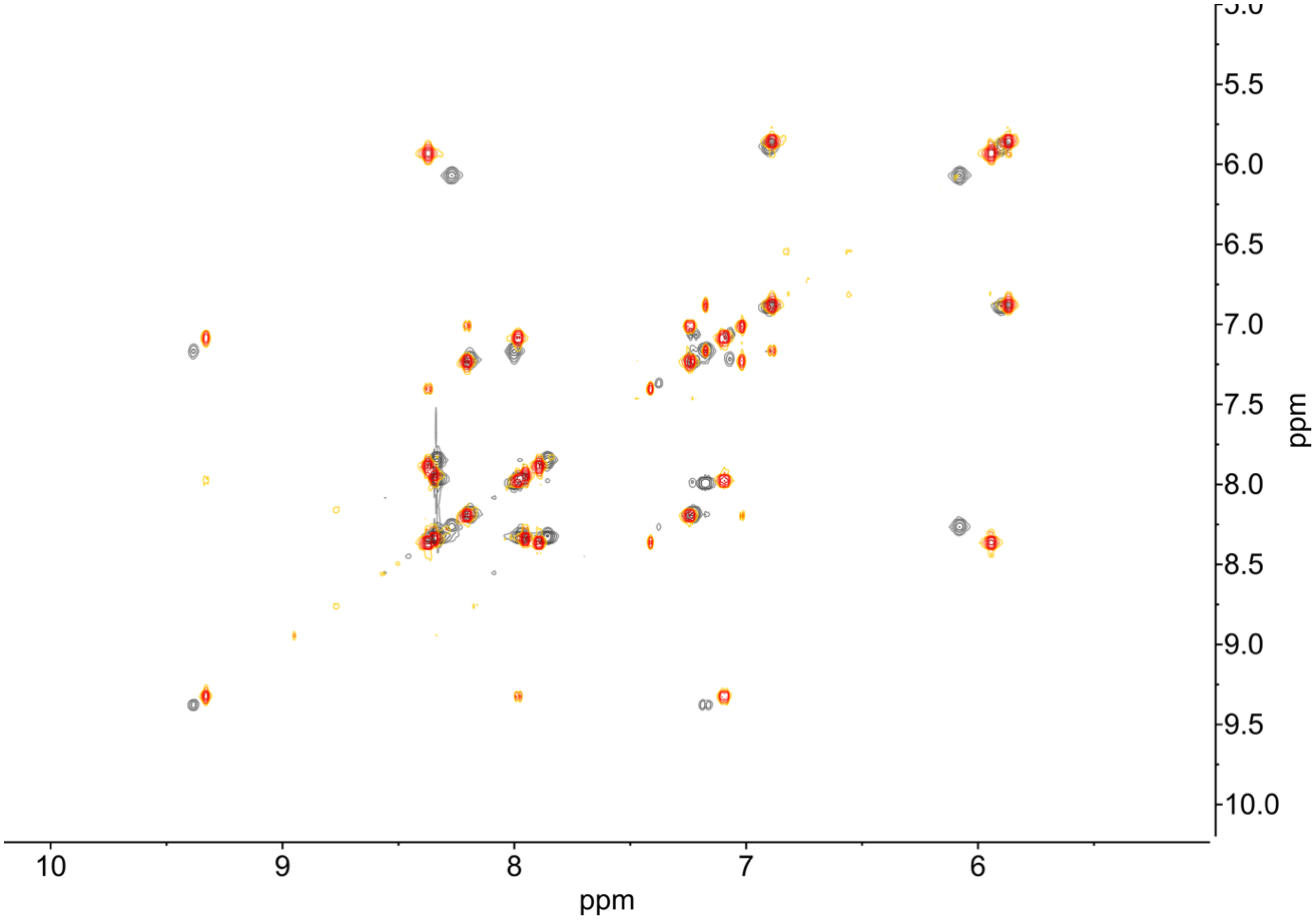

Figure S34: Overlay of the aromatic regions of ^{1}H-^{1}H COSY NMR spectrums (500 MHz, 298 K, CD_3CN) of **11** (grey) and **9** (orange) illustrating the high degree of similarity between the structures. For example, the almost perfect overlap of correlations between 9.5 ppm and 7.5 ppm.

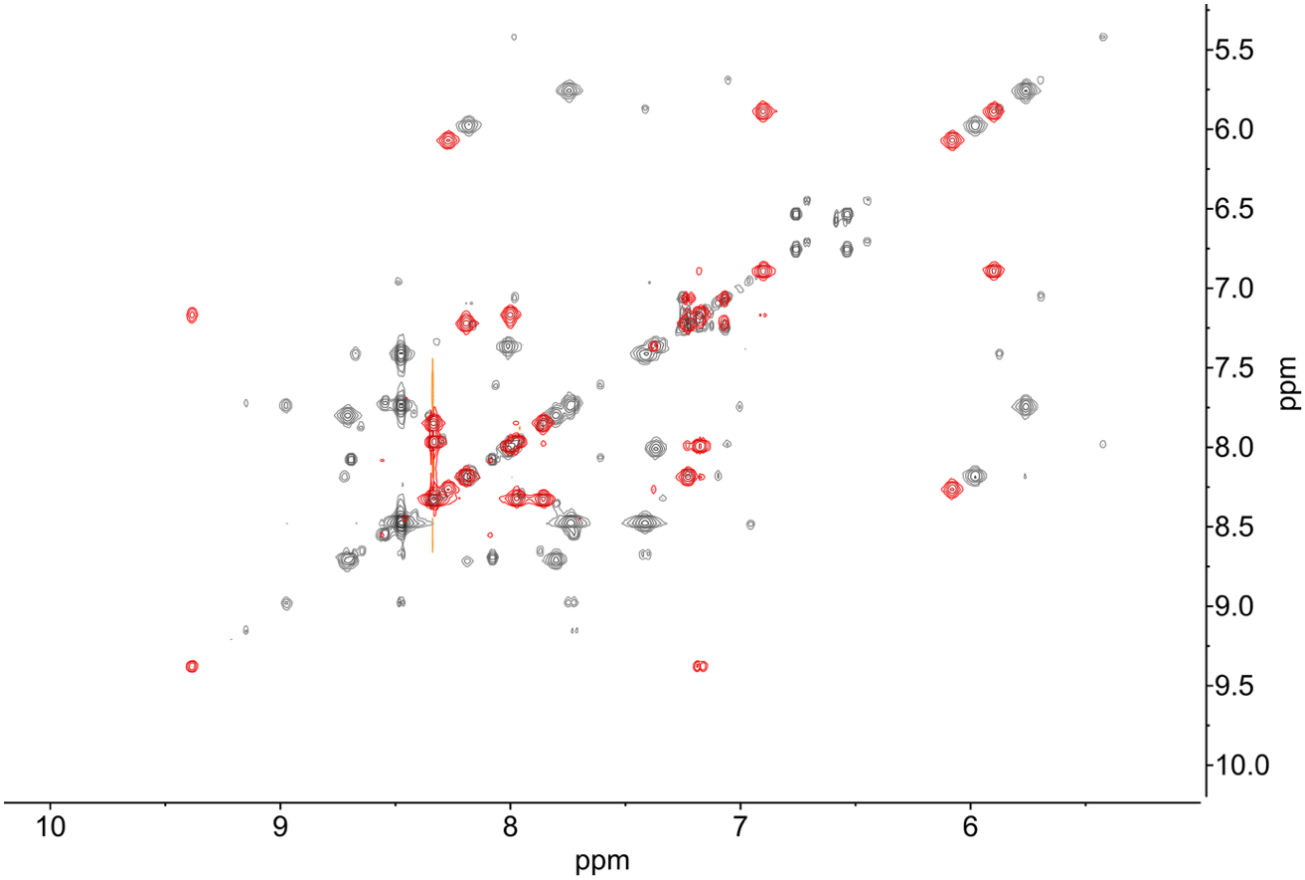

Figure S35: Overlay of the aromatic regions of ^{1}H-^{1}H COSY NMR spectrums (500 MHz, 298 K, CD_3CN) of **10** (grey) and **1** (red) illustrating the low degree of similarity between the structures. Note in particular the correlations around 9 ppm, 8.5 ppm, 7.5 ppm and 5.8 ppm. Note that this lack of overlap is due to differing patterns of correlation being observed, not just changes in the particular chemical shift.

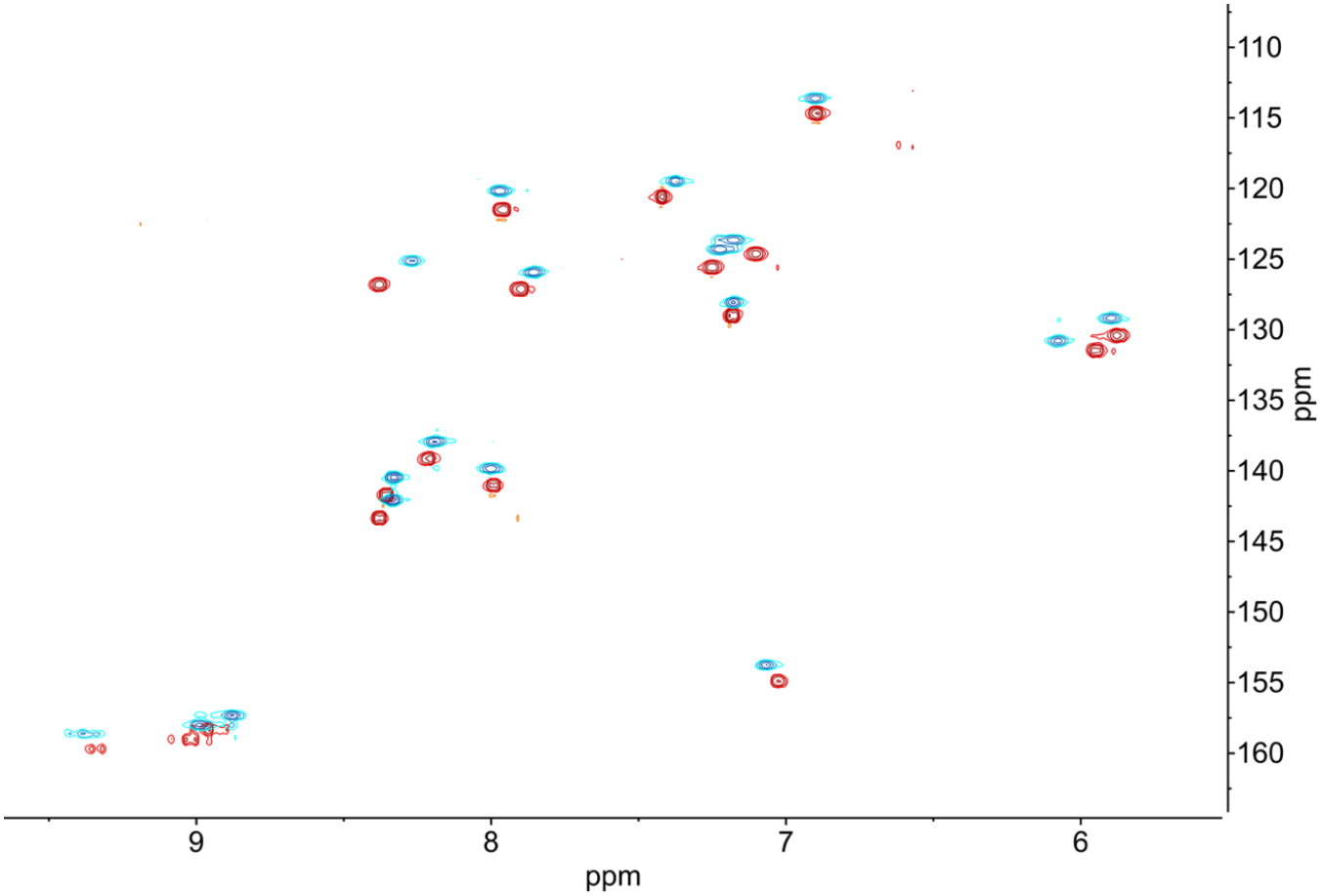

Figure S36: Overlay of the aromatic regions of ^{1}H-^{13}C HSQC NMR spectrums (500 MHz, 298 K, CD_3CN) of **11** (blue) and **9** (red) illustrating the high degree of similarity between the structures. For example, the almost perfect overlap of correlations between 8 ppm and 140 ppm.

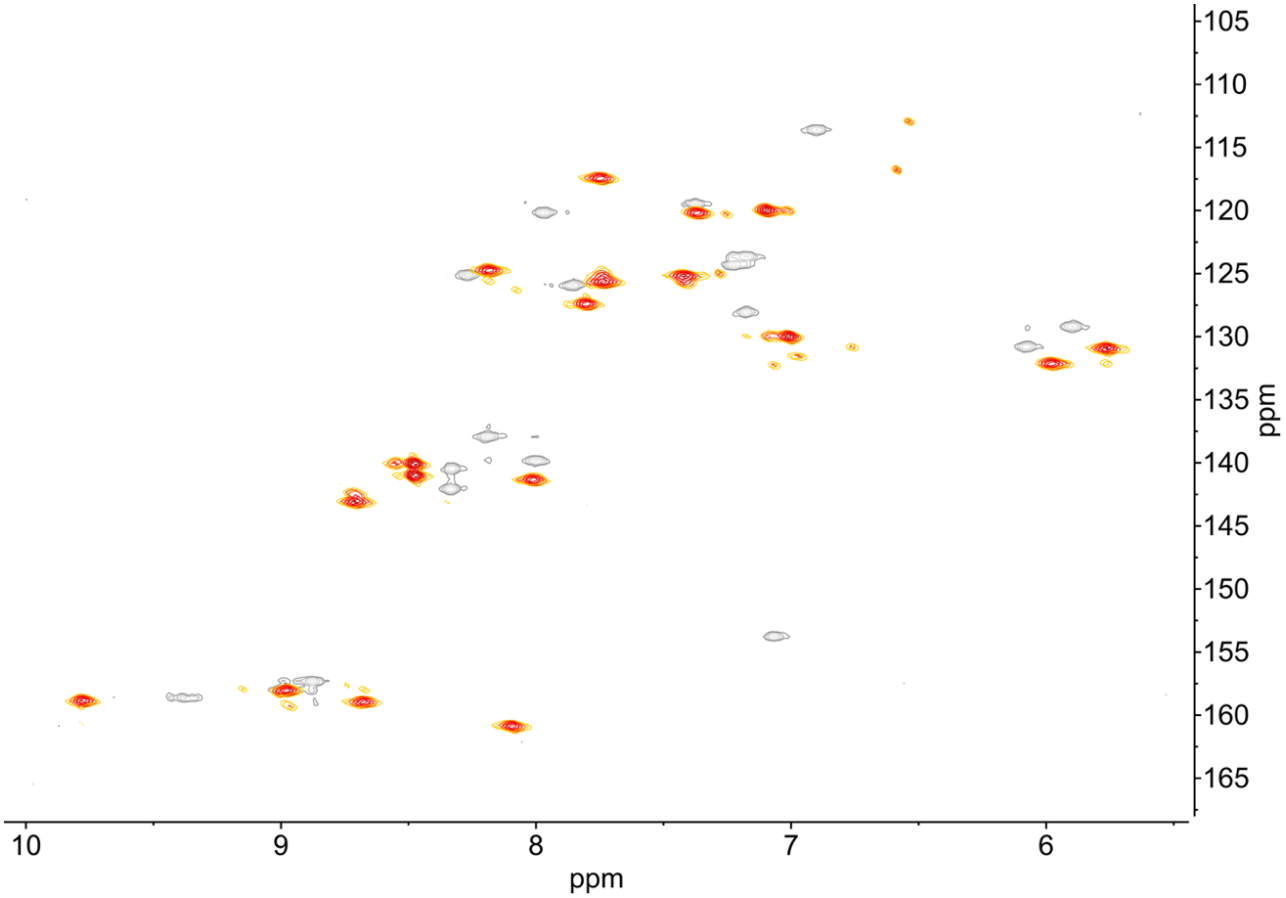

Figure S37: Overlay of the aromatic regions of ^{1}H-^{13}C HSQC NMR spectrums (500 MHz, 298 K, CD_3CN) of **10** (grey) and **11** (orange) illustrating the lower degree of similarity between the structures. Note in particular the correlation at 7 ppm and 153 ppm, which has no closely corresponding signal in **11**.

S6. Investigation of Assembly of Six-Stranded Helicates

S6.1 Generality of silver salts used in assembly

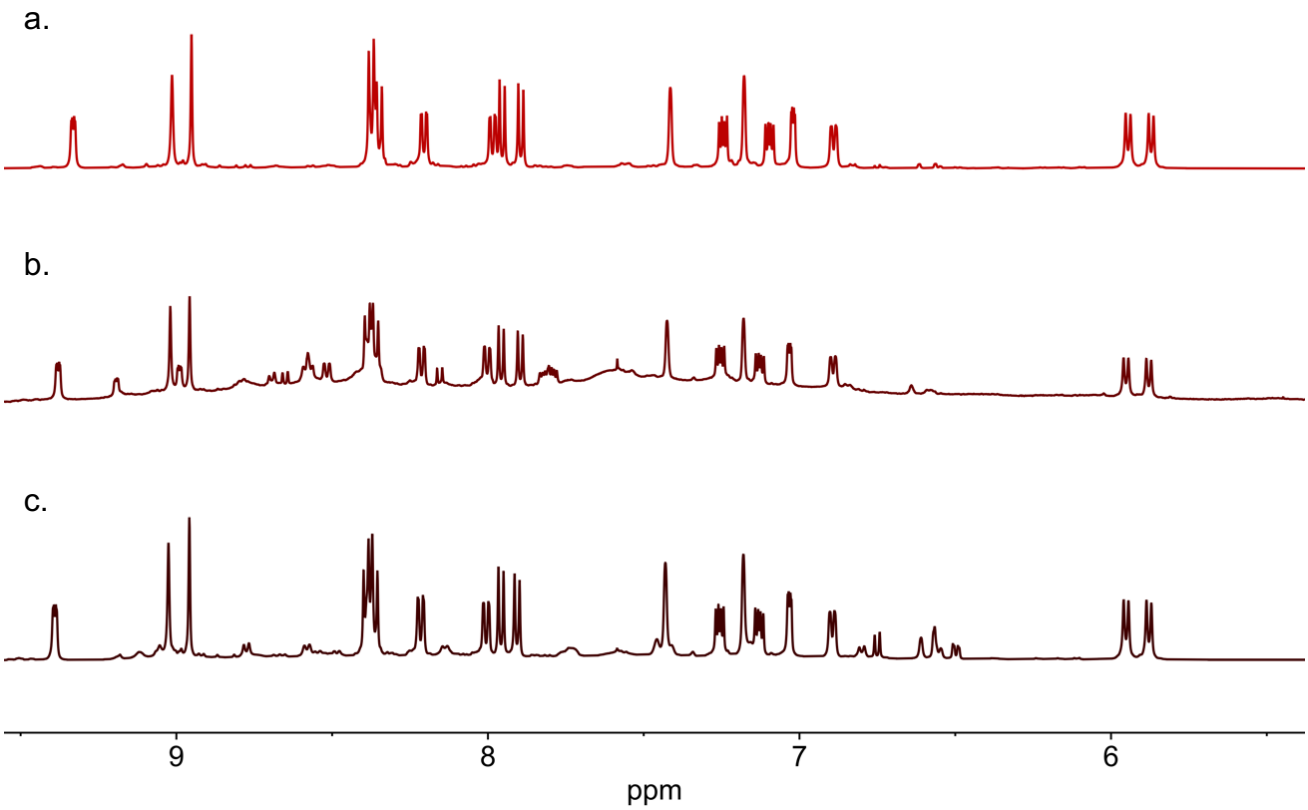

Figure S38: ^{1}H NMR spectrum (500 MHz, 298 K, CD_3CN) of assembly of **1**, **3**, KI and a. $AgNTf_2$, b. $AgBF_4$ or c. AgOTf showing in all cases assembly of the six-stranded helicate **9**. Note that significant by-products were seen when using $AgBF_4$ in b.. With assemblies constructed using $AgBF_4$, $AgClO_4$ and $AgPF_6$, we saw the residual formation of **5** and **6**. We infer that these counterions interact more strongly with the initially-formed **5** and **6**, thus preventing the system of interconverting products from expressing six-stranded helicate **9** alone.

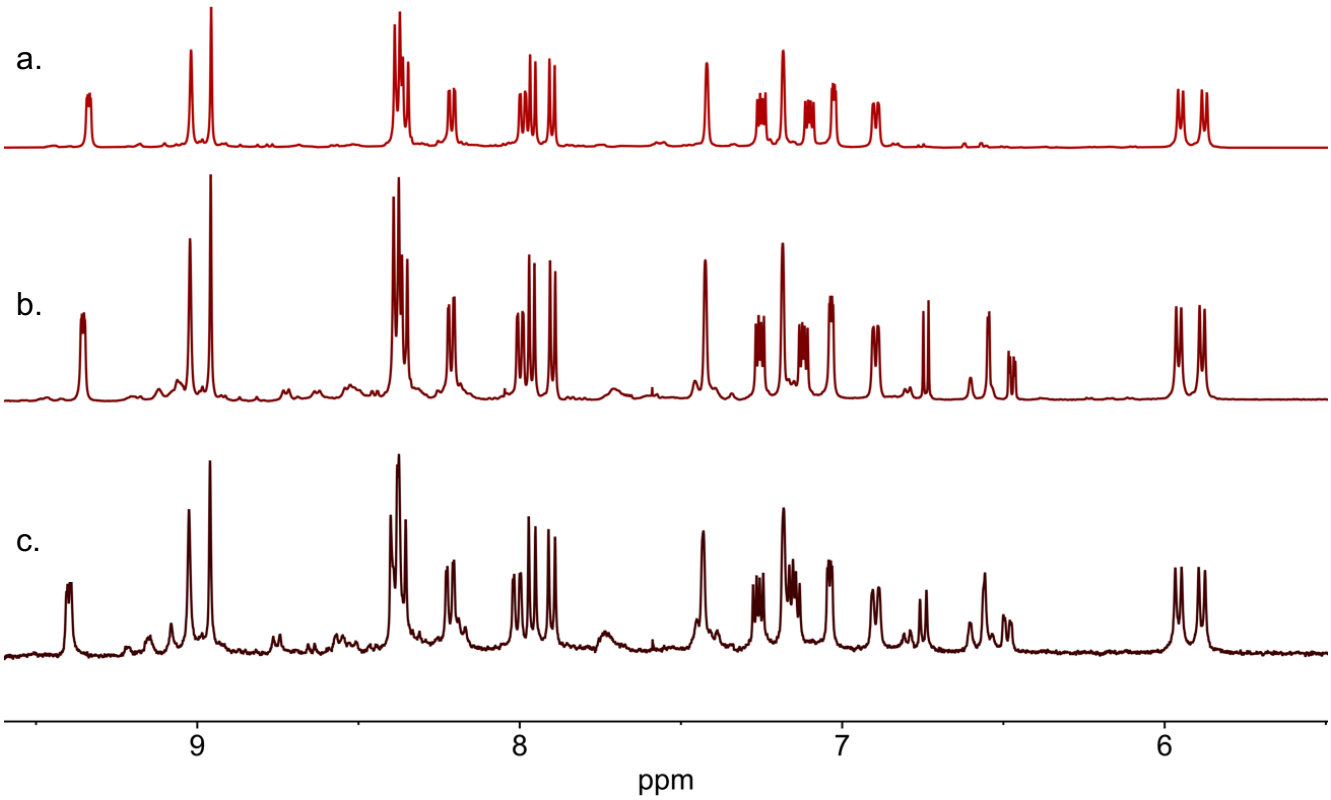

Figure S39: ^{1}H NMR spectrum (500 MHz, 298 K, CD_3CN) of assembly of **1**, **3**, KI and a. $AgNTf_2$, b. $AgPF_6$ or c. $AgClO_4$ showing in all cases assembly of the six-stranded helicate.

S6.2 Addition of anions to 9.

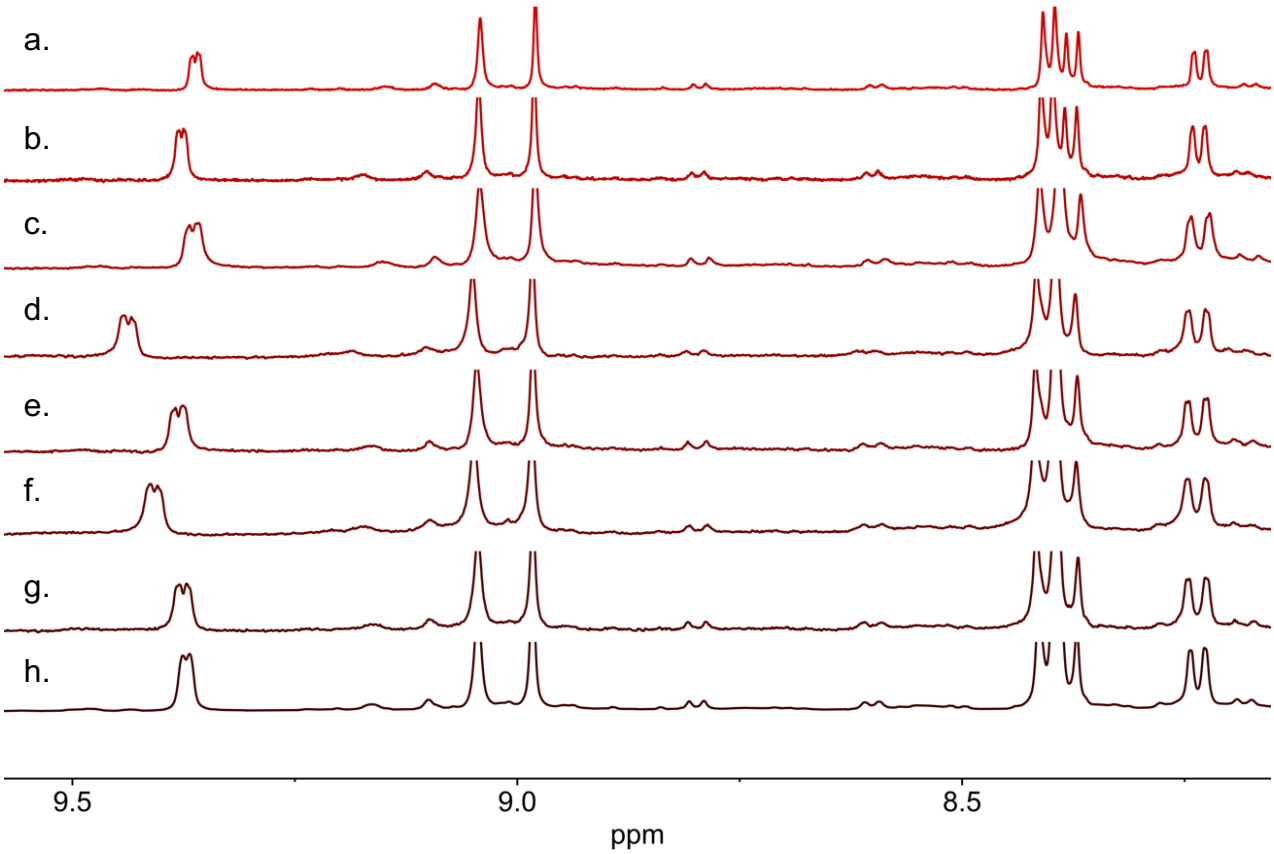

Figure S40: Partial ^{1}H NMR spectrum (500 MHz, 298 K, CD_3CN) of six-stranded helicate **9** after addition of a. $TBAReO_4$, b. $TBAPF_6$, c. TBAOTf, d. TBAOTs, e. $TBANO_3$, f. $TBABF_4$, g. $TBAClO_4$, h. no anion added.

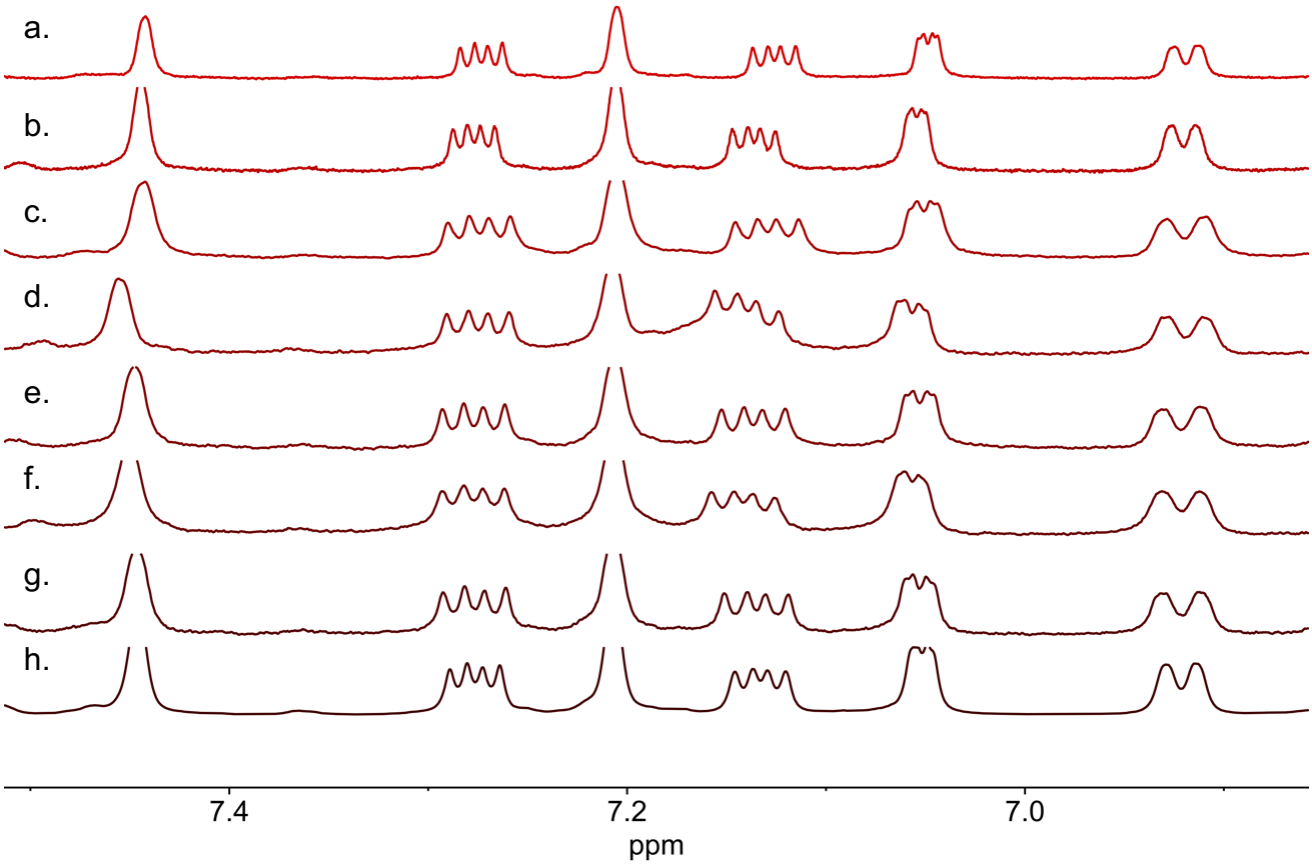

Figure S41: Partial ^{1}H NMR spectrum (500 MHz, 298 K, CD_3CN) of six-stranded helicate **9** after addition of a. $TBAReO_4$, b. $TBAPF_6$, c. TBAOTf, d. TBAOTs, e. $TBANO_3$, f. $TBABF_4$, g. $TBAClO_4$, h. no anion added.

We observe the most significant shifts at in H_{32} (see characterisation for assignment) suggesting that the added anions which show greatest interactions (OTs, BF_4) may be binding at the helix termini, in a manner similar to that seen with sulfate in **9**, with non-classical hydrogen bonding between CH_{32} and the anion stabilising the interaction.

S6.3 Addition of TBAI in substoichiometric quantities

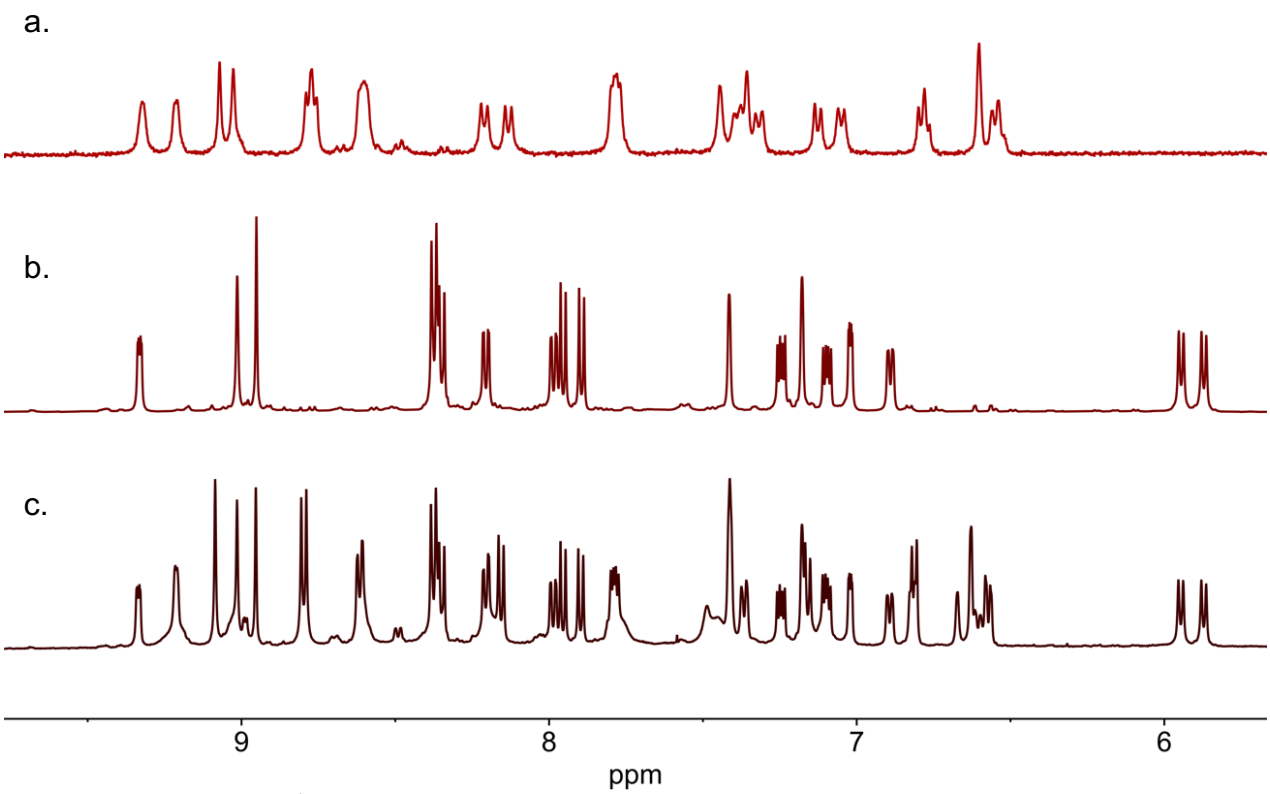

Figure S42: Partial ^{1}H NMR spectrum (500 MHz, 298 K, CD_3CN) of a. mixture of **5** and **6**, b. six-stranded helicate **9**, c. mixture of six-stranded helicate **9**, **5** and **6** formed after addition of a substoichiometric amount (1 eq.) of TBAI.

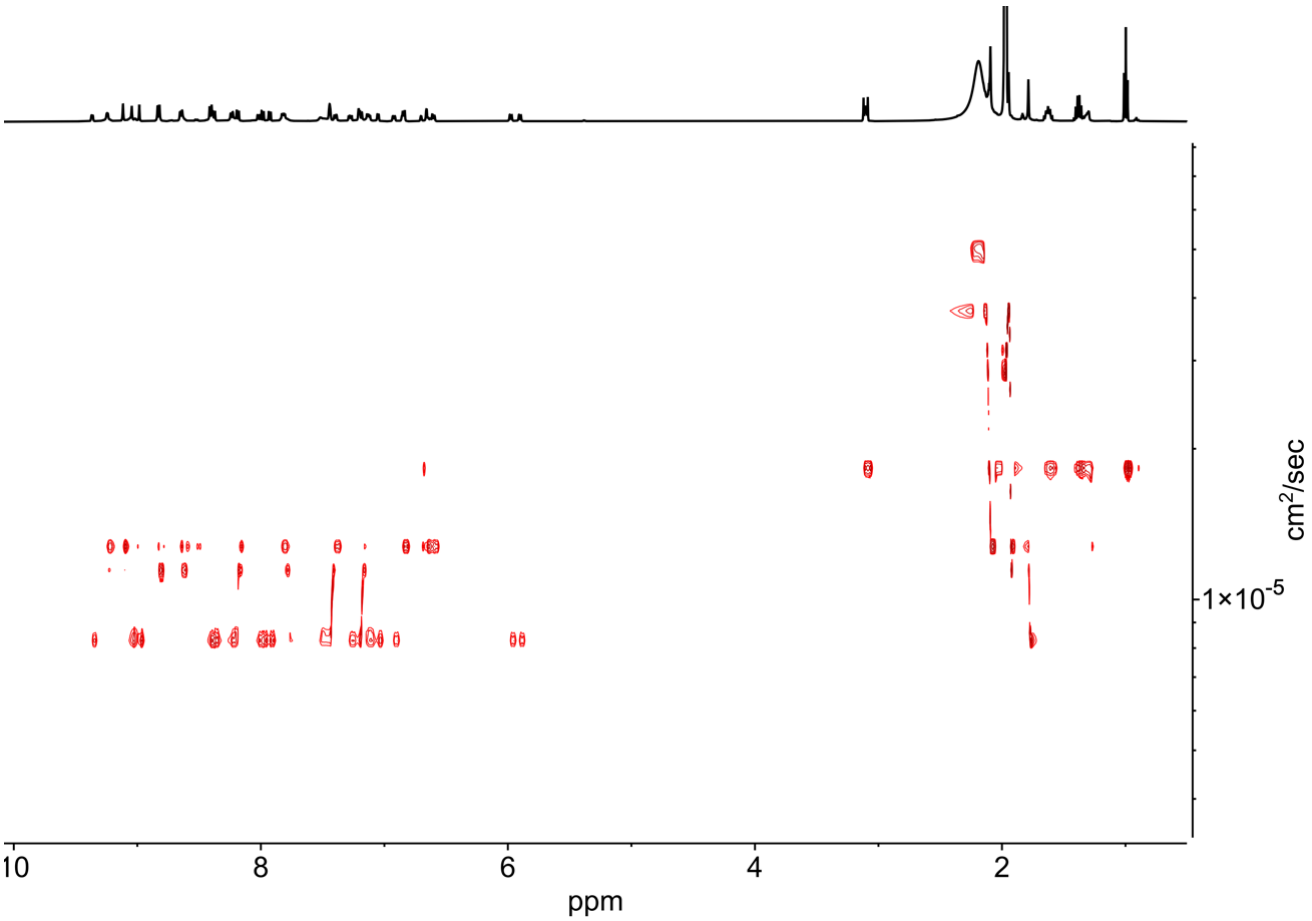

Figure S43: ^{1}H DOSY NMR spectrum (400 MHz, 298 K, CD_3CN) of **5**, **6** and **9** assembled from $AgNTf_2$ and 1 eq. of TBAI (2 eq. required for stoichiometric addition. The diffusion coefficient of **9** was measured to be 8.62 x 10^{-6} cm^2 s^{-1}, of **5** to be 1.27 x 10^{-5} cm^2 s^{-1}, and of **6** to be 1.13 x 10^{-5} cm^2 s^{-1} giving solvodynamic radii of 7.38 Å, 5.01 Å and 5.63 Å. These values are comparable with those generated by models of the proposed structures and the crystal structure of **9**.

S6.4 Effect of dilution on six-stranded helicate 9

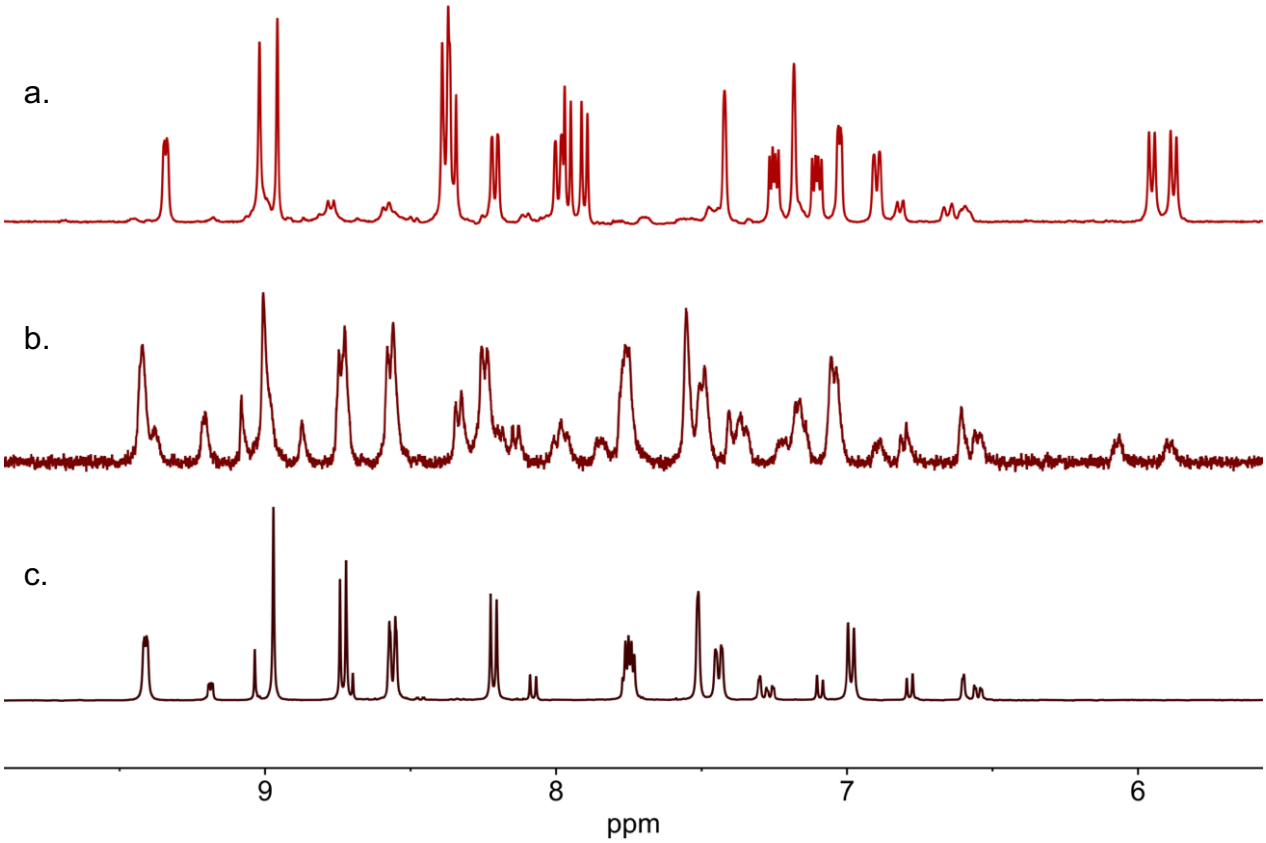

Figure S44: Partial ^{1}H NMR spectrum (500 MHz, 298 K, CD_3CN) of a. six-stranded helicate **9**. b. Ten-fold dilution of assembly of **9**. c. Direct assembly with $AgNTf_2$ to form **5** and **6**. Note reversion of the majority of the material to **5** and **6** after dilution.

S6.5 Effect of addition of different halides to $AgNTf_2$ assembly

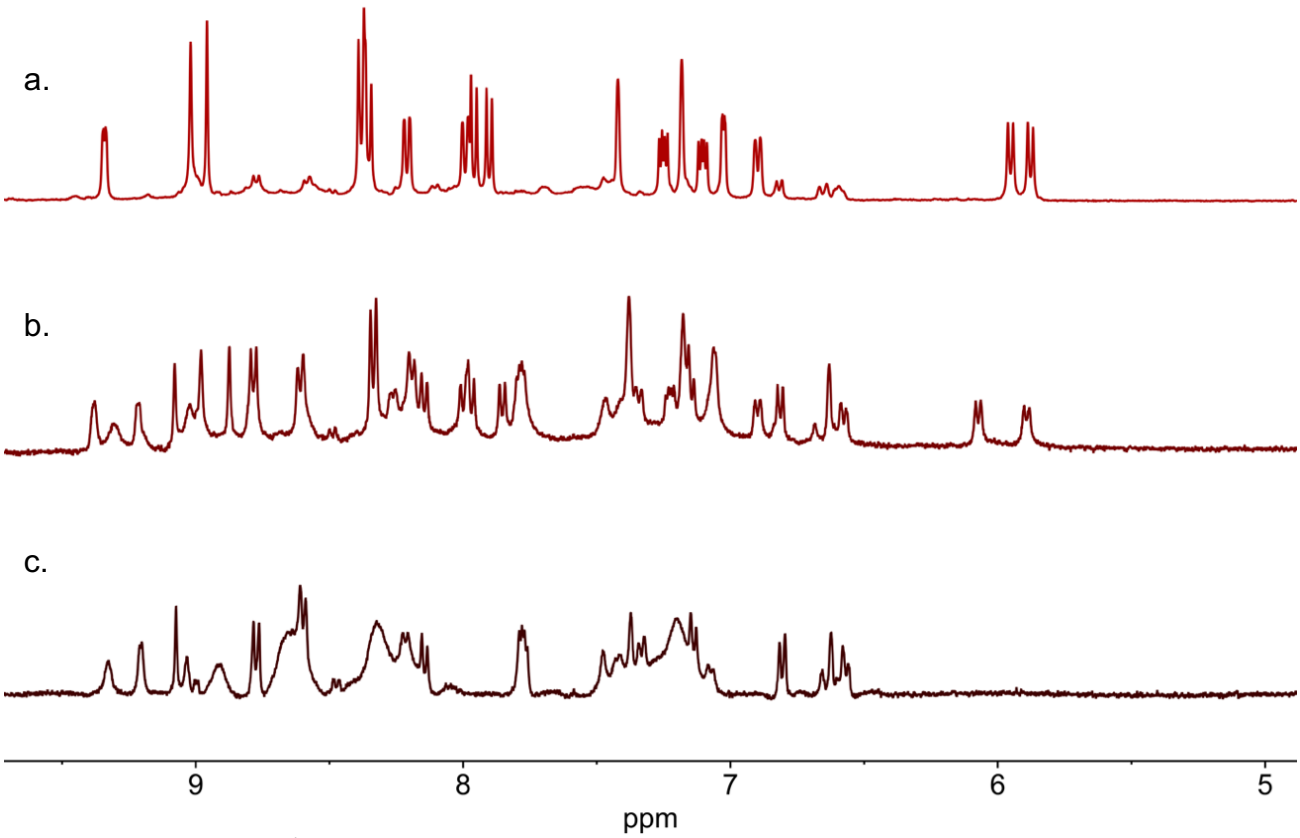

Figure S45: Partial ^{1}H NMR spectrum (500 MHz, 298 K, CD_3CN) a. TBAI addition (2 eq.), b. TBABr addition (2 eq.), c. TBACl addition (2 eq.). Addition of TBAF led to immediate decomposition of the system, and a complex ^{1}H NMR spectra. Clear formation of six-stranded helicate was observed upon addition of TBABr and TBAI, but no evidence of six-stranded helicate was observed on addition of TBACl or TBAF.

The lack of six-stranded helicate formation upon addition of TBACl or TBAF likely stemmed from a different cause in each case. For TBACl, immediate precipitation upon halide addition was seen, with presumed abstraction of chloride from solution. For TBAF, immediate discoloration and disruption of the metal-organic assemblies was seen. The smaller ionic radius and greater electronegativity of fluoride may prevent fluoride serving in a bridging role between the silver ions, precluding six-stranded helicate formation.

S6.6 Titration of TBABr into $AgNTf_2$ Assembly forming Six-Stranded helicate 11

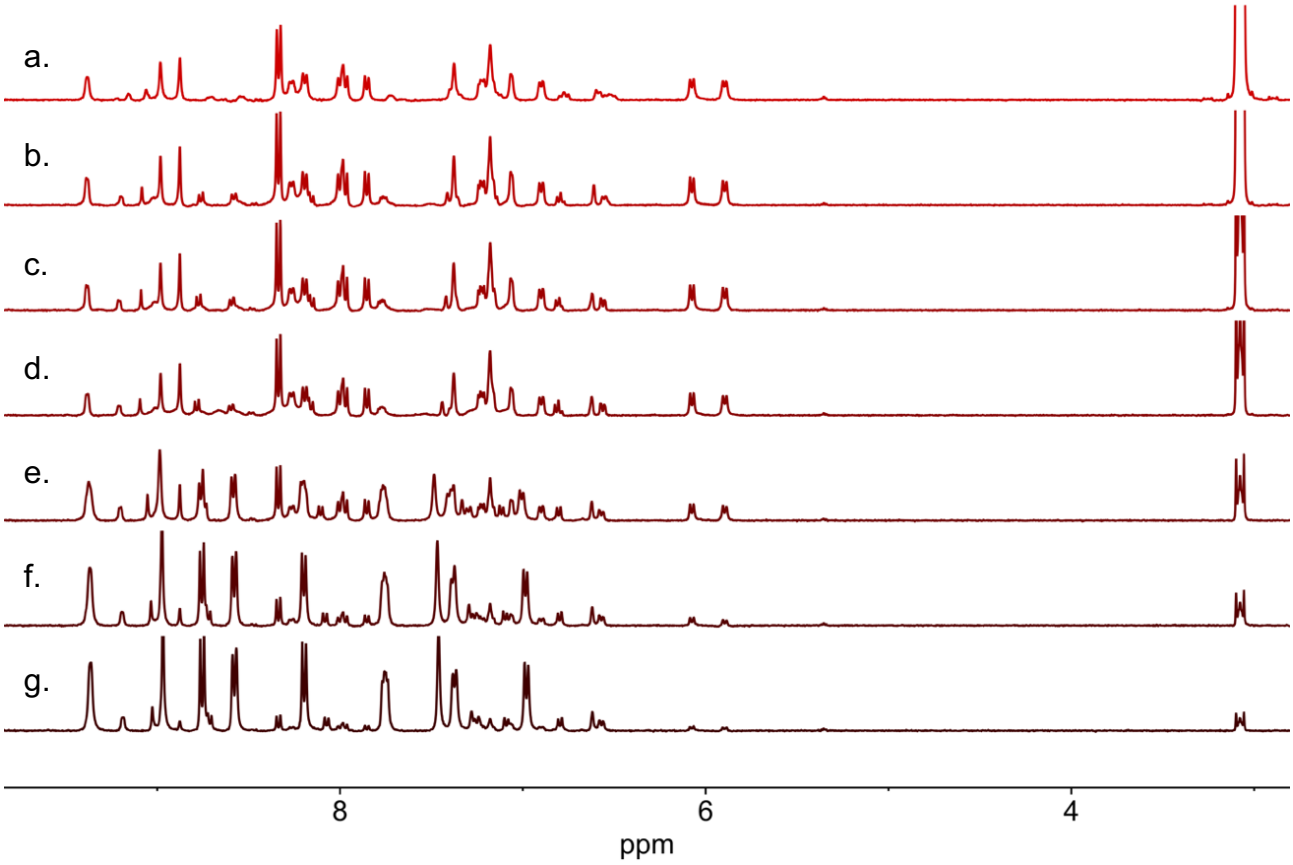

Figure S46: Partial ^{1}H NMR spectrum (500 MHz, 298 K, CD_3CN) showing titration of increasing quantities of TBABr to **1**, **3** and $AgNTf_2$. No evidence was seen of intermediate species – increasing amounts of the starting trimeric helicate **5** and tetrahedron **6** were converted to six-stranded helicate **11** in concert with increasing amounts of TBABr added.

S6.7 Partial induction of Six-Stranded helicate by Iodate, Bromate and thiocyanate.

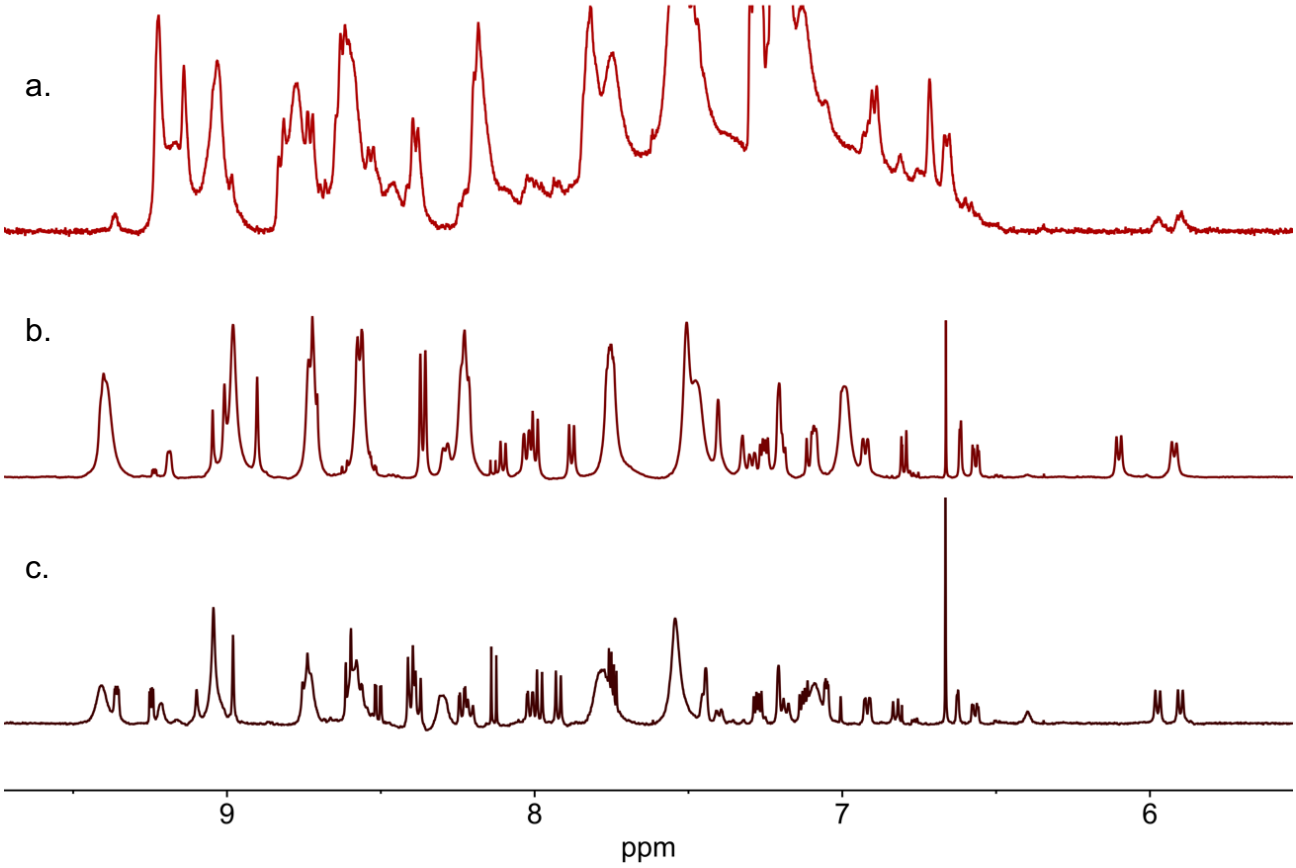

Figure S47: Partial ^{1}H NMR spectrum (500 MHz, 298 K, CD_3CN) of **1**, **3** and $AgNTf_2$ with addition of 2 eq. of a. TBASCN, b. $KBrO_3$, c. KIO_3. Partial six-stranded helicate formation was identified by the appearance of new signals near 6 ppm, and by the symmetry of the formed complex. No conditions could be found where the system could be driven cleanly to the six-stranded helicate.

S6.8 Anions unable to induce six-stranded helicate formation.

Tetrabutylammonium triflimide
Tetrabutylammonium methoxide
Tetrabutylammonium hexafluorophosphate
Tetrabutylammonium tetrafluoroborate
Tetrabutylammonium perrhenate
Tetrabutylammonium chloride
Tetrabutylammonium fluoride
Tetrabutylammonium perchlorate
Tetrabutylammonium triflate
Tetrabutylammonium nitrate
Tetrabutylammonium cyanate
Tetrabutylammonium cyanide
Tetrabutylammonium periodate
Tetrabutylammonium dihydrogen phosphate
Tetrabutylammonium hydrogen phosphate
Tetrabutylammonium acetate
Tetrabutylammonium benzoate
Tetrabutylammonium tosylate
Sodium antimony hexafluoride
Sodium azide
Sodium tetraphenylborate
Sodium tetrakis(4-chlorophenyl)borate
Sodium oxalate
Sodium thiosulfate
Sodium persulfate
Sodium arsenic hexafluoride
Sodium carbonate
Sodium bicarbonate
Potassium dicyanoaurate
Potassium polysulfate
Potassium chromate
Potassium thioacetate

S6.9 Attempted direct assembly from AgBr, AgI or Ag_2SO_4.

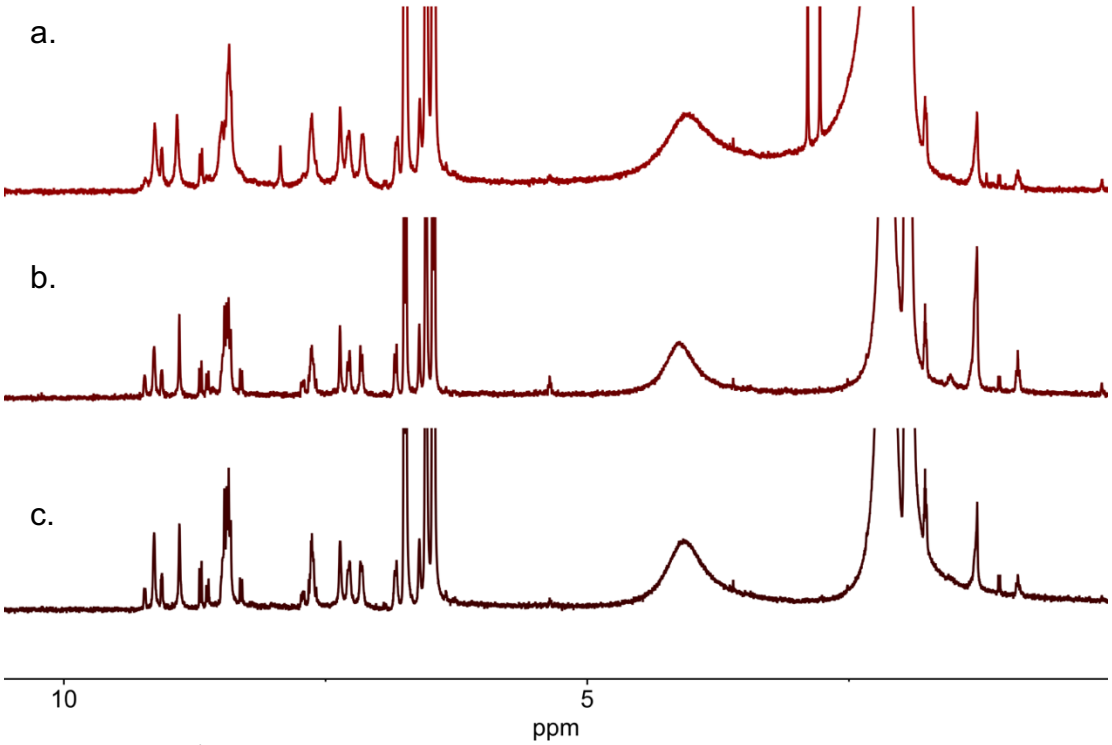

Figure S48: ^{1}H NMR spectra (500 MHz, 298 K, CD_3CN) following attempted direct assembly from a) Ag_2SO_4, b) AgI, or c) AgBr. In all cases, no evidence of six-stranded helicate was observed. Peaks corresponding to free **3** were observed, along with peaks we assign to partially assembled ligand strand. Extensive precipitation was seen in all cases.

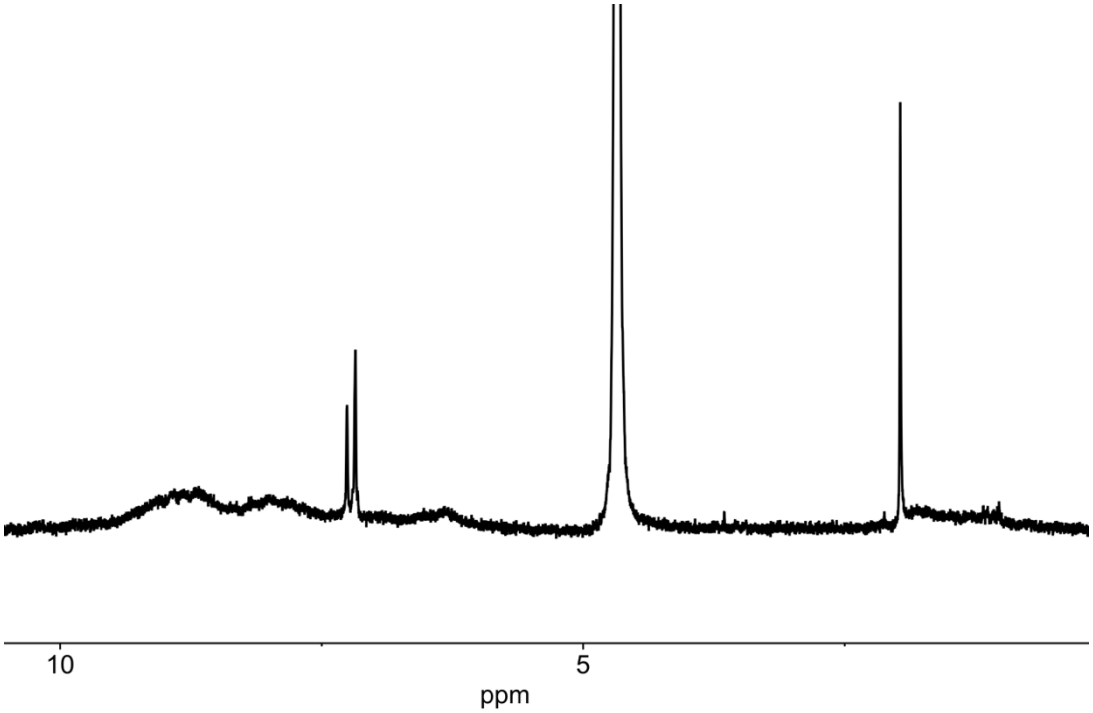

Figure S49: ^{1}H NMR spectrum (500 MHz, 298 K, D_2O) following attempted direct assembly from Ag_2SO_4. No six-stranded helicate formation was observed. Extensive precipitation was seen.

S7. Investigation of Equilibrium between Helicate 5 and Tetrahedron 6

We sought to influence the equilibrium between tetrahedron **6** and helicate **5** by adding prospective guests. The self-assembly of **3**, **1** and silver triflimide in acetonitrile initially formed a 95:5 ratio of tetrahedron **6** to helicate **5**. Although NMR spectral changes consistent with host-guest interactions were seen with multiple anionic species and neutral organic molecules (*vide infra*), no factors were identified that would enable consistent control over the tetrahedron⇌helicate equilibrium. The addition of tetrabutylammonium (TBA) acetate or benzoate led to a 65:35 ratio of **6**:**5**. The greatest shift in the equilibrium was observed on the addition of potassium polysulfide, where a 41:59 ratio of **6**:**5** was observed (Figure S48).

Using silver hexafluorophosphate we observed the predominant formation of Ag_8L_6 species **6** (Figure S30). Hexafluorophosphate has previously been shown to template the assembly tetrahedra of a similar size.[1] However, in this case we observed additional peaks in the ^{19}F and ^{31}P spectra (Figure S31+S32) alongside free hexafluorophosphate. These peaks correspond to difluorophosphate,[2] and integration suggests one equivalent of difluorophosphate forms per **6**. We infer that **6** induced the hydrolysis of an equivalent of hexafluorophosphate to form difluorophosphate, which is bound within the tetrahedral cavity of **6**, and is in turn protected from further hydrolysis by encapsulation.[70]

S7.1 Control of ratio of 5 to 6

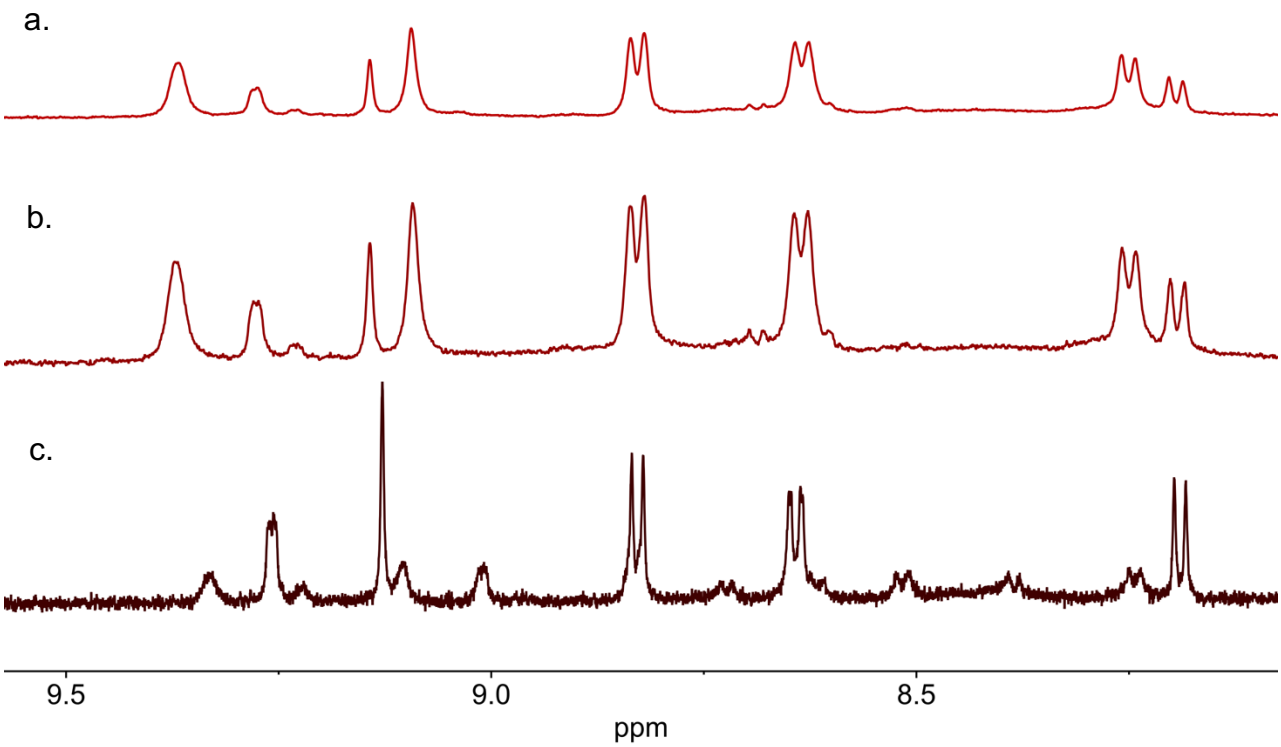

Figure S50: Partial ^{1}H NMR spectrum (500 MHz, 298 K, CD_3CN) of **1**, **3** and $AgNTf_2$ with addition of 2 eq. of a. TBA benzoate (35% **5**, 65% **6**), b. TBA acetate (35% **5**, 65% **6**) and c. Potassium polysulfide (59% **5**, 41% **6**).

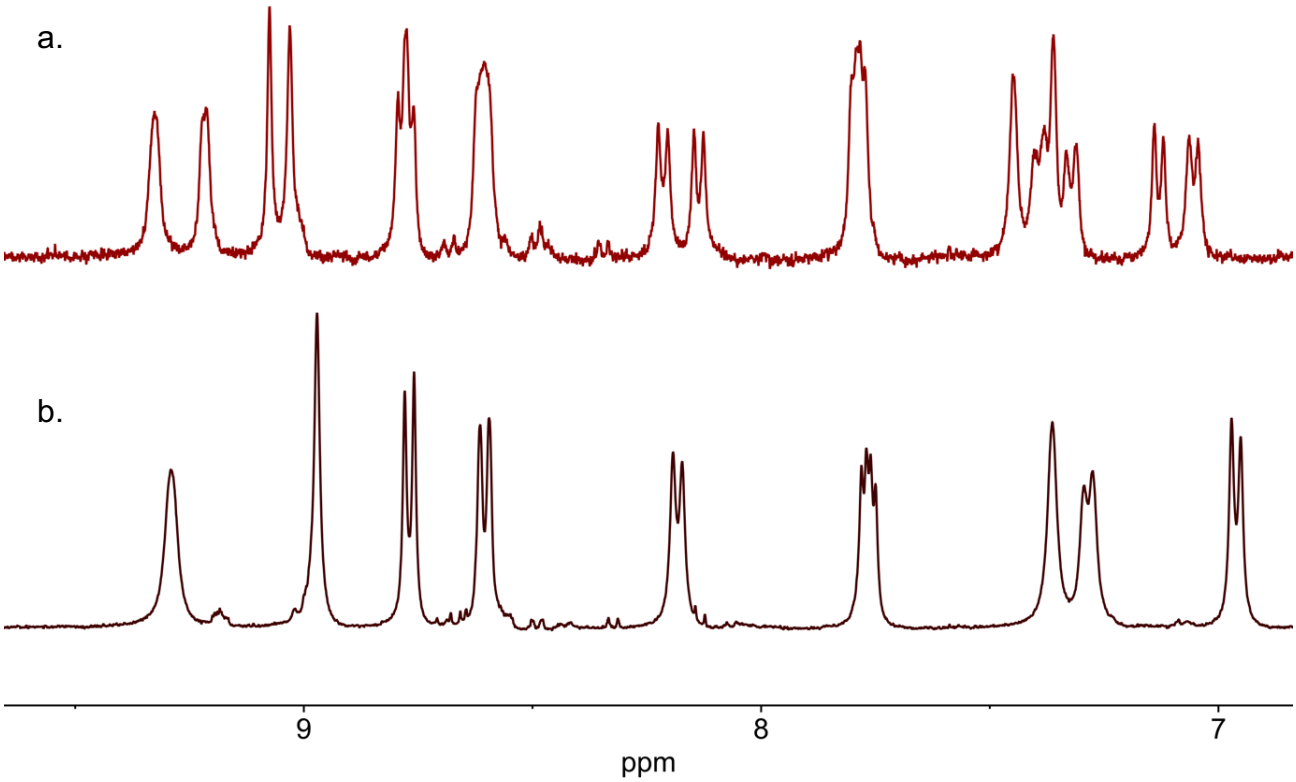

Figure S51: Partial ^{1}H NMR spectrum (500 MHz, 298 K, CD_3CN) of **1**, **3** and a. $AgClO_4$ (50% **5**, 50% **6**) or b. AgOTf (5% **5**, 95% **6**).

No clear correlation between hydrogen-bonding ability or size of the anion and the ratio of **5**:**6** formed could be inferred from these data. We hypothesize that the interplay of hydrogen-bonding ability, size complementarity, and solvation effects together determine the ratio of **5**:**6** formed.

S7.2 Guest binding to 5 and 6

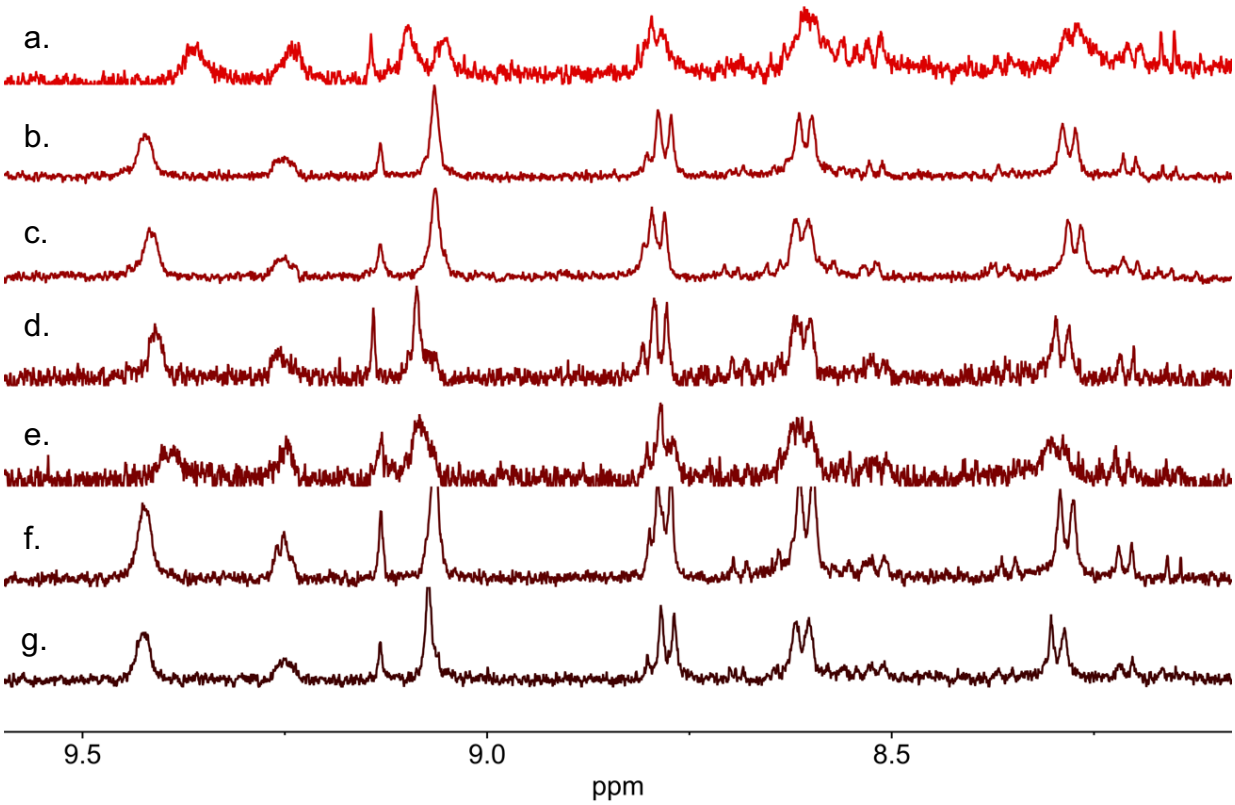

Figure S52: Partial ^{1}H NMR spectrum (500 MHz, 298 K, CD_3CN) of **5**, **6** and a. cyclohexane, b. TBA perrhenate, c. TBA tetrafluoroborate, d. TBA nitrate, e. trimethoxybenzene, f. TBA triflate or g. no added guest. Binding, but no structural transformation, was seen for these guests.

S7.3 Effect of Concentration on Equilibrium between 5 and 6

We saw no effect on the equilibrium between **5**:**6** when changing the overall concentration in the system, corresponding to initial 1,8-naphthyridine carboxaldehyde concentrations between 0.78 mM and 50 mM.

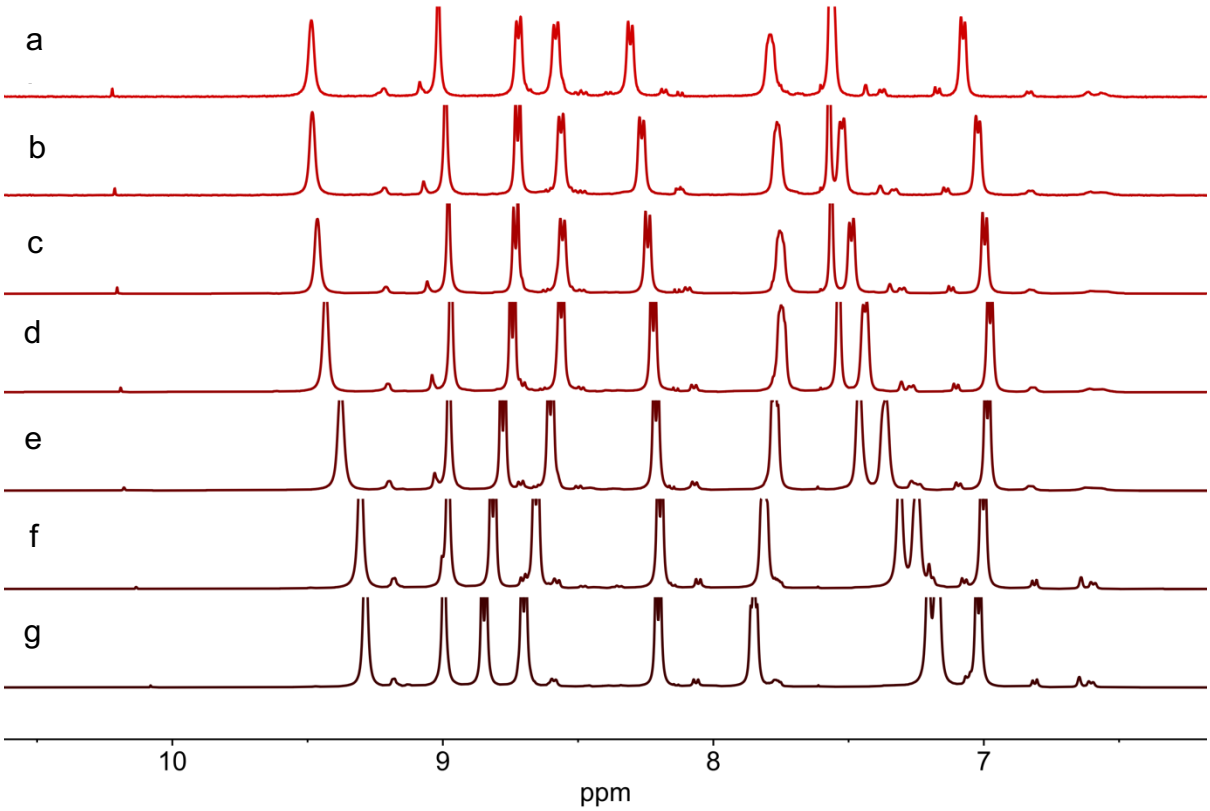

Figure S53: Partial ^{1}H NMR spectra (500 MHz, 298 K, CD_3CN) of assembly of **5** and **6** using $AgNTf_2$. Although concentration-dependent shifts were seen, no shift in the **5**:**6** equilibrium was observed. a. 0.78 mM, b. 1.56 mM, c. 3.13 mM, d. 6.25 mM, e. 12.5 mM, f. 25 mM and g. 50 mM of initial 1,8-naphthyridine carboxaldehyde in the system.

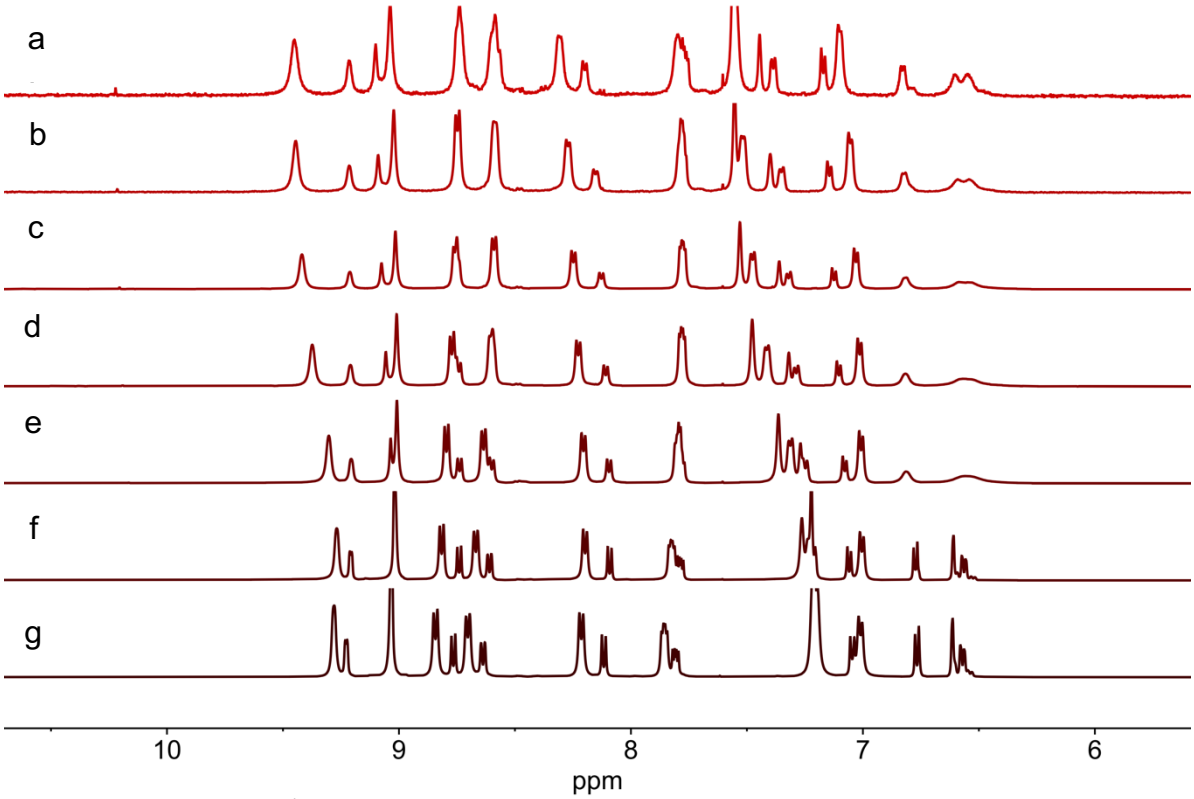

Figure S54: Partial ^{1}H NMR spectra (500 MHz, 298 K, CD_3CN) of assembly of **5** and **6** using AgOTf. Although concentration-dependent shifts were seen, no shift in the **5**:**6** equilibrium was observed. a. 0.78 mM, b. 1.56 mM, c. 3.13 mM, d. 6.25 mM, e. 12.5 mM, f. 25 mM and g. 50 mM of initial 1,8-naphthyridine carboxaldehyde in the system.

S8. Attempts to assemble architectures with 1,1'-biphenyl-4,4'-diamine

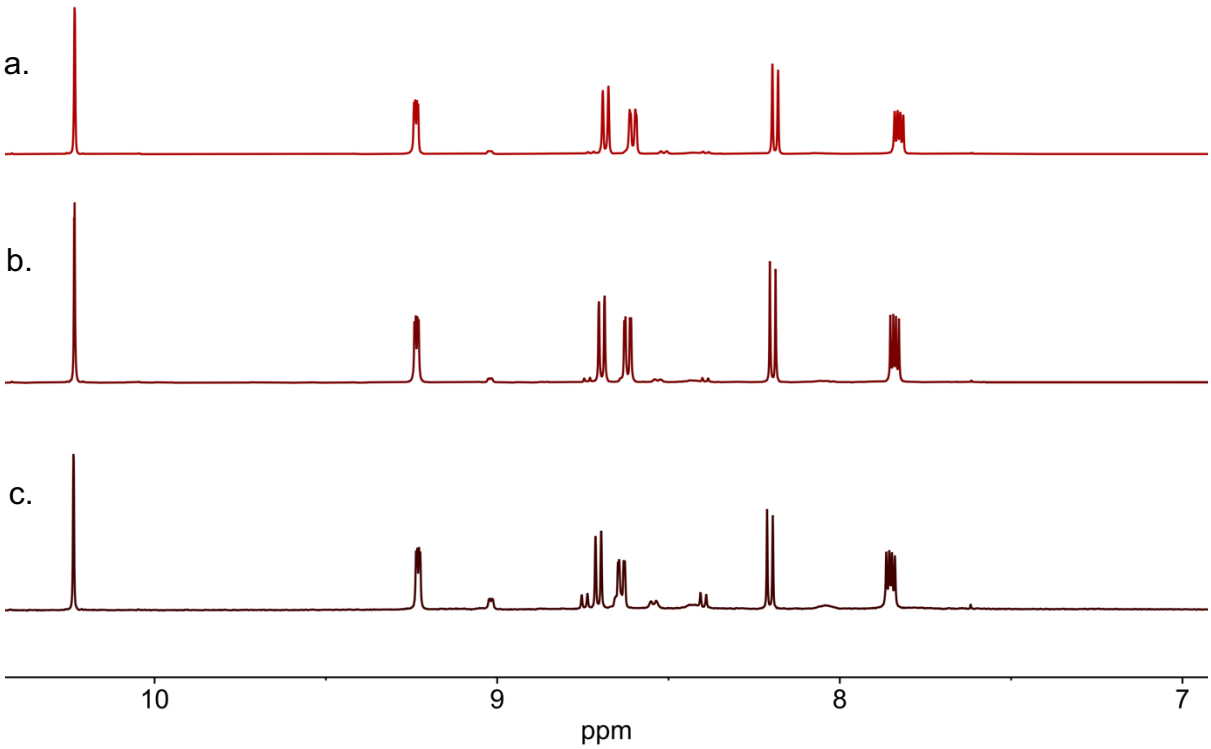

Figure S55: Partial ^{1}H NMR spectrum (500 MHz, 298 K, CD_3CN) of attempted assembly of **1** (2 eq.), **2** (1 eq.) and a. AgOTf (4 eq.), b. $AgNTf_2$ (4 eq.), or c. $AgClO_4$ (4 eq.). In all cases intractable gels formed, and 2-formyl-1,8-naphthyridine **1** remained in solution.

S9. MM3 Models and calculated energies of 6

Structures and energies were calculated using Scigress, running MM2 followed by MM3 calculations until convergence was achieved. The tetrahedral structure proposed in the paper was found to be greatly (c. 3-400 Kcal/mol) more stable than alternate structures, supporting the assignation of this architecture.

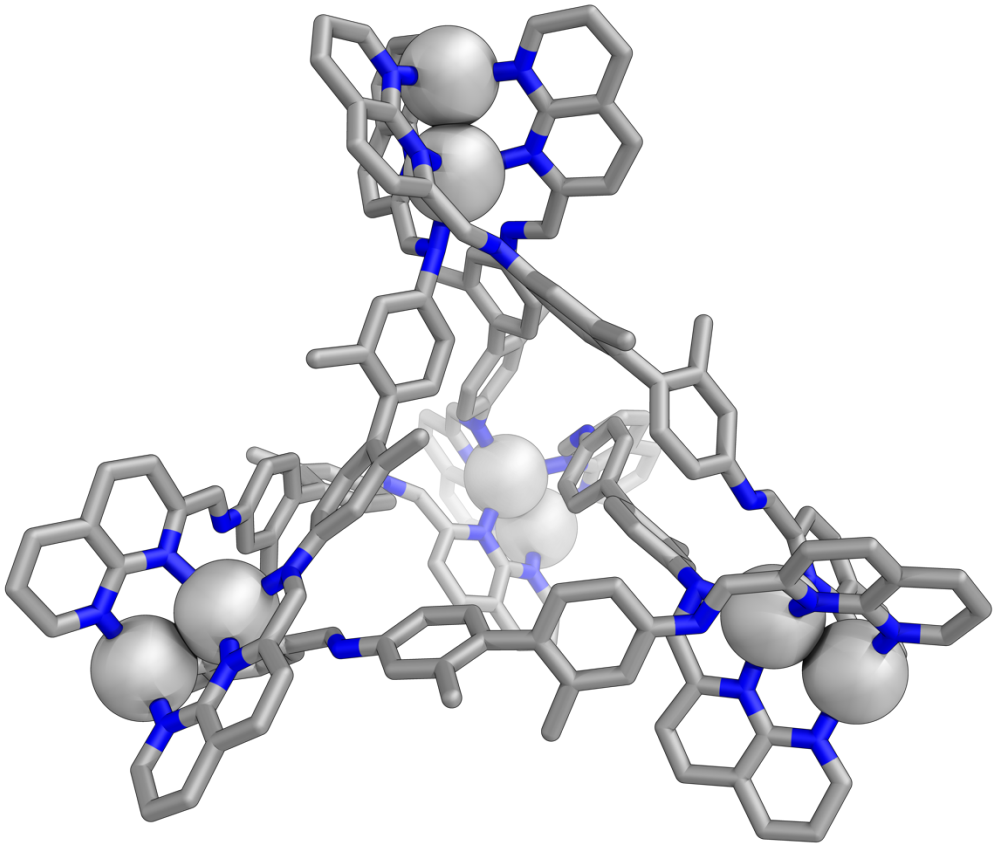

Figure S56: Calculated energy of MM3 optimised structure: 785 Kcal/mol. If we consider an additional acetonitrile ligand on each external silver(I) ion, as coordinating solvent, the calculated energy drops further to 548 kcal/mol.

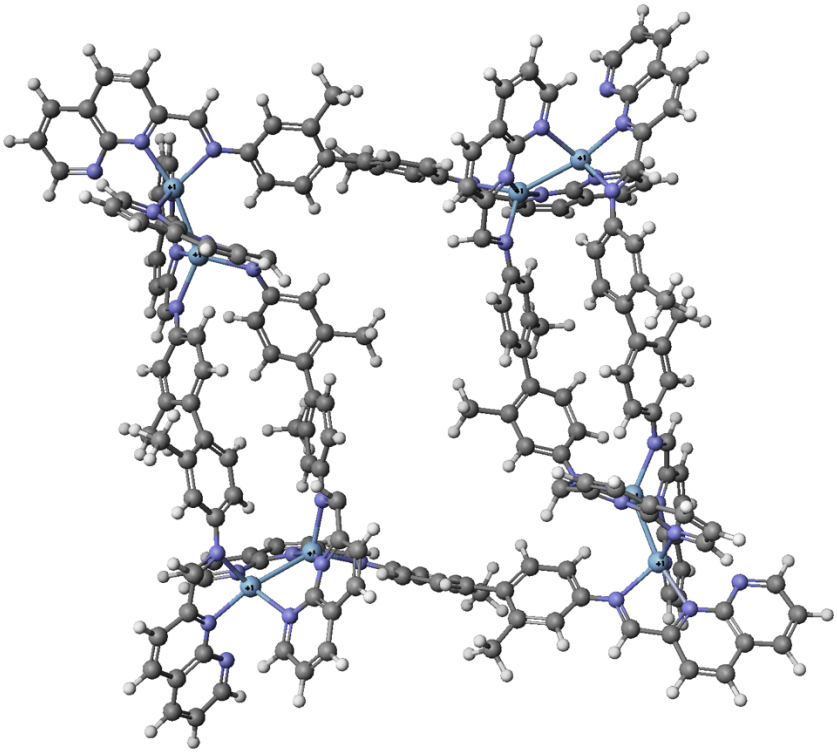

Figure S57: Alternate structure, calculated energy: 1153 kcal/mol

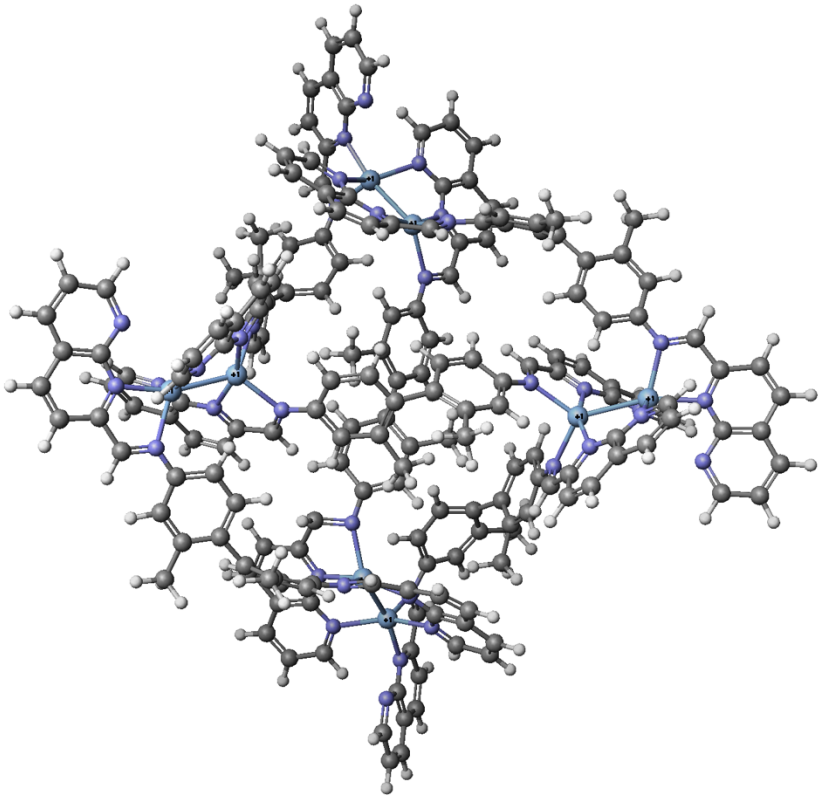

Figure S58: Second alternate structure, calculated energy: 1281 kcal/mol.

S10. Investigation of behaviour of 7 and 8

Similar reaction outcomes to that observed with diamine **3** were observed when diamine **4**, which contains CF_3-substituents in the place of the CH_3-groups of **3**, was used in the self-assembly reaction. Assembly of **4**, **1** and the perchlorate, triflate, hexafluorophosphate or triflimide salt of silver(I) in acetonitrile led to a mixture of helicate **7** and tetrahedron **8**. A **7**:**8** ratio of 6:94 was obtained in the case of silver perchlorate versus 42:58 when silver triflate was used (S61). The two species could again be distinguished by DOSY, which showed two species with the diffusion coefficient of one significantly larger that of the other (Figure S62). Attempts at purification by precipitation resulted in the formation of material that did not redissolve, and was thus inferred to be polymeric. The ions corresponding to **7** and **8** could be observed in the mass spectra, supporting our assignment of Ag_4L_3 and Ag_8L_6 species (Figure S69).

S10.1 Assembly of 7 and 8

To 2,2'-ditrifluoromethyl-[1,1'-biphenyl]-4,4'-diamine (**4**) (8.0 mg, 0.025 mmol, 6 eq.), 2-formyl-1,8-naphthyridine (**1**) (8.0 mg, 0.051 mmol, 12 eq.), and silver triflimide (21.3 mg, 0.055 mmol, 12 eq.) was added a magnetic stirrer and acetonitrile (2.5 ml). The assembly was sonicated until a homogenous solution was formed. This system could not be recovered after precipitation (insoluble polymers were formed) and so was analysed without further purification.

^{1}H NMR (500 MHz, CD_3CN) δ: 9.24 (1H, dd, *J* = 4.6, 1.9, $H_{1\text{-tet}}$), 9.16 (1H, dd, *J* = 4.6, 1.9, $H_{1\text{-hel}}$), 9.07 (1H, s, $H_{9\text{-hel}}$), 9.05 (1H, s, $H_{9\text{-tet}}$), 8.83 (1H, d, *J* = 8.3 Hz, $H_{6\text{-tet}}$), 8.80 (1H, d, *J* = 8.4 Hz, $H_{6\text{-hel}}$), 8.65 (1H, dd, *J* = 8.4, 1.8 Hz, $H_{3\text{-tet}}$), 8.61 (1H, dd, *J* = 8.2, 1.9 Hz, $H_{3\text{-hel}}$), 8.26 (1H, d, *J* = 8.2 Hz, $H_{7\text{-tet}}$), 8.19 (1H, d, *J* = 8.1 Hz, $H_{7\text{-hel}}$), 7.80 (1H, dd, *J* = 8.3, 4.3 Hz, $H_{2\text{-tet}}$), 7.76 (1H, dd, *J* = 7.7, 4.1 Hz, $H_{2\text{-hel}}$), 7.73 (1H, d, *J* = 1.8 Hz, $H_{15\text{-tet}}$), 7.68 (1H, d, *J* = 2.2 Hz, $H_{15\text{-hel}}$), 7.61 (1H, dd, *J* = 8.3, 1.8 Hz, $H_{11\text{-tet}}$), 7.55 (1H, dd, *J* = 8.1, 2.1 Hz, $H_{11\text{-hel}}$), 7.36 (1H, d, *J* = 8.6 Hz, $H_{12\text{-hel}}$), 7.34 (1H, d, *J* = 8.1 Hz, $H_{12\text{-tet}}$).

^{13}C NMR (126 MHz, CD_3CN) δ: 162.1, 161.3, 158.2, 158.1, 156.9, 154.2, 153.9, 153.9, 153.7, 149.6, 149.5, 148.5, 143.0, 142.9, 141.4, 140.2, 140.1, 139.9, 137.1, 135.2, 134.2, 133.5, 127.1, 126.3, 125.8, 125.4, 125.1, 124.6 (q, *J* = 274 Hz), 124.5 (q, *J* = 275 Hz), 120.8 (q, *J* = 321 Hz), 120.1, 117.2, 112.0.

^{19}F NMR (376 MHz, CD_3CN) δ: − 80.16.

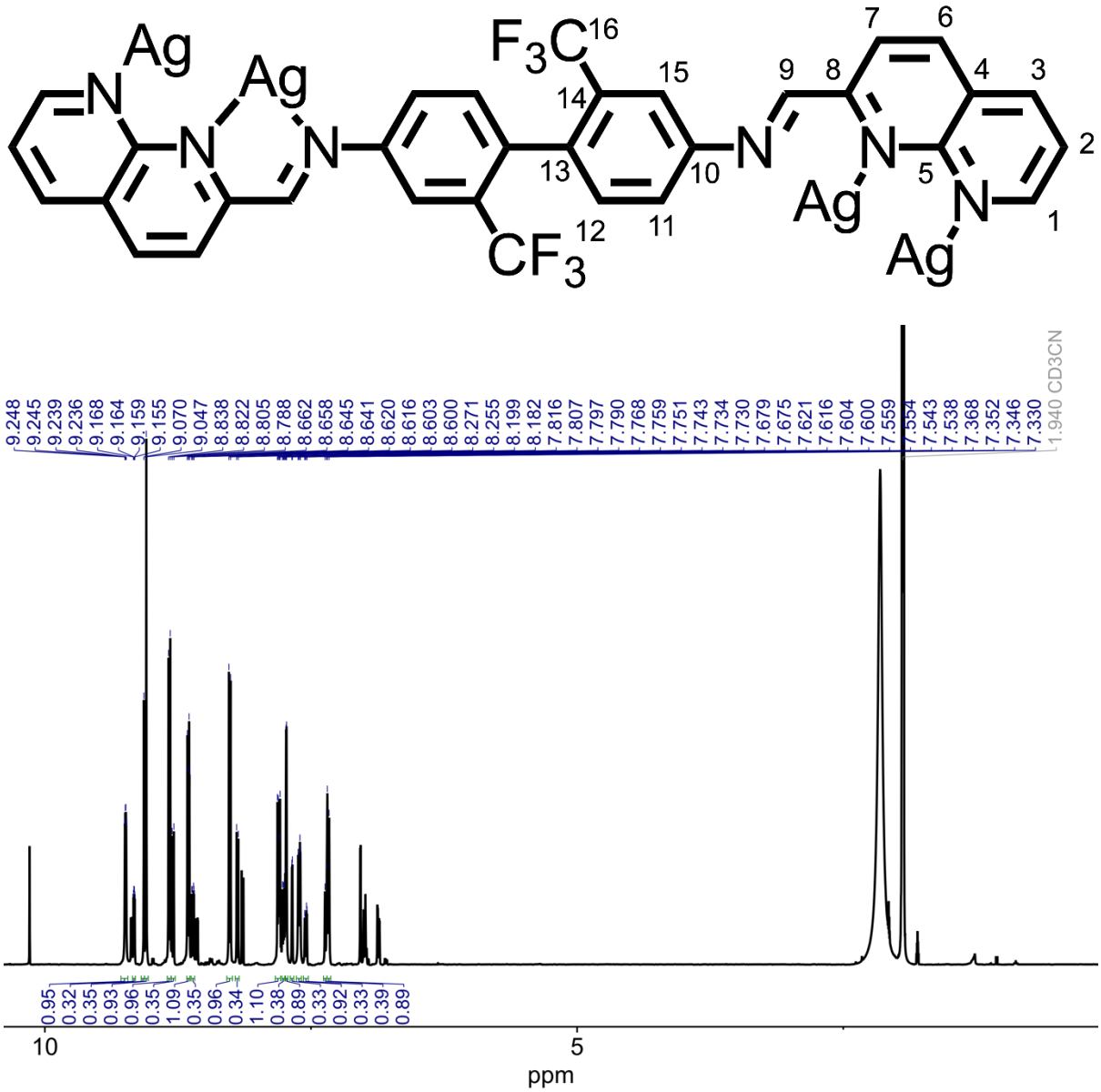

Figure S59: ^{1}H NMR spectrum (500 MHz, 298 K, CD_3CN) of **7** and **8**. Residual naphthyridine and **4** have not been peak picked.

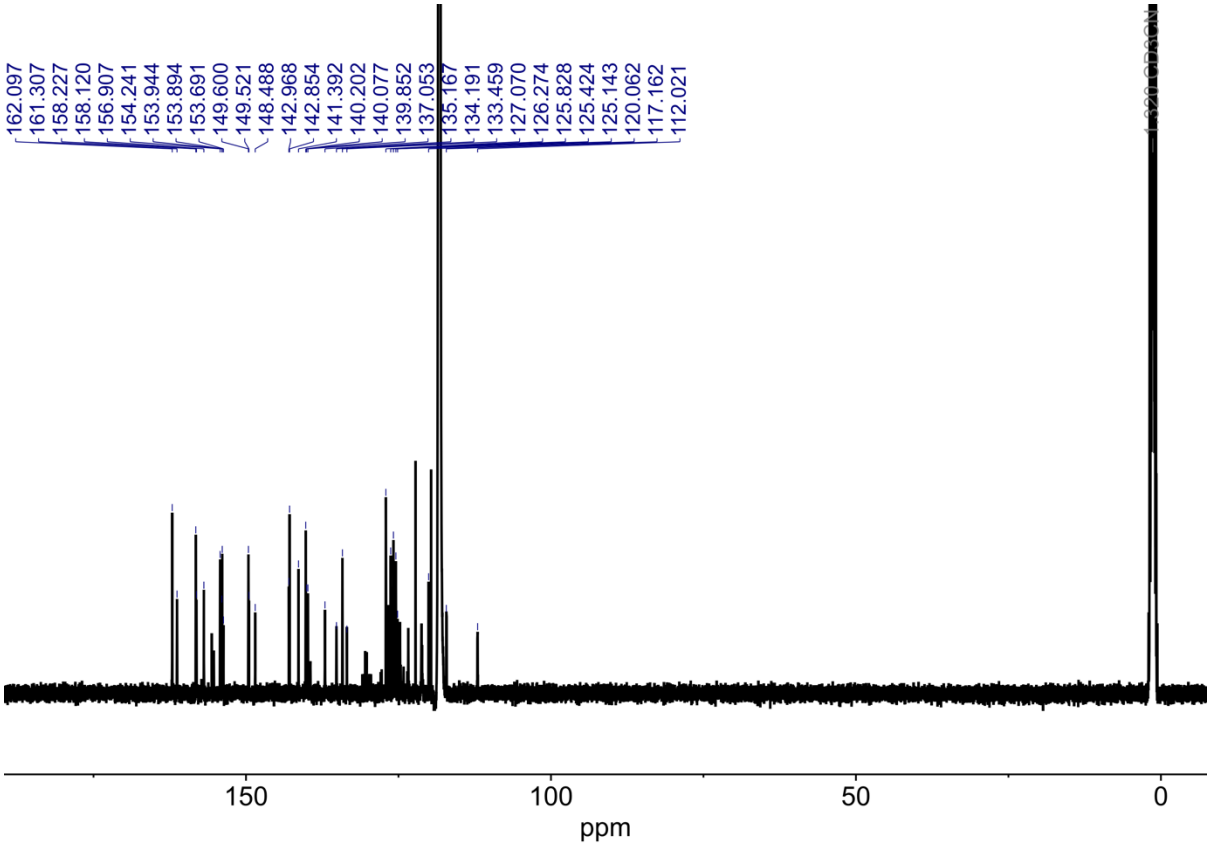

Figure S60: ^{13}C NMR spectrum (126 MHz, 298 K, CD_3CN) of **7** and **8**. Residual naphthyridine and **4** have not been peak picked.

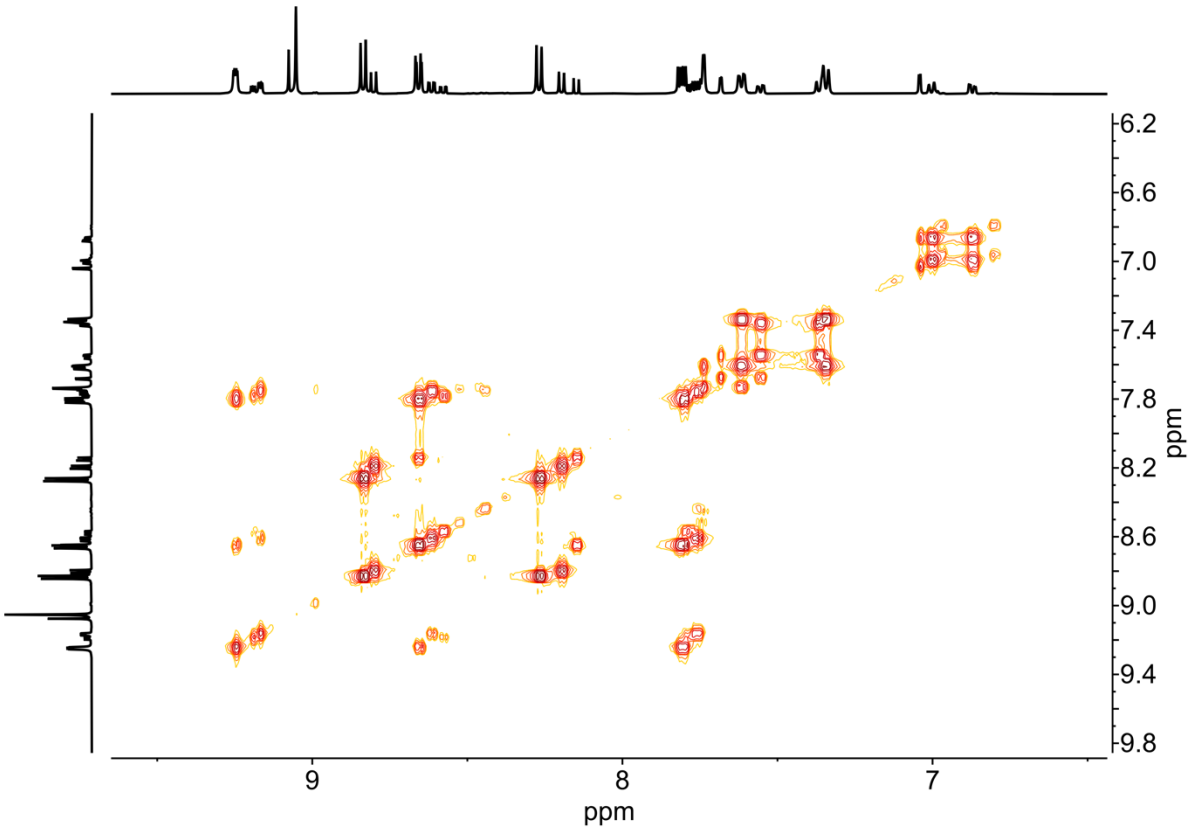

Figure S61: COSY NMR spectrum (500 MHz, 298 K, CD_3CN) of **7** and **8**.

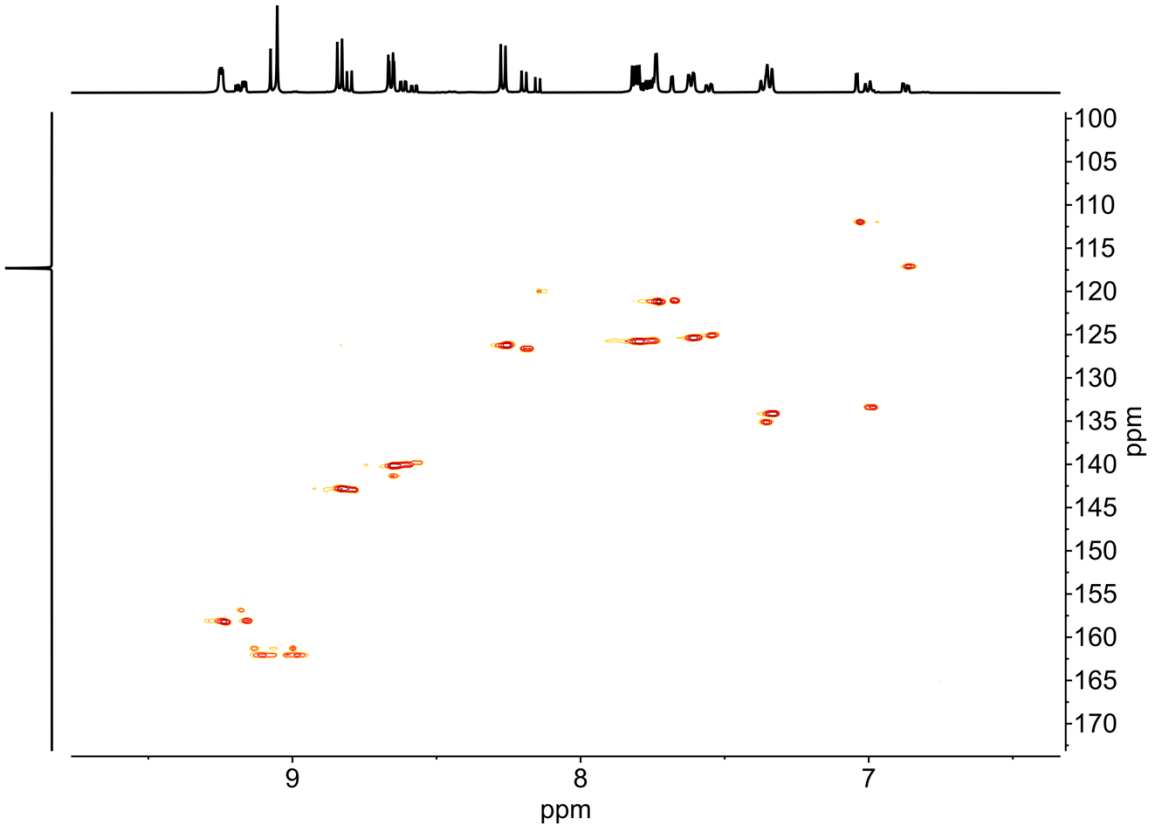

Figure S62: HSQC NMR spectrum (500 MHz, 298 K, CD_3CN) of **7** and **8**.

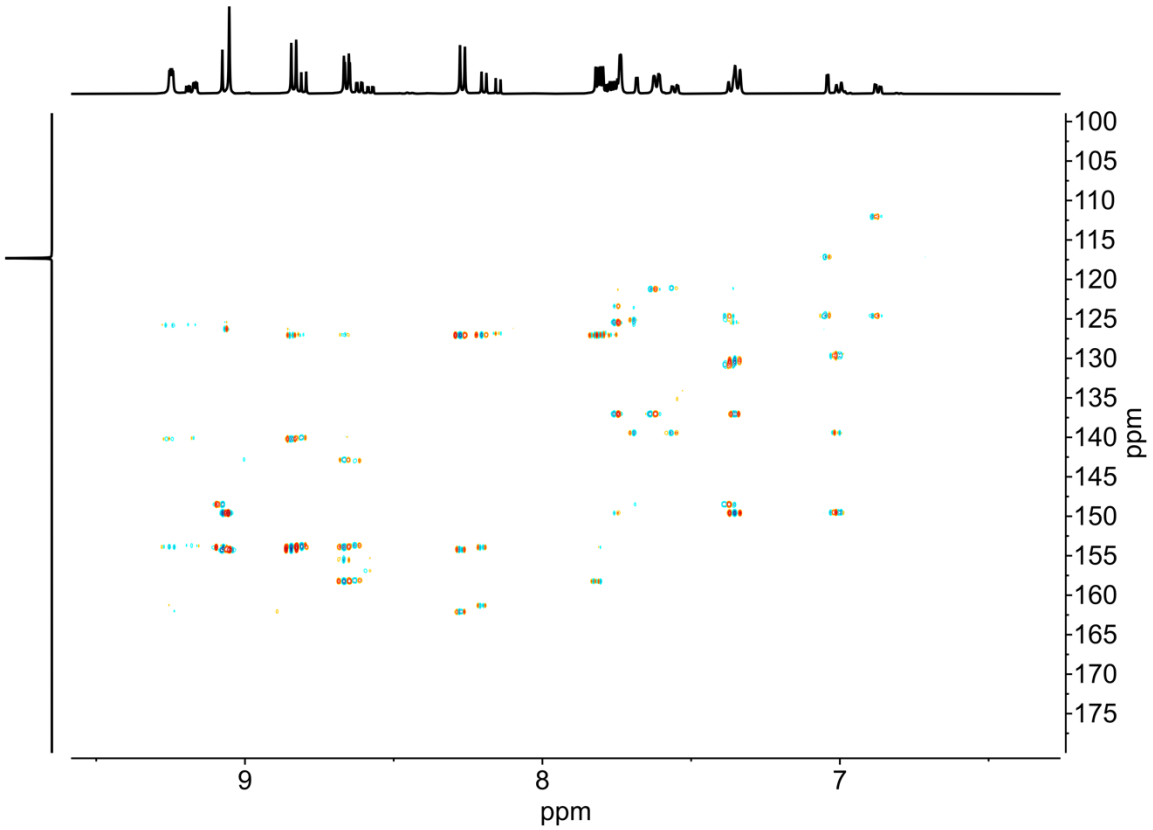

Figure S63: HMBC NMR spectrum (500 MHz, 298 K, CD_3CN) of **7** and **8**.

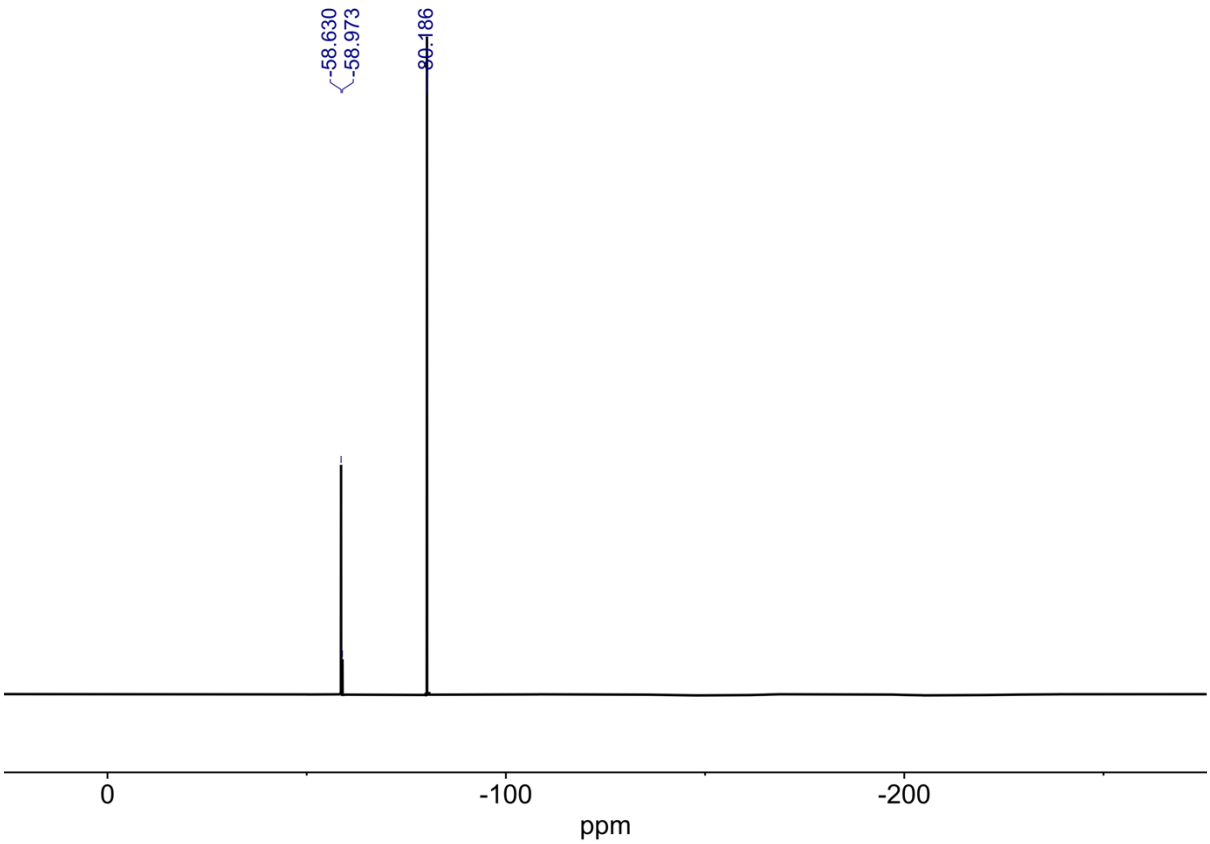

Figure S64: ^{19}F NMR spectrum (471 MHz, 298 K, CD_3CN) of **7** and **8**.

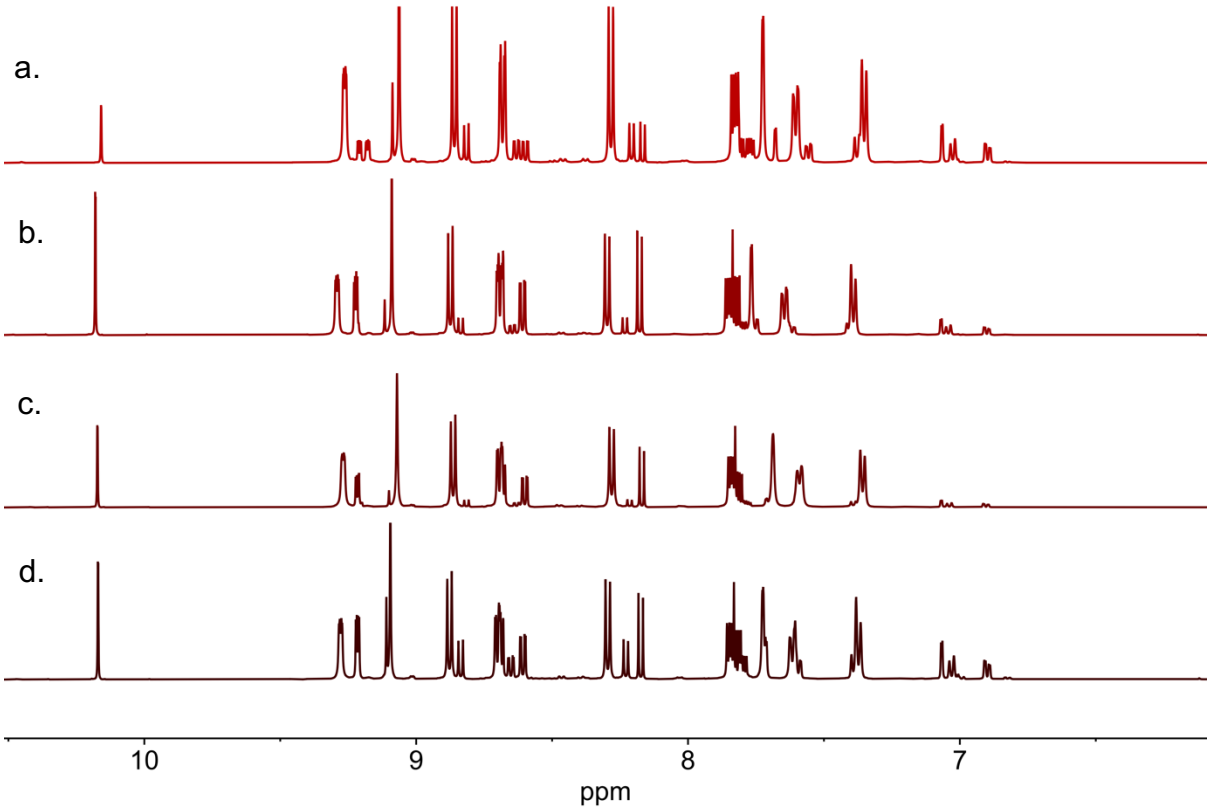

Figure S65: Partial ^{1}H NMR spectrum (500 MHz, 298 K, CD_3CN) of assembly of **1** and **4** with a. $AgNTf_2$ (**7**:**8** ratio 29:71), b. $AgPF_6$ (**7**:**8** ratio 25:75), c. $AgClO_4$ (**7**:**8** ratio 6:94) or d. AgOTf (**7**:**8** ratio 58:42). Residual naphthyridine and **4** were observed in all cases, and the assembly was not stable to precipitation, preventing their removal.

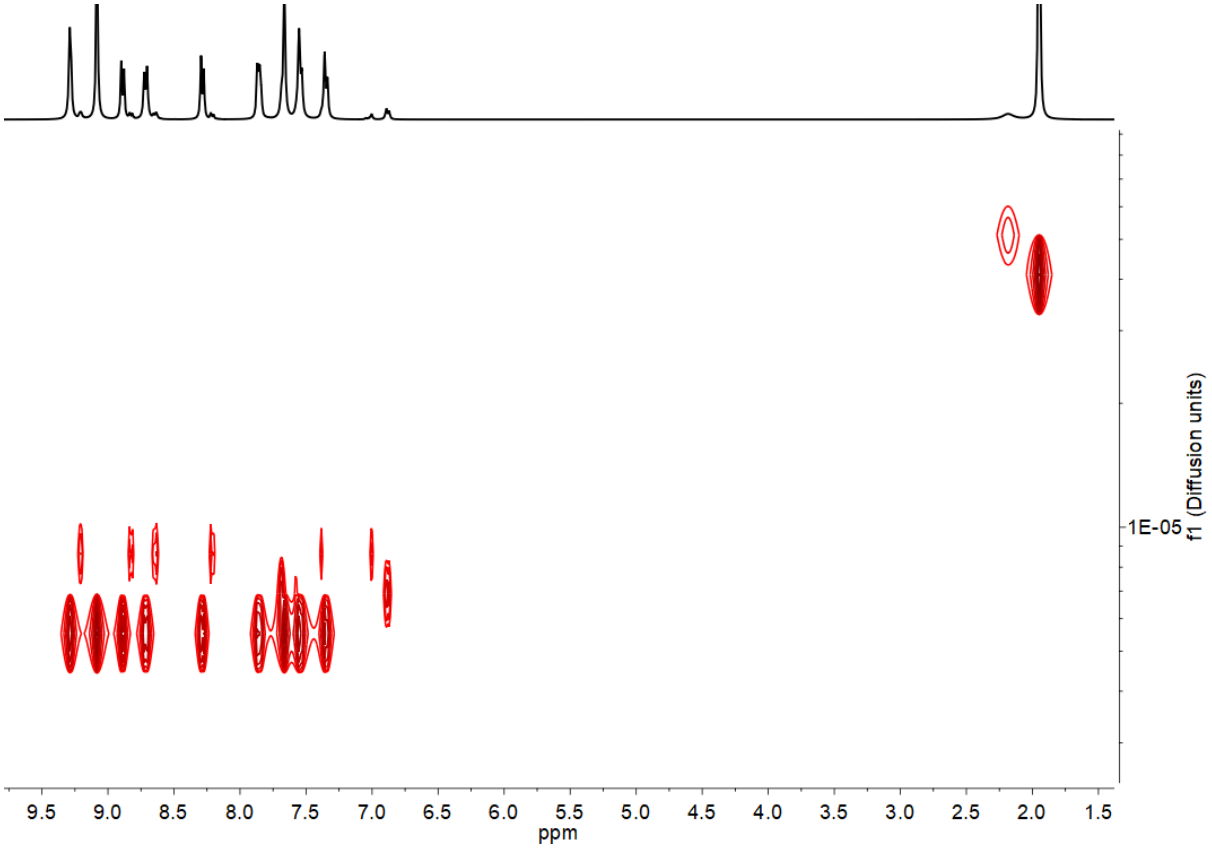

Figure S66: ^{1}H DOSY NMR spectrum (400 MHz, 298 K, CD_3CN) of **7** and **8** assembled with AgOTf. The diffusion coefficient of **7** was measured to be 1.04 x 10^{-5} cm^2 s^{-1}, and of **8** to be 6.17 x 10^{-6} cm^2 s^{-1} giving solvodynamic radii of 6.12 Å and 10.3 Å. These values are comparable with those generated by molecular models of the proposed structures.

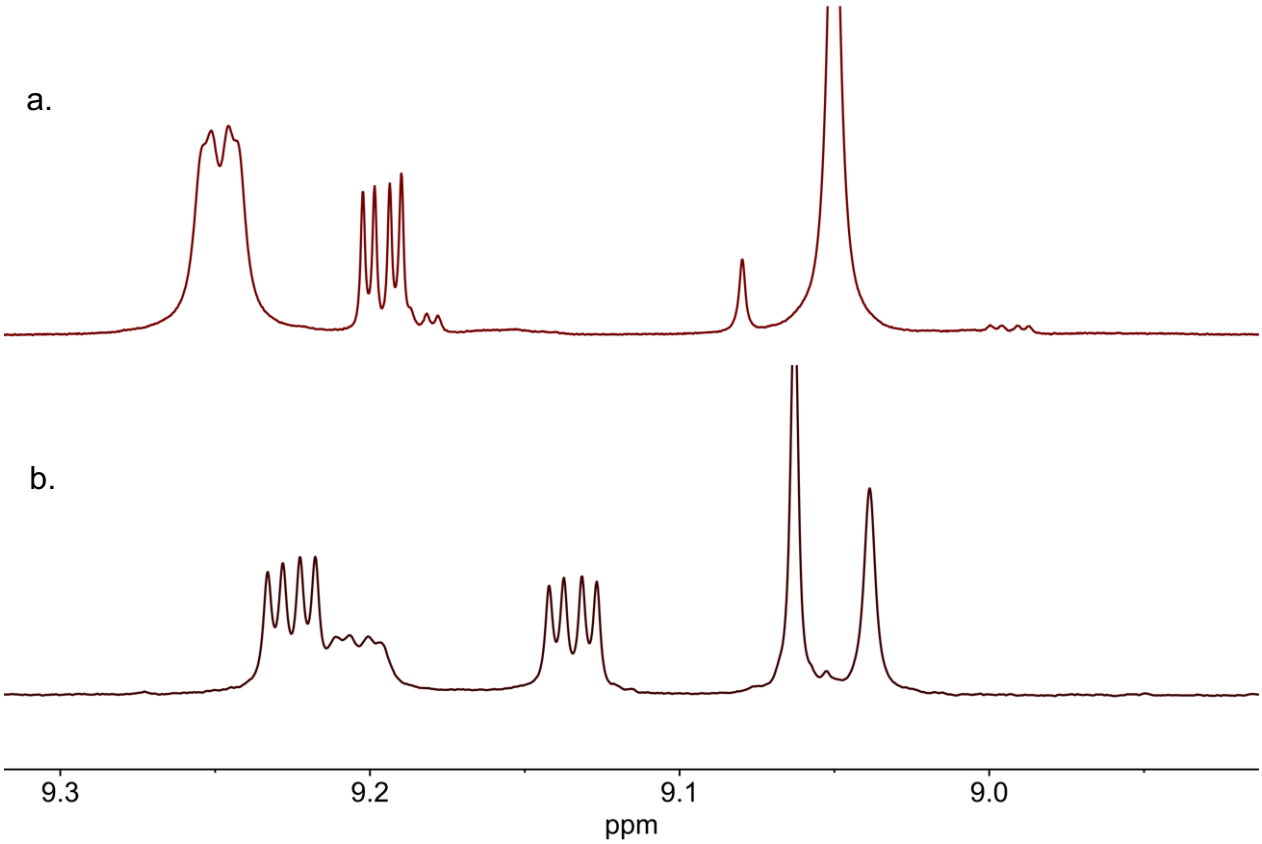

Figure S67: ^{1}H NMR spectrum (500 MHz, 298 K, CD_3CN) of assembly of **1** and **4** with a. AgClO4, showing 94:6 ratio of **8**:**7** architectures. b. AgNTf2 assembly after addition of 1 eq. of TBA bromide. No evidence of six-stranded helicate formation, but equilibrium shifts to 42:58 **8**:**7**, the maximum seen with addition of any anion.

S10.2 Addition of anions to 7 and 8

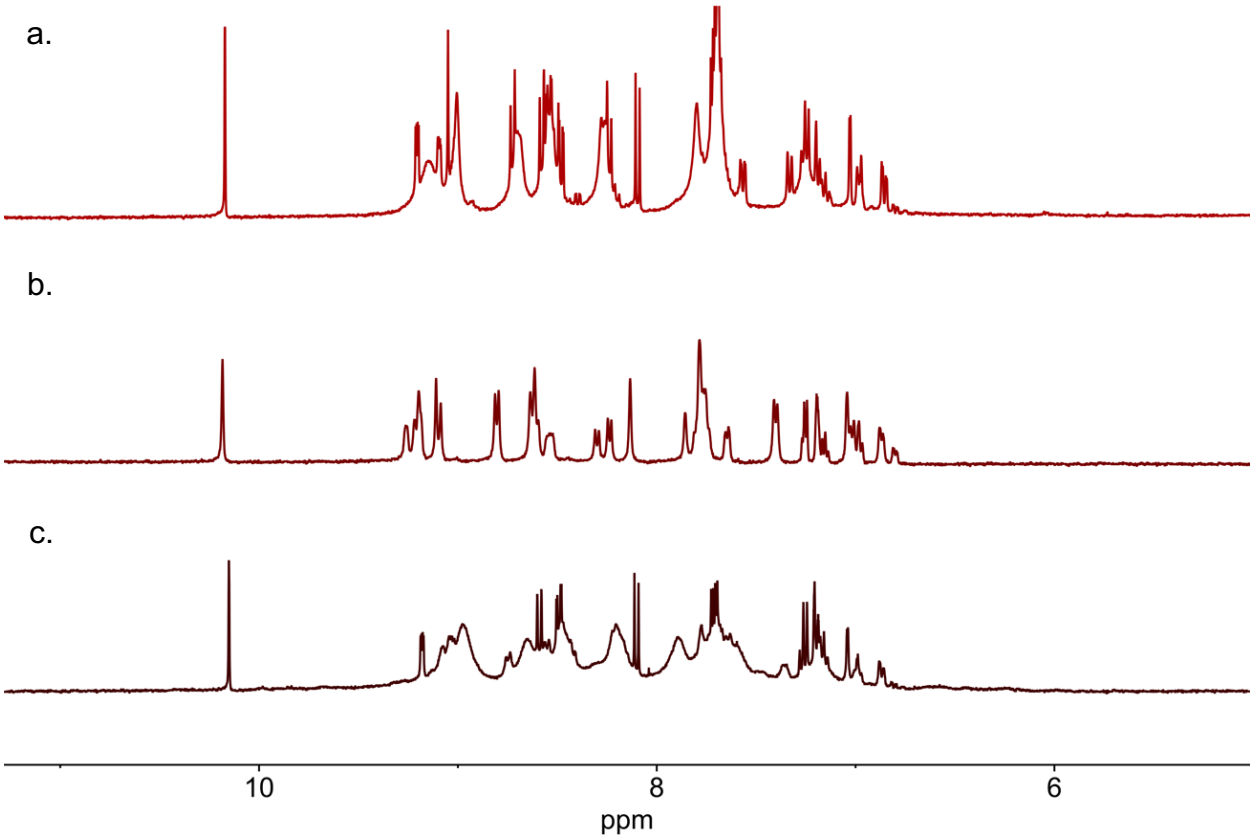

Figure S68: ^{1}H NMR spectrum (500 MHz, 298 K, CD_3CN) of $AgNTf_2$ assembly of **1** and **4** with 2 eq. of a. Tetramethylammonium bromide, b. Tetramethylammonium sulfate or c. TBA iodide. Destruction of **7** and **8** or a shift in **7**/**8** equilibrium was observed in all cases, with no evidence of formation of six-stranded helicate.

S11. Mass Spectrometry Data

Mass spectrometry of these silver complexes is challenging, presumably due to the dynamic nature of the naphthyridine-silver interactions. We see extensive fragmentation of all complexes under even mild conditions. Mass spectrometry data could be gathered with judicious choice of counterion and is detailed below.

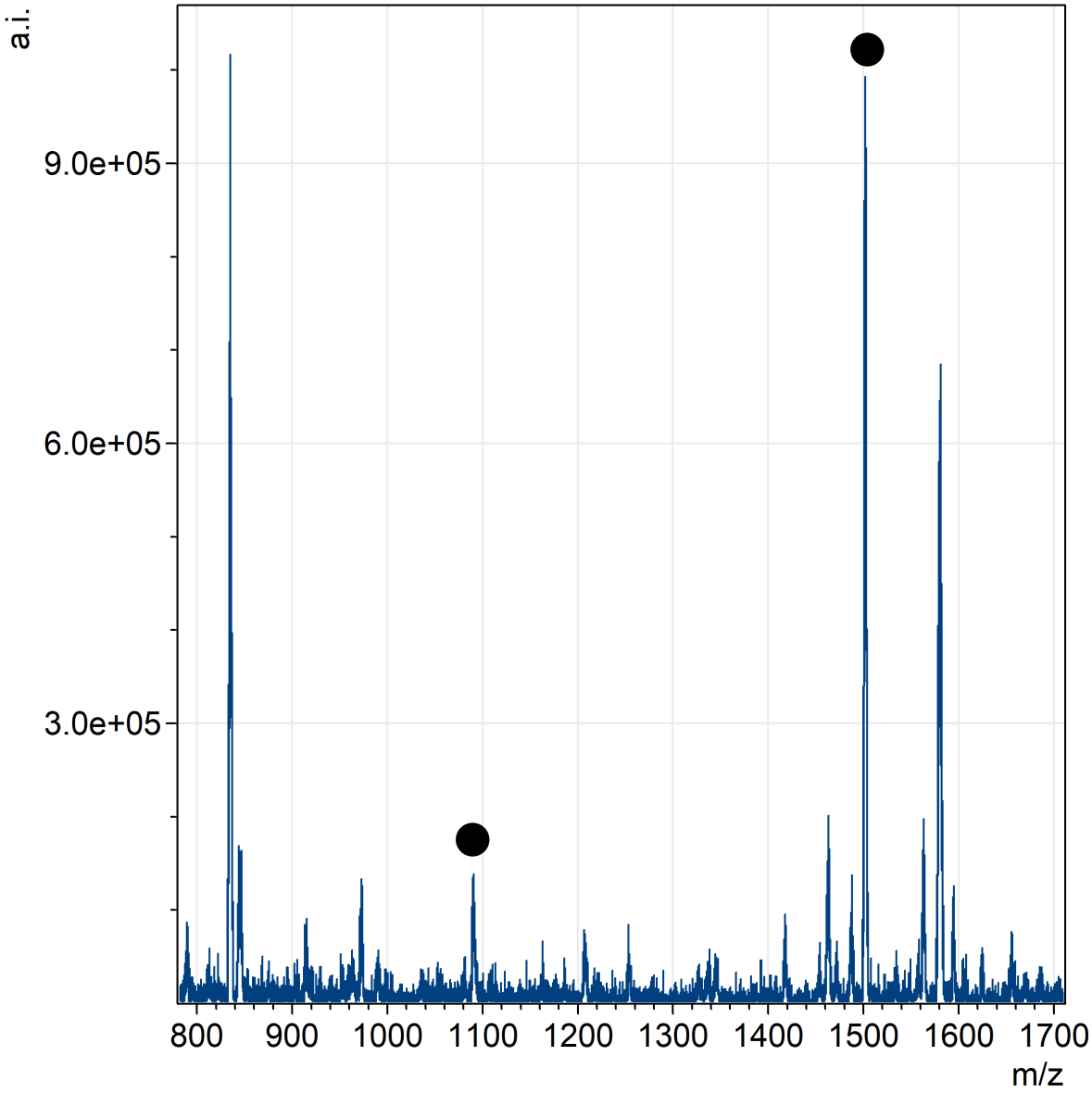

Figure S69: LRMS of iodide-templated six-stranded helicate **9**. Ions at 1502 (+3) and 1089 (+4). Counterion is hexafluorophosphate.

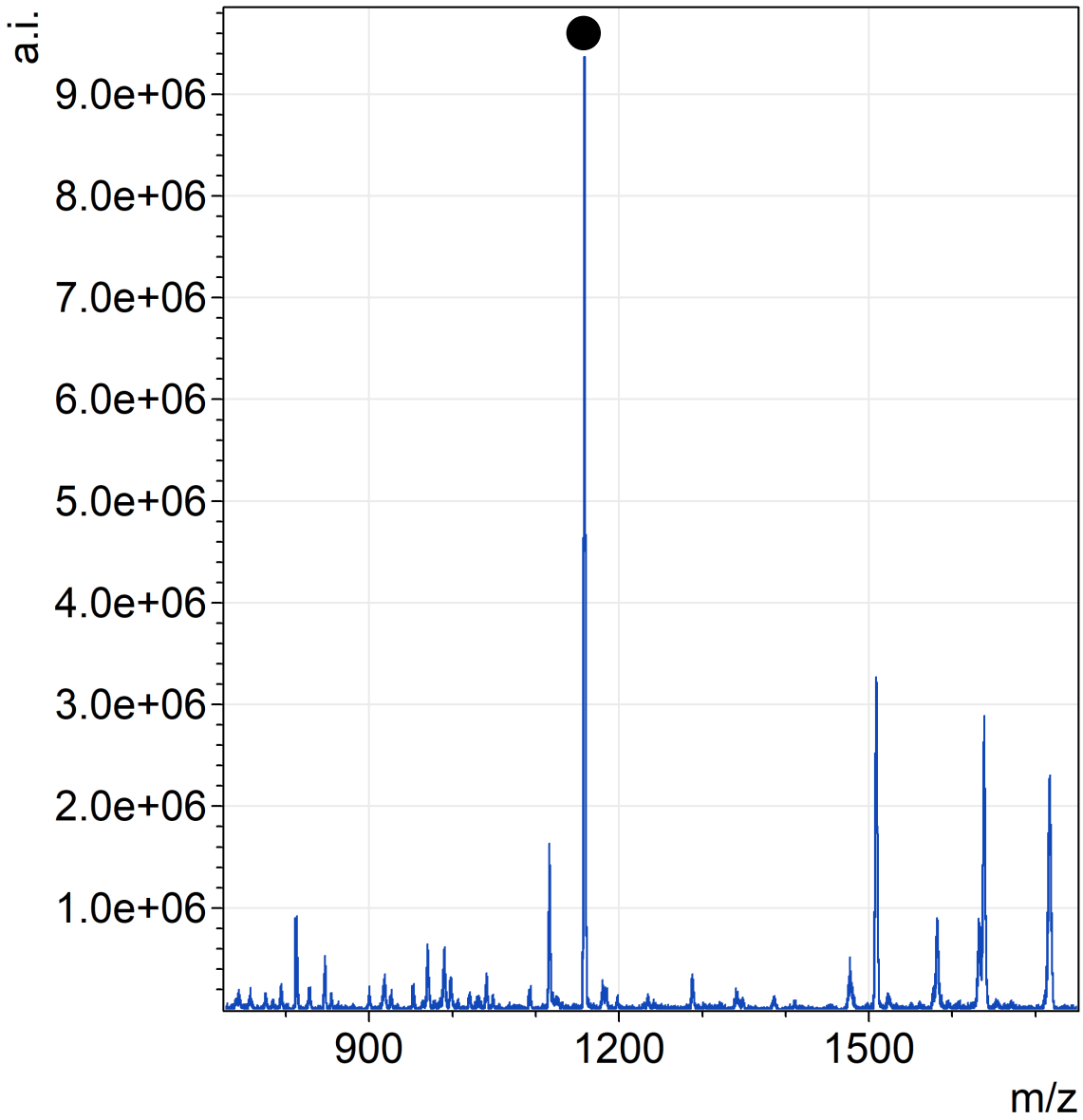

Figure S70: LRMS of sulfate-templated six-stranded helicate **10**. Ion observed at 1158 (+4). Counterion is triflimide.

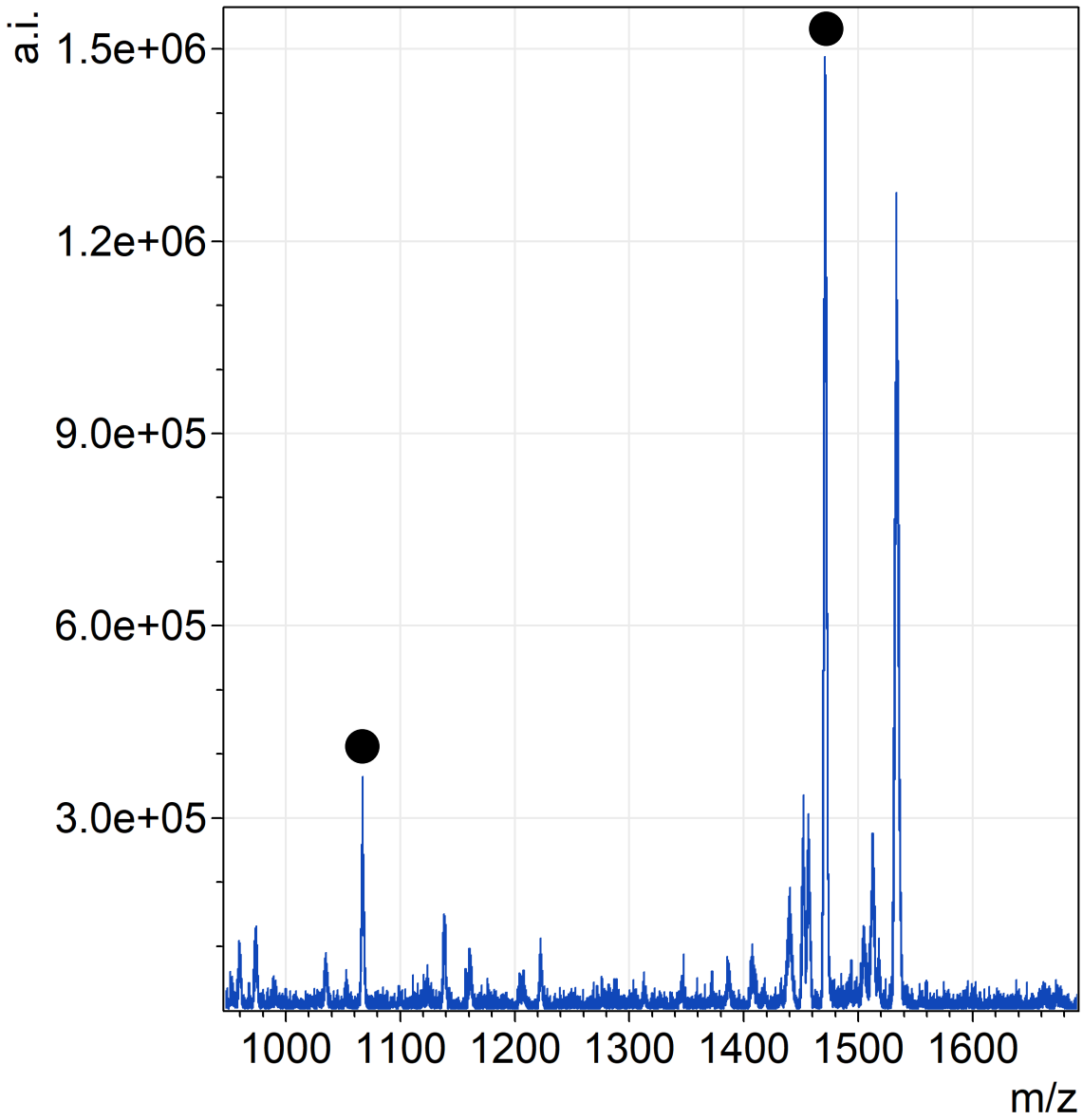

Figure S71: LRMS of bromide-templated six-stranded helicate **11**. Ions at 1067 (+4) and 1471 (+3) observed. Counterion is hexafluorophosphate.

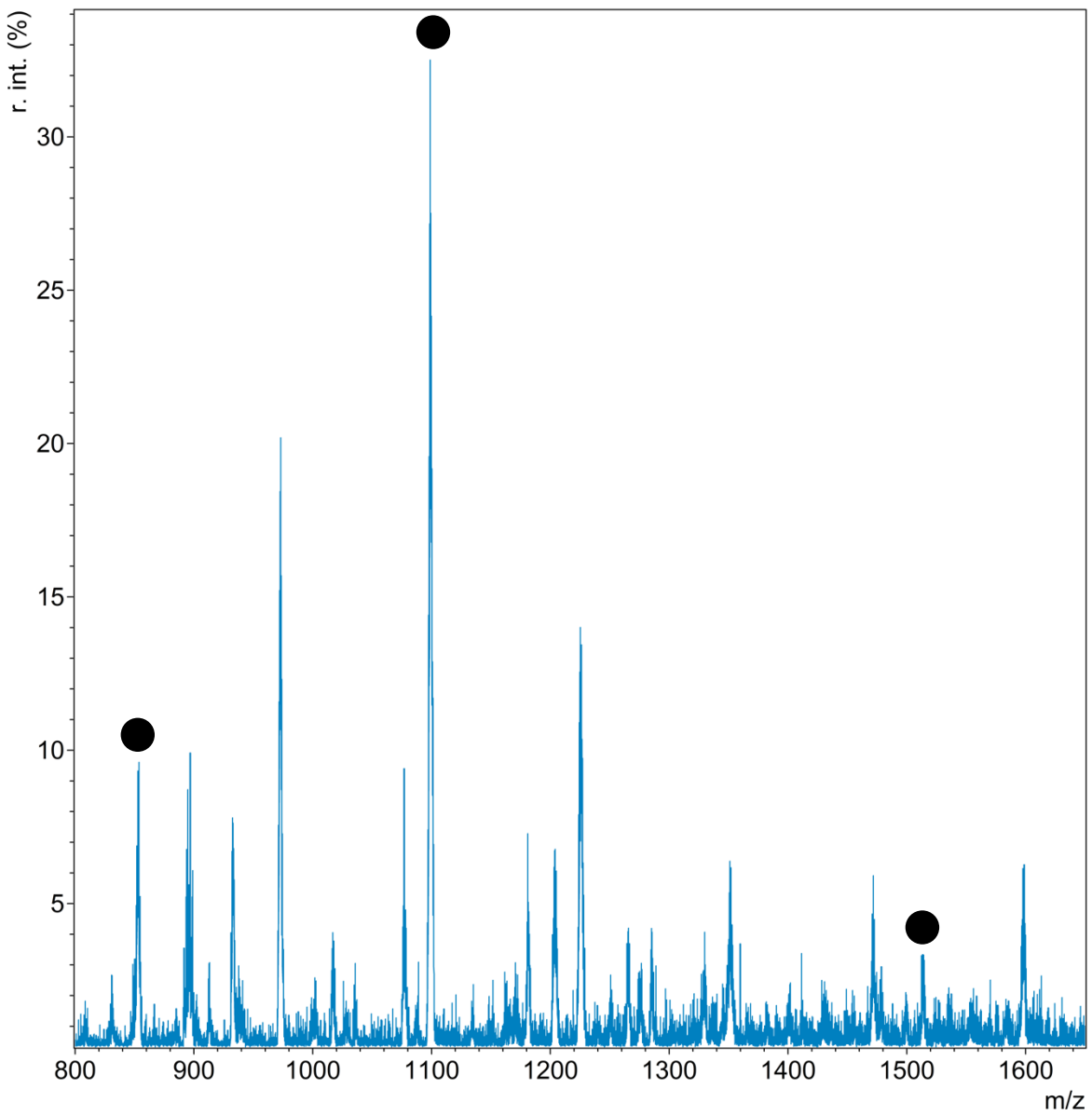

Figure S72: LRMS of helicate **5** and tetrahedron **6**. Counterion is hexafluorophosphate. Observed signals at 849 (tetrahedron, +5), 1098 (tetrahedron +4 or helicate +2) and 1512 (tetrahedron +3).

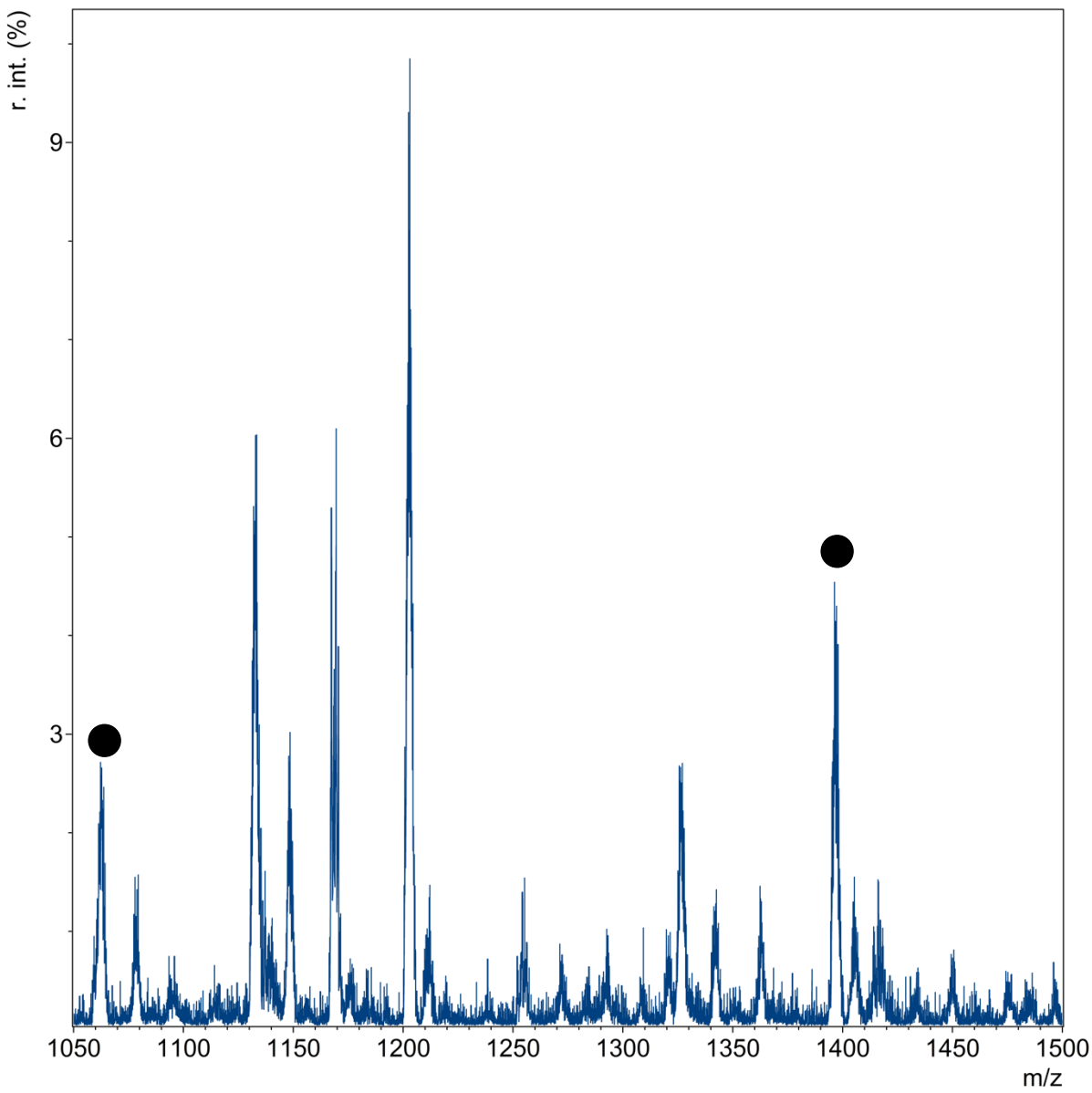

Figure S73: LRMS of helicate **7** and tetrahedron **8**. Counterion is triflimide. Signals observed at 1395 and 1060 corresponding to the +4 (or +2, for the helicate) and +5 states of the tetrahedron.

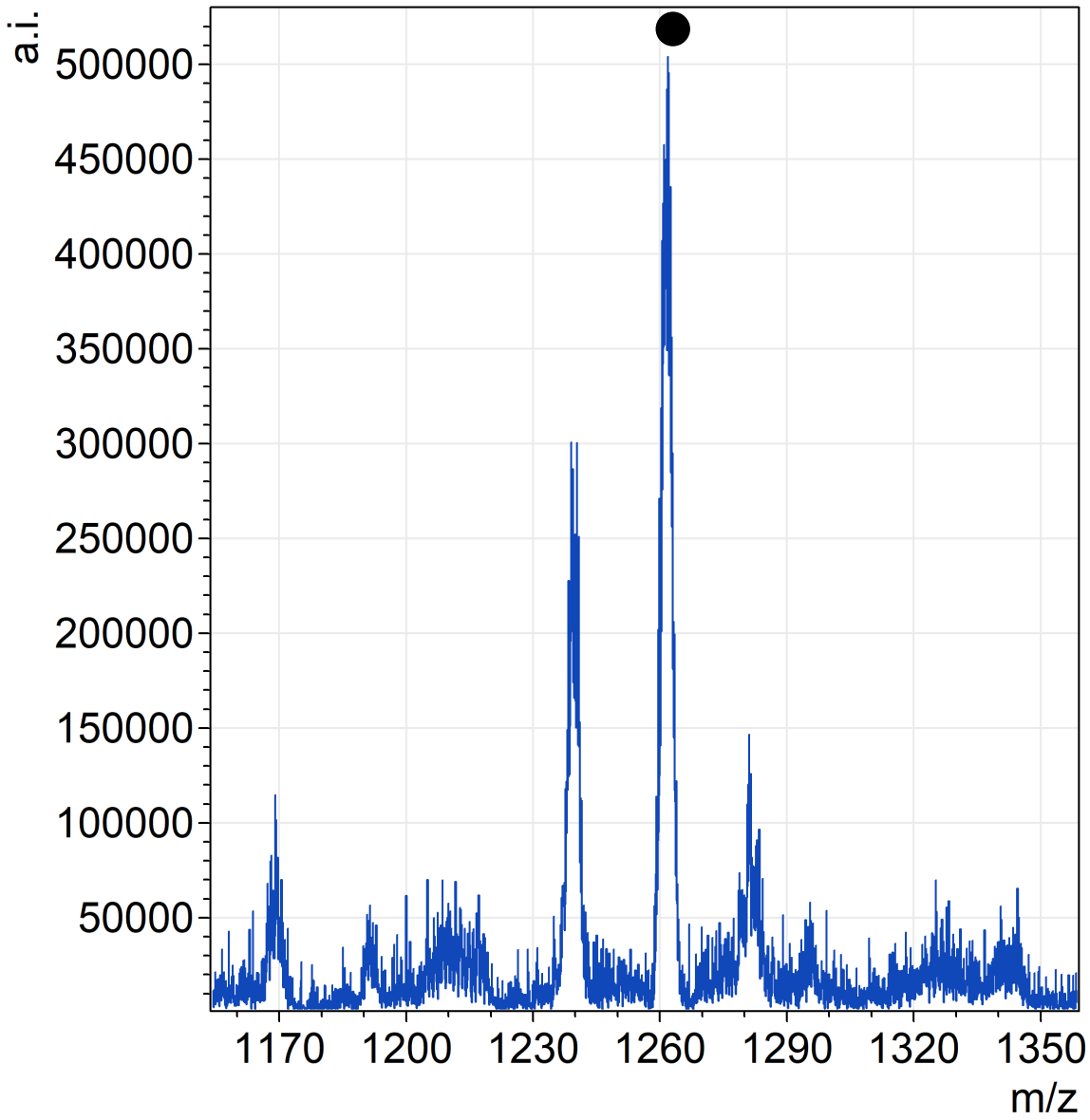

Figure S74: LRMS of helicate **7** and tetrahedron **8**. Counterion is hexafluorophosphate. Observed signal at 1260 corresponds to helicate and tetrahedron (+2 or +4 states respectively).

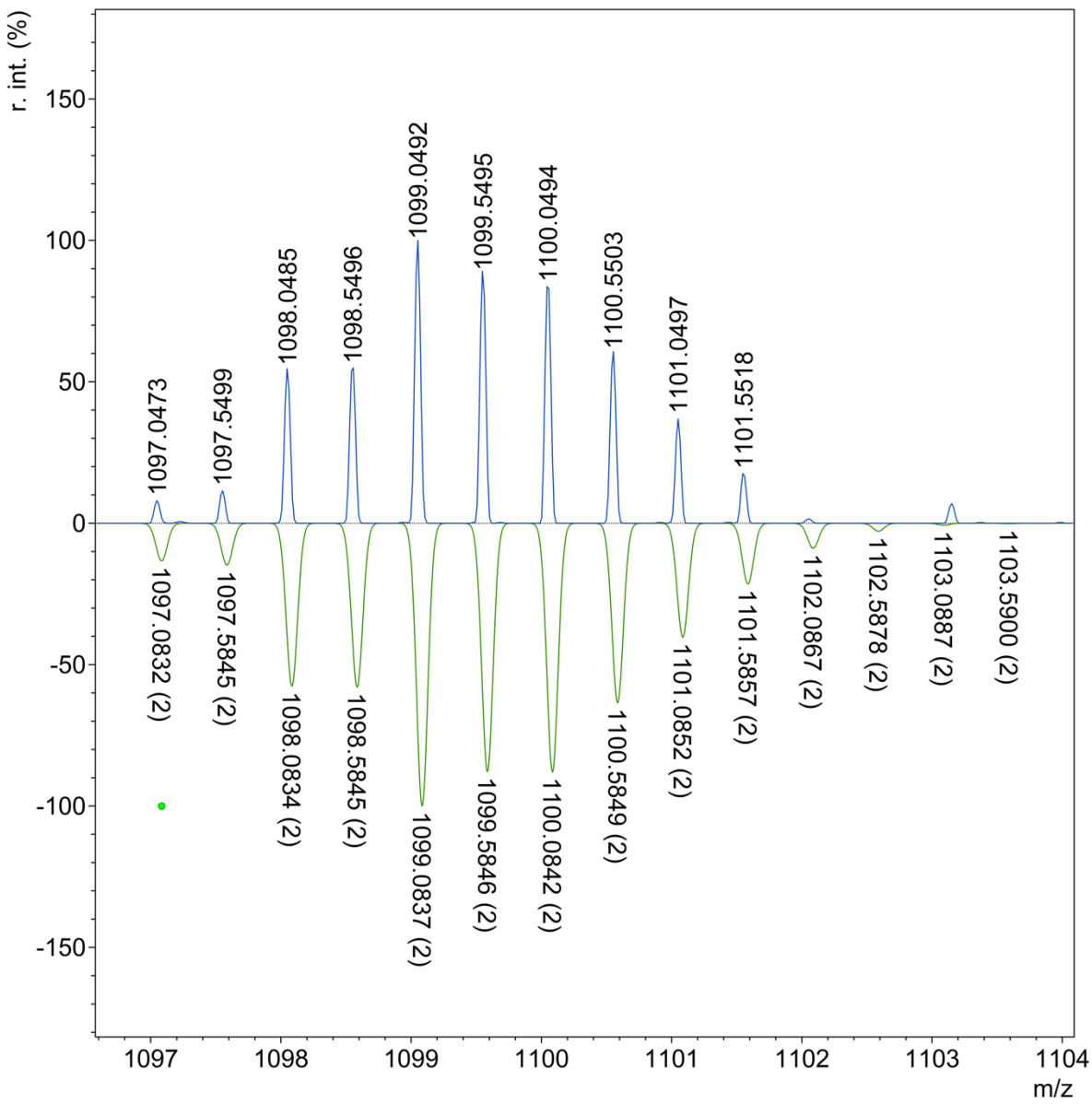

Figure S75: HRMS of helicate **5**. Counterion is hexafluorophosphate. Observed signal top, predicted below.

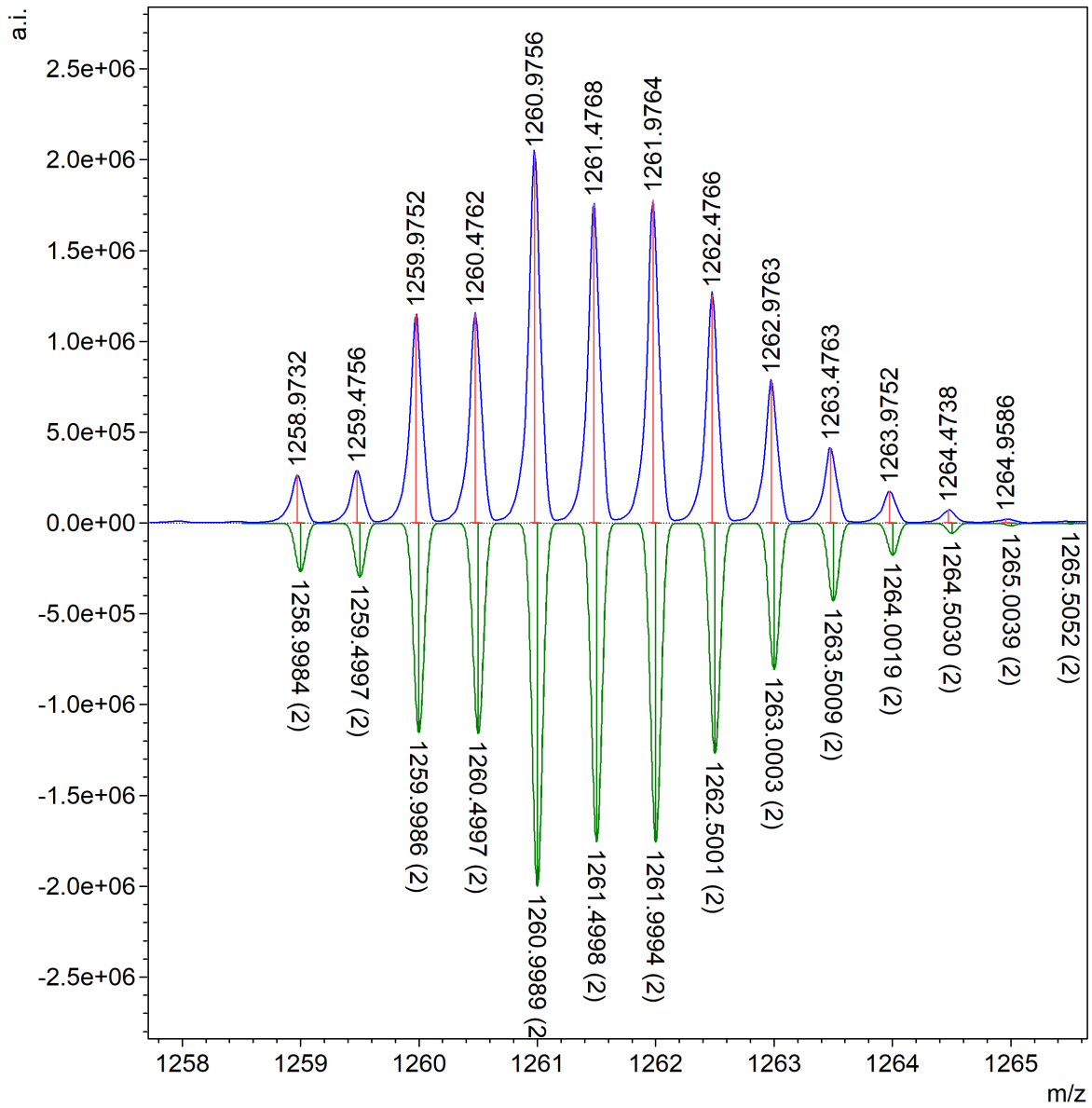

Figure S76: HRMS of helicate **7**. Counterion is hexafluorophosphate. Observed signal top, predicted below.

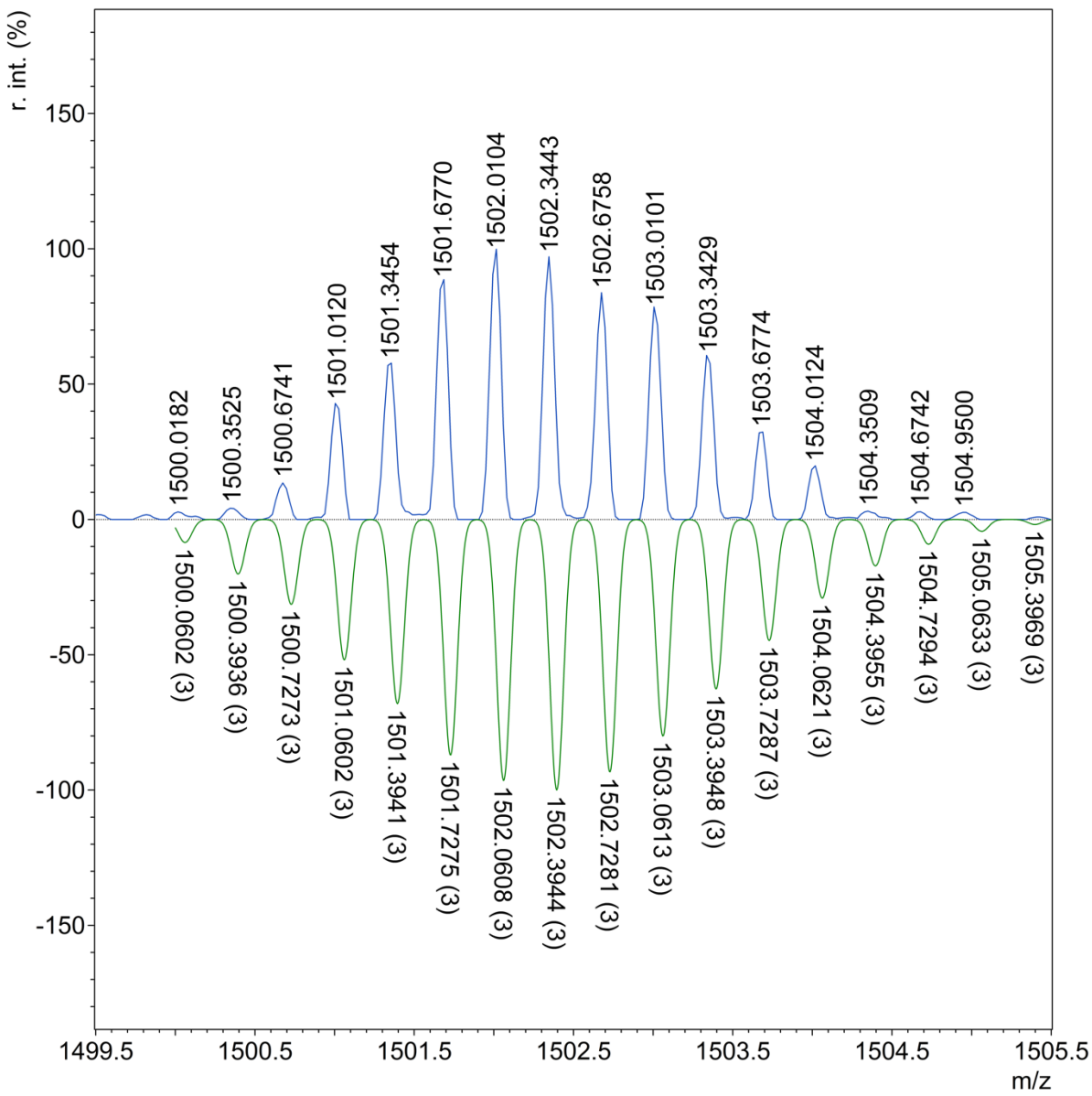

Figure S77: HRMS of six-stranded helicate **9**, templated by iodide. Counterion is hexafluorophosphate. Observed signal top, predicted below.

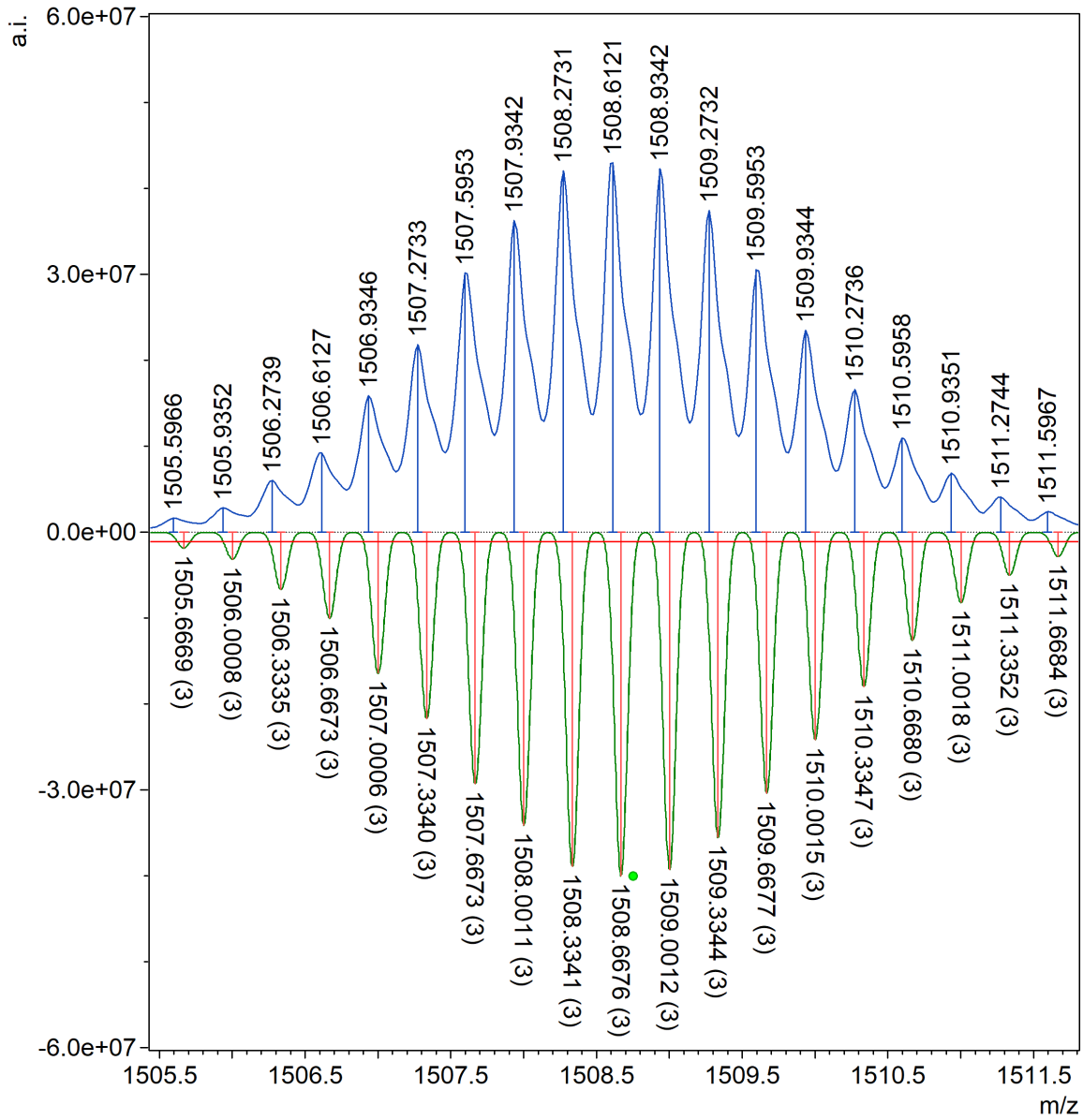

Figure S78: HRMS of six-stranded helicate **10**, templated by sulfate. Counterion is hexafluorophosphate. Observed signal top, predicted below. This species has lost a single Ag+ ion in the mass spectrometer, to form the +3 ion, illustrating the lability of naphthyridine-silver coordination.

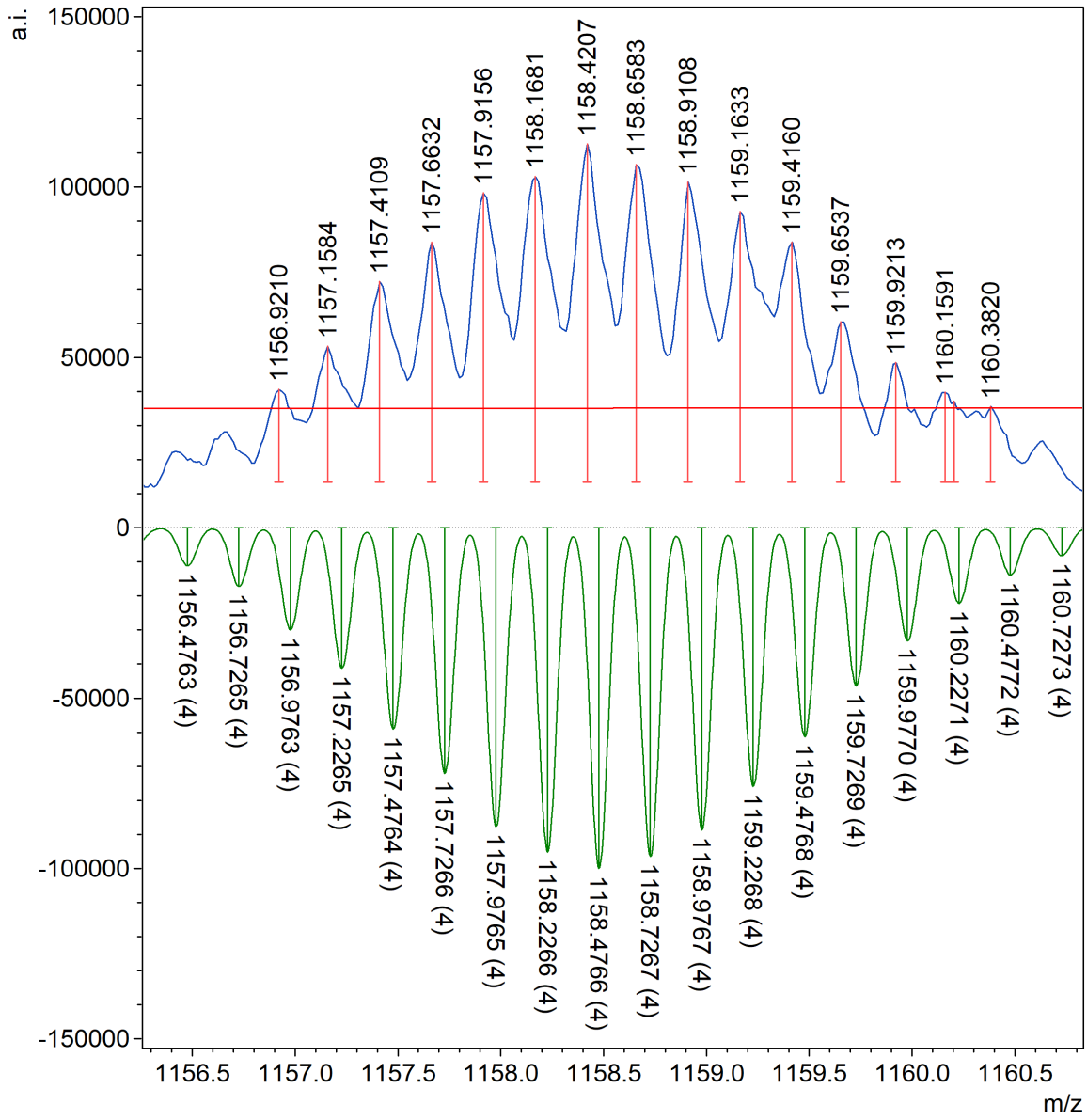

Figure S79: HRMS of six-stranded helicate **10**, templated by sulfate. Counterion is hexafluorophosphate. Observed signal top, predicted below, +4 species.

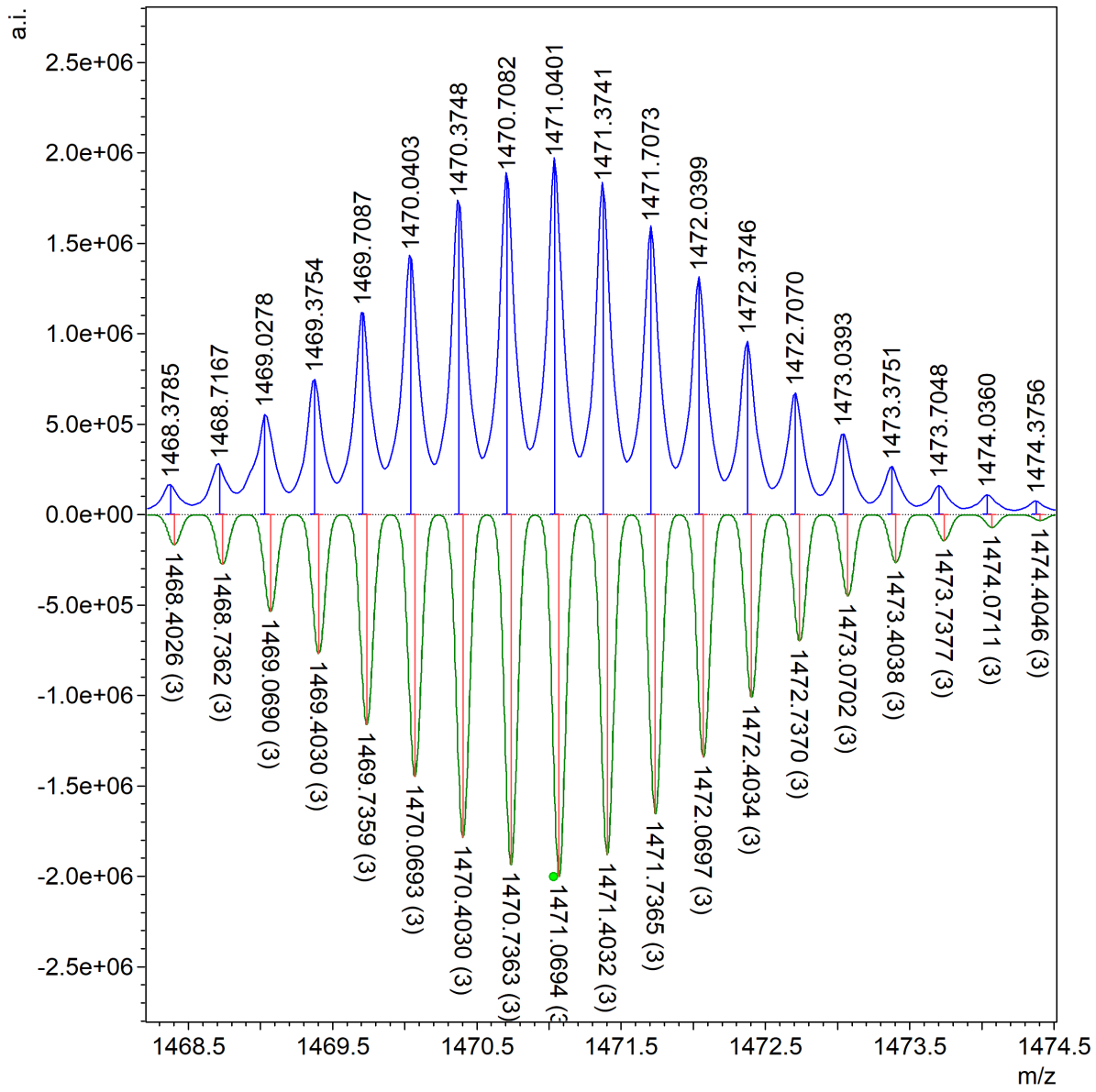

Figure S80: HRMS of six-stranded helicate **11**, templated by bromide. Counterion is hexafluorophosphate. Observed signal top, predicted below, +3 species.

S12. X-Ray Crystallography Data

Data were collected at Beamline I19 of Diamond Light Source employing silicon double crystal monochromated synchrotron radiation (0.6889 Å) with ω and ψ scans at 100(2) K.[3] Data integration and reduction were undertaken with Xia2.[4] Subsequent computations were carried out using the WinGX-32 graphical user interface.[5] Multi-scan empirical absorption corrections were applied to the data using the AIMLESS[6] tool in the CCP4 suite.[7] The structures were solved by direct methods using SHELXT[8] then refined and extended with SHELXL.[9] In general, non-hydrogen atoms with occupancies greater than 0.5 were refined anisotropically. Carbon-bound hydrogen atoms were included in idealised positions and refined using a riding model. Disorder was modelled using standard crystallographic methods including constraints, restraints and rigid bodies where necessary. Crystallographic data along with specific details pertaining to the refinement follow. Crystallographic data have been deposited with the CCDC (2024152-2024153).

$[Ag_8I_2L_6]\cdot 6NTf_2\cdot 6.5MeCN\cdot 1.5Et_2O$ [+ solvent]

Formula $C_{223}H_{178.50}Ag_8F_{36}I_2N_{48.50}O_{25.50}S_{12}$, M 6131.11, Triclinic, space group P-1 (#2), a 21.6420(3), b 24.0386(4), c 25.2054(4) Å, α 80.5920(10), β 81.8190(10), γ 79.0120(10)º, V 12615.5(3) $Å^3$, D_c 1.614 g cm^{-3}, Z 2, crystal size 0.080 by 0.060 by 0.060 mm, colour yellow, habit block, temperature 100(2) Kelvin, λ(Synchrotron) 0.6889 Å, μ(Synchrotron) 0.952 mm^{-1}, T(Analytical)$_{min,max}$ 0.975301320063, 1.0, $2\theta_{max}$ 51.01, *hkl* range -27 27, -30 30, -31 31, N 157389, N_{ind} 50624(R_{merge} 0.1027), N_{obs} 25956(I > 2σ(I)), N_{var} 3693, residuals* $R1(F)$ 0.0741, $wR2(F^2)$ 0.2245, GoF(all) 0.965, $\Delta\rho_{min,max}$ -0.862, 1.586 e^- $Å^{-3}$.

*$R1 = \Sigma||F_o| - |F_c||/\Sigma|F_o|$ for $F_o > 2\sigma(F_o)$; $wR2 = (\Sigma w(F_o^2 - F_c^2)^2/\Sigma(wF_c^2)^2)^{1/2}$ all reflections

$w=1/[\sigma^2(F_o^2)+(0.1255P)^2]$ where $P=(F_o^2+2F_c^2)/3$

Specific refinement details:

The crystals of $[Ag_8I_2L_6]\cdot 6NTf_2\cdot 6.5MeCN\cdot 1.5Et_2O$ [+ solvent] were grown by diffusion of diethyl ether into an acetonitrile solution of the complex. The crystals employed immediately lost solvent after removal from the mother liquor and rapid handling prior to flash cooling in liquid nitrogen was required to collect data. The asymmetric unit was found to contain one complete $[Ag_8I_2L_6]$ assembly and associated counterions and solvent molecules.

The anions and solvent molecules within the structure show evidence of substantial disorder. Five of the six triflimide anions were modelled as disordered over two or three locations. Some lower occupancy disordered atoms were modelled with isotropic thermal parameters and extensive bond length restraints (DFIX, DANG) were applied to facilitate realistic modelling of the disordered triflimide anions. Bond length restraints were also applied to some disordered solvent molecules. Thermal parameter restraints (SIMU, RIGU) were applied to all atoms except for silver and iodine to facilitate anisotropic refinement. The hydrogen atoms of some disordered acetonitrile

molecules could not be located in the electron density map and were therefore not included in the model.
The SQUEEZE[10] function of PLATON[11] was employed to remove the contribution of the electron density associated with a small amount of highly disordered solvent, which gave a potential solvent accessible void of 643 Å^3 per unit cell (a total of approximately 204 electrons). Since the diffuse solvent molecule(s) could not be assigned conclusively to acetonitrile or diethyl ether only those solvent molecules that could be modelled with discrete atom positions are included in the formula. The remaining electron density peaks (up to 1.586 e$^-$Å^3) are close to the silver centers reflecting absorption effects.
CheckCIF gives five B level alerts. These alerts all result from the disordered acetonitrile molecules for which hydrogens were not modelled (apparent singly bonded carbon atoms).

$[Ag_{12}(SO_4)_4L_6]\cdot 4BF_4\cdot 10.5MeCN\cdot 2Et_2O\cdot 4.5H_2O$ [+ solvent]
Formula $C_{221}H_{204.50}Ag_{12}B_4F_{16}N_{46.50}O_{22.50}S_4$, *M* 5641.72, Trigonal, space group R -3 (#148), *a* 23.97750(10), *b* 23.97750(10), *c* 70.6392(3) Å, γ 120º, *V* 35170.9(3) Å^3, D_c 1.598 g cm^{-3}, *Z* 6, crystal size 0.100 by 0.080 by 0.070 mm, colour yellow, habit prism, temperature 100(2) Kelvin, λ(Synchrotron) 0.6889 Å, μ(Synchrotron) 0.997 mm^{-1}, T(Analytical)$_{min,max}$ 0.9813060754116014, 1.0, $2\theta_{max}$ 64.00, *hkl* range -36 36, -36 36, -108 108, *N* 183793, N_{ind} 29726(R_{merge} 0.0538), N_{obs} 21845(I > 2σ(I)), N_{var} 1100, residuals* *R*1(*F*) 0.0474, *wR*2(F^2) 0.1703, GoF(all) 1.071, $\Delta\rho_{min,max}$ -2.158, 1.437 e$^-$ Å^{-3}.
*$R1 = \Sigma||F_o| - |F_c||/\Sigma|F_o|$ for $F_o > 2\Sigma(F_o)$; $wR2 = (\Sigma w(F_o^2 - F_c^2)^2/\Sigma(wF_c^2)^2)^{1/2}$ all reflections
$w=1/[\sigma^2(F_o^2)+(0.1077P)^2]$ where $P=(F_o^2+2F_c^2)/3$

Specific refinement details:
The crystals of $[Ag_{12}(SO_4)_4L_6]\cdot 4BF_4\cdot 10.5MeCN\cdot 2Et_2O\cdot 4.5H_2O$ [+ solvent] were grown by diffusion of diethyl ether into an acetonitrile solution of the complex containing excess $TBABF_4$. The crystals employed immediately lost solvent after removal from the mother liquor and rapid handling prior to flash cooling in liquid nitrogen was required to collect data. The asymmetric unit was found to contain one third of a $[Ag_{12}(SO_4)_4L_6]$ assembly and associated counterions and solvent molecules.
The anions and solvent molecules within the structure show evidence of disorder. One of the outer coordinated sulfates was modelled as disordered over two locations corresponding to different coordination modes with occupancies of 0.59/0.41. The other outer coordinated sulfate shows evidence of thermal motion or minor unresolved disorder. One tetrafluoroborate anion was modelled as disordered over two locations and several acetonitrile molecules were modelled as disordered over multiple locations. Some lower occupancy disordered atoms were modelled with isotropic thermal parameters and extensive bond length restraints (DFIX, DANG) were applied to the disordered residues. Thermal parameter restraints (SIMU, RIGU) were applied to all atoms except for silver to facilitate anisotropic refinement. The hydrogen atoms of some disordered acetonitrile molecules and one water molecule could not be located in the electron density map and were therefore not included in the model.

The SQUEEZE[10] function of PLATON[11] was employed to remove the contribution of the electron density associated with a small amount of highly disordered solvent, which gave a potential solvent accessible void of 261 $Å^3$ per unit cell (a total of approximately 31 electrons). Since the identity of the diffuse solvent molecule could not be conclusively assigned only those solvent molecules that could be modelled with discrete atom positions are included in the formula. The remaining electron density peaks and holes (up to 1.437 or −2.158 $e^{-}Å^3$) are close to the silver centers reflecting absorption effects.
CheckCIF gives nine B level alerts. These alerts all result from the disordered anions and solvent molecules (high MainMol Ueq ratios due to unresolved disorder from the outer coordinated sulfate anions, acetonitriles for which hydrogens were not modelled and a short contact involving a low occupancy disordered acetonitrile).

S13. References

1. Clegg, J. K.; Cremers, J.; Hogben, A. J.; Breiner, B.; Smulders, M. M. J.; Thoburn, J. D.; Nitschke, J. R. A Stimuli Responsive System of Self-Assembled Anion-Binding $Fe_4L_6^{8+}$ Cages. *Chem. Sci.* **2013**, *4*, 68–76.

2. Fernández-Galán, R.; Manzano, B. R.; Otero, A.; Lanfranchi, M.; Pellinghelli, M. A. ^{19}F and ^{31}P NMR Evidence for Silver Hexafluorophosphate Hydrolysis in Solution. New Palladium Difluorophosphate Complexes and X-ray Structure Determination of [Pd(η^3-2-Me-C_3H_4)(PO_2F_2)(PCy_3)]. *Inorg. Chem.* **1994**, *33*, 2309–2312.

3. Allan, D.; Nowell, H.; Barnett, S.; Warren, M.; Wilcox, A.; Christensen, J.; Saunders, L.; Peach, A.; Hooper, M.; Zaja, L.; Patel, S.; Cahill, L.; Marshall, R.; Trimnell, S.; Foster, A.; Bates, T.; Lay, S.; Williams, M.; Hathaway, P.; Winter, G.; Gerstel, M.; Wooley, R., A Novel Dual Air-Bearing Fixed-χ Diffractometer for Small-Molecule Single-Crystal X-ray Diffraction on Beamline I19 at Diamond Light Source. *Crystals* **2017**, *7*, 336.

4. (a) Collaborative Computational Project, N., The CCP4 suite: programs for protein crystallography. *Acta Cryst.* **1994**, *D50*, 760; (b) Evans, P., Scaling and assessment of data quality. *Acta Cryst.* **2006**, *D62*, 72; (c) Winter, G., xia2: an expert system for macromolecular crystallography data reduction. *J. Appl. Crystallogr.* **2010**, *43*, 186.

5. Farrugia, L., WinGX and ORTEP for Windows: an update. *J. Appl. Crystallogr.* **2012**, *45*, 849.

6. Evans, P. R.; Murshudov, G. N., How good are my data and what is the resolution? *Acta Cryst.* **2013**, *D69*, 1204.

7. Winn, M. D.; Ballard, C. C.; Cowtan, K. D.; Dodson, E. J.; Emsley, P.; Evans, P. R.; Keegan, R. M.; Krissinel, E. B.; Leslie, A. G. W.; McCoy, A.; McNicholas, S. J.; Murshudov, G. N.; Pannu, N. S.; Potterton, E. A.; Powell, H. R.; Read, R. J.; Vagin, A.; Wilson, K. S., Overview of the CCP4 suite and current developments. *Acta Cryst.* **2011**, *D67*, 235.

8. Sheldrick, G., SHELXT - Integrated space-group and crystal-structure determination. *Acta. Cryst.* **2015**, *A71*, 3.

9. Sheldrick, G. M., Crystal structure refinement with SHELXL. *Acta. Cryst.* **2015**, *C71*, 3.

10. van der Sluis, P.; Spek, A. L., BYPASS: an effective method for the refinement of crystal structures containing disordered solvent regions. *Acta Cryst.* **1990**, *A46*, 194.

11. Spek, A. L., *PLATON: A Multipurpose Crystallographic Tool*. Utrecht University: Utrecht, The Netherlands, 2008.